APPLICATION OF REMOTE SENSING DATA TO COMPLEMENT HYDROLOGIC MODELLING, THE UPPER BLUE NILE BASIN

A Dissertation

Presented to the Faculty of the Graduate School

of Cornell University

in Partial Fulfillment of the Requirements for the Degree of

Doctor of Philosophy

by

Abeyou Wale Worqlul

August 2015

APPLICATION OF REMOTE SENSING DATA TO COMPLEMENT HYDROLOGIC MODELLING, THE UPPER BLUE NILE BASIN

Abeyou Wale Worqlul, Ph.D.

Cornell University 2015

It has been recognized that reliable, long-term and well distributed climate information is essential to inform any development policy that aims to address the consequences of climate variability and change on water resources. However, in developing countries planning of such activity is greatly hampered by the lack of a sufficiently dense network of weather stations measuring precipitation. The objective of this dissertation is, therefore, to evaluate the freely available high resolution satellite rainfall estimates in the Lake Tana Basin which has a relatively denser ground rainfall stations network. Rainfall estimates of Tropical Rainfall Measuring Mission (TRMM) 3B42 version 7, EUMETSAT's Meteorological Product Extraction Facility (MPEF), Multi-Sensor Precipitation Estimate-Geostationary (MPEG) and Climate Forecast System Reanalysis (CFSR) are considered. The satellite rainfall is validated by a direct comparison with the gauged rainfall data, and through hydrological modelling to capture the observed flow using a semi-distributed hydrological model Hydrologiska Byråns Vattenbalansavdelning (HBV) and Parameter Efficient Distributed (PED).

The result of direct comparison indicated that, the MPEG and CFSR rainfall provided the most accurate rainfall estimates. On average, for 38 stations, 78 and 86 % of the observed rainfall variation is explained by MPEG and CFSR data, respectively, while TRMM explained only 17% of the variation. The hydrological modelling indicated that both the gauged and the CFSR precipitation estimates were able to reproduce the stream flow well for either of the models. The

TRMM data was not be able to capture the observed flow through model calibration for both models. Bias corrected MPEG rainfall by the gauged monthly means performed as well as or better than the gauged rainfall data in capturing the observed flow through hydrologic model calibration.

This dissertation has also identified potential irrigable areas by considering hydrological and landscape factors that determine lack of irrigation development in the Ethiopian highland. Potential land areas suitable for surface irrigation were determined by using a GIS based Multi-Criteria Evaluation (MCE) technique by considering climate characteristics (rainfall and evaporation), land features (soil type, land use and slope), market access (town and road proximity) and proximity to a perennial river. The available water for surface irrigation was quantified by analysing historical river flow data during the dry season of the major rivers in the Lake Tana Basin. The result indicated that the main limitation for surface irrigation in the Ethiopian highlands is the availability of water and not land suitable for irrigation.

BIOGRAPHICAL SKETCH

Abeyou Wale Worqlul was born in Gondar and grown up in Bahir Dar, Ethiopia, the oldest of four. After he completed high school at Tana Haik Secondary School, he joined Arba Minch Water Technology Institute in 2003 with a degree in Hydraulic Engineering. From 2004-2005 he worked at the Bahir Dar Construction Technology College as an Assistant Lecturer and head of Building Construction Department and in 2006 he was appointed as a Lecturer in the School of Civil and Water Resource Engineering of Bahir Dar University. In 2008 Abeyou was awarded a Master's degree from Faculty of Geo-Information Science and Earth Observation, University of Twente, Netherlands (ITC). His thesis was concerned with the Hydrological Balance of Lake Tana focused on runoff estimation from ungauged catchments using regionalization. After his M.Sc. he served Bahir Dar University as a lecturer for the undergraduate and graduate programs. In 2011, Abeyou joined the Department of Biological and Environmental Engineering, Cornell University, for a PhD program and derived this dissertation.

Dedicated to my parents who guided my education since my childhood.

ACKNOWLEDGEMENTS

This dissertation would have not been finalised without the help and support of many people. Therefore, it is a great pleasure for me to acknowledge those who contributed to the completion of this PhD dissertation.

First, I would like to express my sincere thanks and appreciation to Prof. Tammo S. Steenhuis for his scientific advice, guidance, critical comments and for facilitating the financial support throughout my study. I would like to thank my special committee members Prof. Wilfried H. Brutsaert, Prof. William D. Philpot and Prof. Jean-Yves Parlange for their invaluable support throughout my academic program and PhD research.

My deepest gratitude also goes to Dr. Essayas K. Ayana, Dr. Amy S. Collick and Dr. Ben Maathuis for their precious time reading my dissertation chapters and for their constrictive comments. I would like to acknowledge Dr. Charlotte McAlistere, Dr. Simon Langan, Aschalew Teshome, David van Eyck from IWMI office and Dr. Seifu A. Tilahun, Fasikaw Atanaw, Anwar A. Adem and Mamaru Ayalew from Bahir Dar University for their invaluable support throughout my study period. I would like to thank colleagues and friends in Ithaca and Riley Robb that made my stay enjoyable especially to Christian Guzman, Pastor Scott Hathorn, Daniel Fuka, Jacky Luna and Haimanote Kebede.

This work is supported by Norman E. Borlaug Leadership Enhancement in Agriculture Program funded by USAID, International Water Management Institute (IWMI) and Cornell University provided assistantship funds. I am grateful to the National Meteorological Agency and Ministry of Water, Irrigation and Energy of Ethiopia for providing daily meteorological and hydrological

data for multiple stations free of charge. Am also grateful to Bahir Dar University for providing me leave for the study period.

I would like to express my sincere appreciation to friends Tsegaye Cherinet, Surafel Bekele, Temesgen Abrehem and Ashenafi Belay for always being there for me during my stay in Addis Ababa. I would like to say thank you to colleagues in the Faculty of Civil and Water Resources Engineering, Bahir Dar University, staff of IWMI East Africa office and to Cornell soil and water lap group for their supporting and engorgements.

Finally, I would like to extend my appreciation to my parents (Wale, Marta, Meseret, Tilahun, Abayneh and Tewdros) for their kindness, unconditional love and moral support.

TABLE OF CONTENTS

LIST OF FIGURES

LIST OF TABLES

CHAPTER 1: INTRODUCTION

The uneven distribution of water in space and time has significant implications for society. This is especially true in developing countries where rain fed agriculture is the single most important driver of the economy (Conway et al., 2009). It has been recognized that reliable, long-term and well distributed climate information is essential to informing any development policy that aims to address economic development (Hut et al., 2010; Washington et al., 2006). Uneven water distribution necessitates investments to ensure water availability for agriculture, domestic water supply and sanitation, flood protection, soil and water conservation and ecosystem services. The design, operation and maintenance of these infrastructures require adequately accurate estimation of quantity and quality of water. However, in many developing countries, and specifically in Ethiopia ground-based observation stations are relatively sparse (Conway, 2000; Kaba et al., 2014; Worqlul et al., 2014). Ground data collection systems are characterized by inadequate monitoring, gaps in observations, decline in number of stations and difference in processing and quality control (Harvey and Grabs, 2003; Vörösmarty et al., 2001). Rainfall is one of the major water balance component of the water cycle, the quality of data collected is poor in developing countries due to uneven and scarcely distributed ground-based observation networks (Conway, 2000; Creutin and Borga, 2003; Kaba et al., 2014; Kidd, 2001; Worqlul et al., 2014).

Water resource assessment tools have improved enormously with advances in computational power and understanding of the processes in data scarce areas (Letcher et al., 2007; RESH et al., 1995; Silberstein, 2006). Often modelers tend to conceptualize based on simplified views of the system (Dozier, 1992). The major water balance component, rainfall is probably one of the climate variables that is highly affected by simplified conceptualization. Although the spatial and

temporal variability of precipitation is important, unless large numbers of rain gauge stations are available, capturing variability is difficult (Chaubey et al., 1999; Pardo-Igúzquiza, 1998). Recently, satellite remote sensing has received much attention in measuring precipitation (Aonashi et al., 2009; Barrett, 1989; Ebert and McBride, 2000; Ferriday, 1994; Hong, 2003; Huffman et al., 2007; Joyce et al., 2004; Kidd, 2001; Scofield and Kuligowski, 2003; Sorooshian et al., 2000). Very few studies evaluate satellite rainfall over Africa (Ali et al., 2005; Thorne et al., 2001; Worqlul et al., 2014). Studies also indicate large differences in algorithm performance depending on season and local climate (Dinku et al., 2007; Dinku et al., 2008; Jobard et al., 2007). This dissertation focuses on evaluation of satellite rainfall estimate in Lake Tana sub-basin of the Upper Blue Nile basin, Ethiopia.

The main hypothesis of this dissertation is that, satellite precipitation measurements can provide better spatial and temporal estimates of precipitation events in a data scarce region, and thus can replace ground based measurement for calibrating and validating hydrologic models. Therefore the main goals of this study are to validate satellite rainfall estimates (SRE)[1] and assess the predictive capability of the best performing SRE using a semi-distributed Hydrologiska Byråns Vattenbalansavdelning (HBV) and Parameter Efficient Distributed (PED) hydrological models over the modestly and scarcely gauged watershed in the Upper Blue Nile Basin, Ethiopia.

The first three chapters of this dissertation focus on the validation of satellite rainfall estimate using ground rainfall data, hydrological modelling and bias correction respectively. Chapter one presents the SRE validation results for TRMM, CFSR and MPEG using observations from dense

[1] Most widely known satellite precipitation estimates (SPE) include Tropical Rainfall Measuring Mission (TRMM), EUMETSAT's Meteorological Product Extraction Facility (MPEF) Multi-Sensor Precipitation Estimate-Geostationary (MPEG), Climate Forecast System Reanalysis (CFSR), the NOAA/Climate Prediction Centre morphing technique (CMORPH), Precipitation Estimation from Remotely Sensed Information using Artificial Neural Network (PERSIANN), the Naval Research Laboratory's blended product (NRLB)

in situ rainfall measurements in the Lake Tana sub-Basin. The satellite rainfall estimate is compared in two ways: first the grids of satellite rainfall estimation (MPEG, TRMM and CFSR) are compared to the ground rainfall observation data within the satellite grid box and then SRE is compared to interpolated observed rainfall stations over Lake Tana major sub-basins. The performance is tested using standard statistics coefficient of determination (R-square), root mean square error (RMSE) and Bias. In the second and third chapters the output from two watershed models; HBV-IHMS and PED, is presented. TRMM, CFSR and MPEG precipitation estimates are used to excite hydrological models to capture the observed flow and the result is compared with flow simulated by traditional gauges.

A major application of validated SREs is in planning and expansion of irrigation infrastructures. Recently a lot of effort has been exerted toward irrigation development in Ethiopia, but little has been done to quantify the irrigation potential land and available water for surface irrigation. Strategic spatial planning and mapping of land suitability is regarded as important in the past decayed. It is a fundamental approach to achieve sustainable development (Chen et al., 2008; Yu et al., 2011). The fifth chapter addresses spatial mapping of potential land areas suitable for small, medium and large-scale irrigations by applying a GIS based Multi-Criteria Evaluation (MCE) technique. The irrigation potential of the available water is estimated by analyzing the historical dry season river flow data.

The sixth chapter presents the impacts of physical catchment characteristics (PCC) which includes climate, geography and physiographic, geology, soil, land-use and land cover conditions on river flow. Two adjacent watersheds of comparable area but annual yield of one over 2.4 times the other are used to examine what PCC drive such disparities in a monsoon climate. The

Soil Water Assessment Tool (SWAT) distributed hydrological model is used to investigate the effect of PCCs on the dissimilar stream flow of those watersheds.

Reference

Ali, A., Amani, A., Diedhiou, A., and Lebel, T.: Rainfall estimation in the Sahel. Part II: Evaluation of rain gauge networks in the CILSS countries and objective intercomparison of rainfall products, Journal of Applied Meteorology, 44, 1707-1722, 2005.

Aonashi, K., Awaka, J., Hirose, M., Kozu, T., Kubota, T., Liu, G., Shige, S., Kida, S., Seto, S., and Takahashi, N.: GSMaP passive microwave precipitation retrieval algorithm: Algorithm description and validation, 気象集誌 第2 輯 87, 119-136, 2009.

Barrett, E. C.: Satellite remote sensing of rainfall. In: Applications of remote sensing to agrometeorology, Springer, 1989.

Chaubey, I., Haan, C., Grunwald, S., and Salisbury, J.: Uncertainty in the model parameters due to spatial variability of rainfall, Journal of Hydrology, 220, 48-61, 1999.

Chen, Y., Khan, S., and Padar, Z.: Irrigation intensification or extensification assessment: a GIS-based spatial fuzzy multi-criteria evaluation, 2008, 309-318.

Conway, D.: The climate and hydrology of the Upper Blue Nile River, The Geographical Journal, 166, 49-62, 2000.

Conway, D., Persechino, A., Ardoin-Bardin, S., Hamandawana, H., Dieulin, C., and Mahé, G.: Rainfall and water resources variability in sub-Saharan Africa during the twentieth century, Journal of Hydrometeorology, 10, 41-59, 2009.

Creutin, J. D. and Borga, M.: Radar hydrology modifies the monitoring of flash- flood hazard, Hydrological processes, 17, 1453-1456, 2003.

Dinku, T., Ceccato, P., Grover- Kopec, E., Lemma, M., Connor, S., and Ropelewski, C.: Validation of satellite rainfall products over East Africa's complex topography, International Journal of Remote Sensing, 28, 1503-1526, 2007.

Dinku, T., Chidzambwa, S., Ceccato, P., Connor, S., and Ropelewski, C.: Validation of high-resolution satellite rainfall products over complex terrain, International Journal of Remote Sensing, 29, 4097-4110, 2008.

Dozier, J.: Opportunities to improve hydrologic data, Reviews of Geophysics, 30, 315-331, 1992.

Ebert, E. and McBride, J.: Verification of precipitation in weather systems: Determination of systematic errors, Journal of Hydrology, 239, 179-202, 2000.

Ferriday, J. G.: Satellite remote sensing of global rainfall using passive microwave radiometry, Univ. of Colorado, Colorado Center For Astrodynamics Research, Boulder, CO (United States), 1994.

Harvey, K. and Grabs, W.: WMO report of the GCOS, 2003, 18-20.

Hong, Y.: Precipitation Estimation from Remotely Sensed Information using Artificial Neural Network-Cloud Classification System, 2003. 2003.

Huffman, G. J., Bolvin, D. T., Nelkin, E. J., Wolff, D. B., Adler, R. F., Gu, G., Hong, Y., Bowman, K. P., and Stocker, E. F.: The TRMM multisatellite precipitation analysis (TMPA): Quasi-global, multiyear, combined-sensor precipitation estimates at fine scales, Journal of Hydrometeorology, 8, 38-55, 2007.

Hut, R., van de Giesen, N., Selker, J., and Andreini, M.: The Trans African Hydro Meteorological Observatory, 2010, 0793.

Jobard, I., Chopin, F., Bergés, J., Ali, A., Lebel, T., and Desbois, M.: Presentation of the EPSAT-SG method and comparison with other satellite precipitation estimations in the frame of Precip-AMMA, 2007, 10062.

Joyce, R. J., Janowiak, J. E., Arkin, P. A., and Xie, P.: CMORPH: A method that produces global precipitation estimates from passive microwave and infrared data at high spatial and temporal resolution, Journal of Hydrometeorology, 5, 487-503, 2004.

Kaba, E., Philpot, W., and Steenhuis, T.: Evaluating suitability of MODIS-Terra images for reproducing historic sediment concentrations in water bodies: Lake Tana, Ethiopia, International Journal of Applied Earth Observation and Geoinformation, 26, 286-297, 2014.

Kidd, C.: Satellite rainfall climatology: a review, International Journal of Climatology, 21, 1041-1066, 2001.

Letcher, R. A., Croke, B. F., and Jakeman, A. J.: Integrated assessment modelling for water resource allocation and management: A generalised conceptual framework, Environmental Modelling & Software, 22, 733-742, 2007.

Pardo-Igúzquiza, E.: Optimal selection of number and location of rainfall gauges for areal rainfall estimation using geostatistics and simulated annealing, Journal of Hydrology, 210, 206-220, 1998.

RESH, V. H., NORRIS, R. H., and BARBOUR, M. T.: Design and implementation of rapid assessment approaches for water resource monitoring using benthic macroinvertebrates, Australian Journal of Ecology, 20, 108-121, 1995.

Scofield, R. A. and Kuligowski, R. J.: Status and outlook of operational satellite precipitation algorithms for extreme-precipitation events, Weather and Forecasting, 18, 1037-1051, 2003.

Silberstein, R.: Hydrological models are so good, do we still need data?, Environmental Modelling & Software, 21, 1340-1352, 2006.

Sorooshian, S., Hsu, K.-L., Gao, X., Gupta, H. V., Imam, B., and Braithwaite, D.: Evaluation of PERSIANN system satellite-based estimates of tropical rainfall, Bulletin of the American Meteorological Society, 81, 2035-2046, 2000.

Thorne, V., Coakeley, P., Grimes, D., and Dugdale, G.: Comparison of TAMSAT and CPC rainfall estimates with raingauges, for southern Africa, International Journal of Remote Sensing, 22, 1951-1974, 2001.

Vörösmarty, C., Askew, A., Grabs, W., Barry, R., Birkett, C., Döll, P., Goodison, B., Hall, A., Jenne, R., and Kitaev, L.: Global water data: A newly endangered species, Eos, Transactions American Geophysical Union, 82, 54-58, 2001.

Washington, R., Kay, G., Harrison, M., Conway, D., Black, E., Challinor, A., Grimes, D., Jones, R., Morse, A., and Todd, M.: African climate change: taking the shorter route, Bulletin of the American Meteorological Society, 87, 1355-1366, 2006.

Worqlul, A. W., Maathuis, B., Adem, A. A., Demissie, S. S., Langan, S., and Steenhuis, T. S.: Comparison of rainfall estimations by TRMM 3B42, MPEG and CFSR with ground-observed data for the Lake Tana basin in Ethiopia, Hydrology and Earth System Sciences, 18, 4871-4881, 2014.

Yu, J., Chen, Y., Wu, J., and Khan, S.: Cellular automata-based spatial multi-criteria land suitability simulation for irrigated agriculture, International journal of geographical information science, 25, 131-148, 2011.

CHAPTER 2: COMPARISON OF RAINFALL ESTIMATIONS BY TRMM 3B42, MPEG AND CFSR WITH GROUND-OBSERVED DATA FOR THE LAKE TANA BASIN, ETHIOPIA[2]

Abstract

Planning for drought relief and floods in developing countries is greatly hampered by the lack of a sufficiently dense network of weather stations measuring precipitation. In this paper we test the utility of three satellite products to augment the ground-based precipitation measurement to provide improved spatial estimates of rainfall. The three products are the Tropical Rainfall Measuring Mission (TRMM) product (3B42), Multi-Sensor Precipitation Estimate-Geostationary (MPEG) and the Climate Forecast System Reanalysis (CFSR). The accuracy of the three products is tested in the Lake Tana basin in Ethiopia where 38 weather stations were available in 2010 with a full record of daily precipitation amounts. Daily gridded satellite-based rainfall estimates were compared to: (1) point-observed ground rainfall and (2) areal rainfall in the major river sub-basins of Lake Tana. The result shows that the MPEG and CFSR satellites provided the most accurate rainfall estimates. On average, for 38 stations, 78 and 86 % of the observed rainfall variation is explained by MPEG and CFSR data, respectively, while TRMM explained only 17% of the variation. Similarly, the areal comparison indicated a better performance for both MPEG and CFSR data in capturing the pattern and amount of rainfall. MPEG and CFSR also have a lower RMSE compared to the TRMM 3B42 satellite rainfall. The Bias indicated that

[2] Worqlul, A. W., Maathuis, B., Adem, A. A., Demissie, S. S., Langan, S., and Steenhuis, T. S.: Comparison of rainfall estimations by TRMM 3B42, MPEG and CFSR with ground-observed data for the Lake Tana basin in Ethiopia, Hydrology and Earth System Sciences, 18, 4871-4881, 2014b.

TRMM 3B42 was, on average, unbiased, whereas MPEG consistently underestimated the observed rainfall. CFSR often produced large overestimates.

2.1 Introduction

Precipitation is a major component of the water cycle, and is responsible for depositing approximately 505,000 km^3 (or on average 990 mm) of the fresh water on the planet (Ramakrishna and Nasreen, 2013). It is one of the major water balance components of the global water budget. Although the spatial and temporal variability of precipitation is important, unless large numbers of rain gauge stations are available, capturing variability is difficult (Chaubey et al., 1999; Pardo-Igúzquiza, 1998). However, ground-based rainfall observation station networks are often unevenly and sparsely distributed especially in developing countries (Kaba et al., 2014). For example, the Rahad, Dindir and Welaka sub-basins in the Blue Nile basin, Ethiopia each had only one rainfall station, despite catchment area greater than 5,000 km^2. This is far below the World Meteorological Organization (WMO) standard of one station for 100 to 250 km^2 in area for mountainous regions (WMO, 1994). This situation is not likely to improve in the near future. The poor coverage introduces large uncertainties into rainfall distribution estimation, and will evidently undermine the dependability of hydrologic models used in simulating flow (both low flows and floods), sediment load and nutrient fluxes (Kaba et al., 2014). The unavailability of good quality rainfall data renders hydrologists reluctant to deal confidently with pressing and unprecedented societal questions vis-à-vis food deficits, global warming, climate change, water scarcity and water shortage issues (Baveye, 2013).

The growing availability of high-resolution (and near-real-time) satellite rainfall products can help hydrologists to obtain more accurate precipitation data, particularly in developing countries

and remote locations where weather radars are absent and conventional rain gauges are sparse (Creutin and Borga, 2003; Kidd, 2001). Satellite-derived rainfall estimates have become a powerful tool for supplementing the ground based rainfall estimates. Recently, Earth observation data for environmental or societal purposes have become readily available through Earth observation (EO) satellites and data distribution systems. Some of the freely available spatially distributed rainfall estimates are the Tropical Rainfall Measuring Mission (TRMM) (Simpson et al., 1988), EUMETSAT's Meteorological Product Extraction Facility (MPEF), Multi-Sensor Precipitation Estimate-Geostationary (MPEG), the Climate Forecast System Reanalysis (CFSR), the NOAA/Climate Prediction Centre morphing technique (CMORPH), precipitation estimation from remotely sensed information using artificial neural network (PERSIANN), the Naval Research Laboratory's blended product (NRLB), and more.

Passive microwave (PM) and thermal infrared (TIR) sensors are the most widely used channels of the electromagnetic spectrum for satellite rainfall estimation (Huffman et al., 2007; Joyce et al., 2004; Kidd et al., 2003; Negri et al., 1984). A TIR sensor provides useful information on storm clouds based on top cloud temperature. The assumption in the TIR is that relatively cold clouds are associated with thick and high clouds that tend to be associated with the production of high rainfall rates (Haile et al., 2010). One of the limitations with a TIR sensor is that it only uses the top cloud temperature from which the depth of the cloud is inferred (Todd et al., 2001) and it also underestimates warm rain and misidentifies cirrus clouds as rain (Dinku et al., 2011). Microwave sensors utilize a more direct way of retrieving precipitation from satellites; they gather information about the rain rather than the cloud (Todd et al., 2001). The absorption of microwave radiation by liquid water and its scattering by ice particles can be related to rainfall over the ocean and over land (Ferraro, 1997). The disadvantage of PM sensors is that they are

not available on geostationary satellites, which makes them have a longer latency (Heinemann et al., 2002). A combination of both, microwave (MW) data from polar orbiting satellites and IR data from geostationary systems, is an obvious approach to overcome some of the shortcomings in the estimation of precipitation. In this study, satellite-estimated rainfall by TRMM 3B42 (hereafter, simply "TRMM"), MPEG and CFSR is validated by comparing the estimates with the ground observation rainfall data in the Lake Tana basin Ethiopia.

Validation of satellite rainfall products in the Ethiopian highlands will give an insight into how the different products perform in this region. In general, three seasons exist in Ethiopia. The main rainfall season from June to September, called the "Kremt" season, accounts for a large proportion of the annual rainfall (approximately 86%), and the dry season extending from October to January called "Bega" is followed by a small rainy season called "Belg". The most important weather systems that cause rain over the country includes the intertropical convergence zone (ITCZ), the Red Sea convergence zone (RSCZ), tropical easterly jet (TEJ) and Somalia jet (NMSA, 1996; Seleshi and Zanke, 2004). The main rainy seasons were found to be significantly correlated with the El Niño-Southern Oscillation (ENSO) (Camberlin, 1997) and most of the drought seasons in Ethiopia are more likely to occur during warm ENSO events (Seleshi and Demaree, 1995).

A number of studies have been done to validate TRMM in the Ethiopian highlands (Dinku et al., 2010; Tsidu, 2012). These studies have focused on comparisons of gridded satellite rainfall estimations to a ground rainfall observation data. This study validates satellite rainfall products in two ways: by comparing satellite-gridded rainfall data to point observation data and, second, by comparing satellite areal rainfall estimates to areal ground-observed rainfall interpolated by the Thiessen polygon method for the major sub-basins of Lake Tana. The Lake Tana basin is

selected to take advantage of a relatively higher rainfall observation station density and the availability of daily rainfall data. These rainfall products are selected for comparison given the fact that the state-of-the-art algorithms are used to generate them. They are also freely available for use in Africa. For example, Bahir Dar University, in collaboration with the Tana sub-basin office and the University of Twente, the Netherlands, have established a GEONETCast ground-receiving station (Wale et al., 2011), that makes the MPEG satellite rainfall product locally available. In addition, all three rainfall estimates (TRMM, CFSR and MPEG) have a relatively high spatial resolution, global coverage and high temporal resolution.

The general objective of the study is to examine which of the three freely available satellite products gives the best estimates of the spatial distribution of rainfall in mountainous terrain of Ethiopia. The satellite estimates are compared with a relatively dense network of ground rainfall observation stations distributed across the Lake Tana basin for year 2010 for which we were able to obtain the most dense distribution of daily precipitation data.

2.1.1 Description of study area

The study is carried out in the Lake Tana basin source of Blue Nile River in the northwest highlands of Ethiopia, with a total catchment area of 15,000 km^2. The lake covers around 3,060 km^2 at an altitude of 1786 m. The lake is located at 12^{o}00'N, 37^{o}15'E around 564 km from the capital Addis Ababa (Wale, 2008). The basin has a complex topography with significant elevation variations ranging from 1786 to 4107 m. The long-term annual average rainfall from 1994 to 2008 ranges from 2500 mm south of Lake Tana to 830 mm west of Lake Tana. Figure 2-1 shows the spatial distribution of the rain gauge station network in and around Lake Tana basin with a TRMM and CFSR grid.

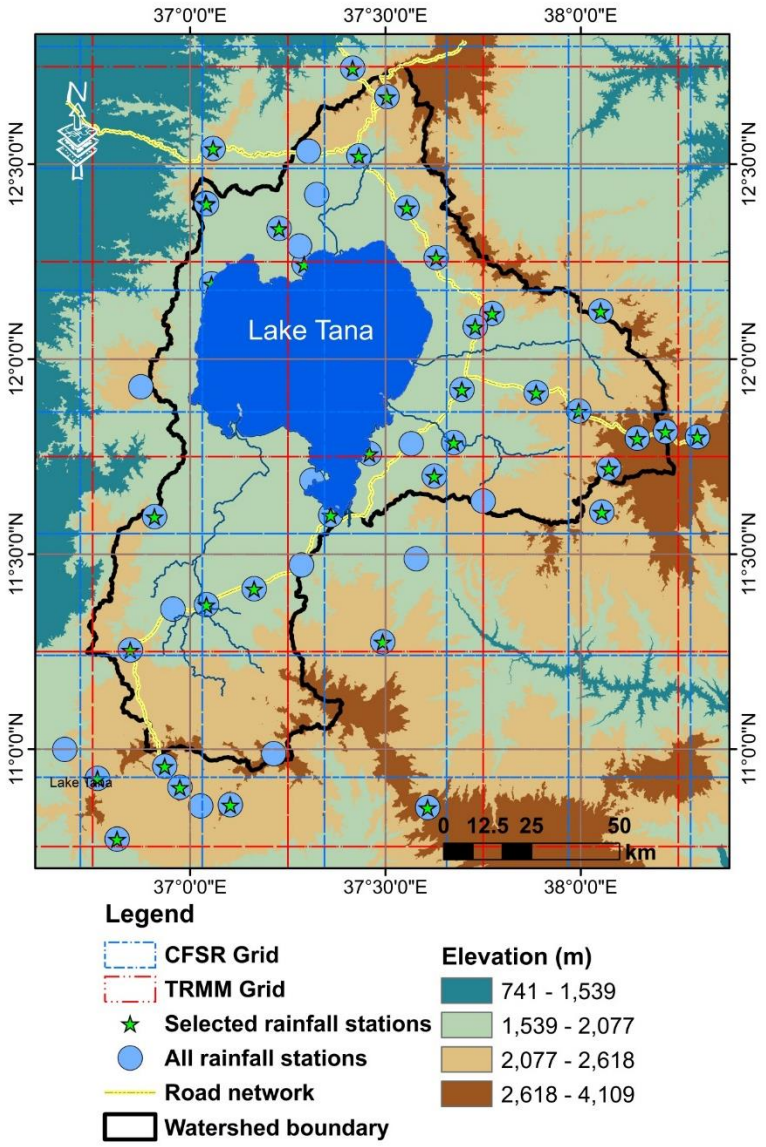

Figure 2-1: The Lake Tana watershed, showing the TRMM and CFSR grids and the location of the available and selected rainfall stations (90 meter digital elevation model as background).

2.1.2 Data availability

The data required for this study, gauge-observed rainfall data, are collected from the Ethiopian National Meteorological Agency (ENMA). Long-term average annual rainfall from 1994 to 2008, daily rainfall data for the year 2010 and station location and elevation for 51 stations in

and around the Lake Tana basin are obtained from ENMA. Some stations did not record the rainfall consistently on a daily basis, or for other stations the location and the elevation were not known. Thirty-eight stations remained that have continuous daily rainfall data for the selected study period (2010). Of these 38, there are seven stations classified as Class 1 (synoptic stations), where all meteorological parameters are measured every hour. The majority of the seventeen stations are Class 3 (ordinary stations) where only rainfall and maximum and minimum temperature are collected on a daily basis. The remaining 14 stations are Class 4; only daily rainfall amounts are recorded.

Some of the MPEG data at 15 minutes temporal interval are acquired in near real time from the low-cost satellite image reception station established at Bahir Dar University, Institute of Technology (Wale et al., 2011). The daily aggregated MPEG data from 00:00 till 23:45 UTC, in mm/day, are available online at ftp://ftp.itc.nl/pub/mpe/msg/. TRMM gridded rainfall estimates are collected from the ftp site, available at: ftp://disc2.nascom.nasa.gov/data/s4pa/TRMM_L3/TRMM_3B42_daily/. The daily gridded CFSR rainfall data can be collected from http://rda.ucar.edu/datasets/ds094.1/.

2.2 Methods

The predicted satellite rainfall estimate and observed gauged rainfall data have different spatial and temporal scales. The ground observation consists of 38 daily observations of point rainfall amounts irregularly distributed across the Lake Tana basin (Figure 2-1). The MPEG, TRMM and CFSR rainfall consists of spatially distributed time series regularly gridded data with spatial resolution of 3 km, 0.25^{o} (≈27 km at the Equator) and 38 km, respectively. A detailed description of TRMM, MPEG and CFSR data is provided in Appendix A. The average annual rainfall from

1994 to 2008 is plotted against the station elevation to see the stations likely affected by convective precipitation and those very much affected by a combination of orographic and convective precipitation. The backwards elimination technique was used to obtain the linear trends with elevation in the long-term average rainfall. The backward elimination technique successively eliminates the weakest independent station (variable), after which the regression will be recalculated (Xu and Zhang, 2001). If removing the variable significantly weakens the linear model, then the variable is re-entered; otherwise, it is deleted. This procedure is then repeated by classifying the data in two groups until we found a maximum coefficient of determination.

The gridded satellite rainfall estimation is linked to the ground rainfall observations in two ways:

Point-to-grid comparison: The grids of satellite rainfall estimation (MPEG, TRMM and CFSR) are compared to the ground rainfall observation data within the satellite grid box. This means that a point ground observation data are compared against a satellite grid data of sizes 3 by 3 km, 0.25 by 0.25 degree and 38 by 38 km for MPEG, TRMM and CFSR, respectively. Finally, the comparison on monthly and annual basis is done by applying standard statistics.

Areal comparison: Satellite rainfall estimation is compared with the interpolated observed rainfall stations. The ground rainfall observations are interpolated adopting a Thiessen polygon method and compared with the respective satellite rainfall estimation for the major gauged river basins of Lake Tana; the accuracy is measured using standard statistics. The major river basins in Lake Tana used for this study are Gilgel Abay, Gumara, Ribb and Megech according to Kebede et al. (2006), these rivers contribute approximately 93% of the surface water inflow.

2.2.1 Ground rainfall observation station (GROS)

There are 51 meteorological stations operated by ENMA in the study area. Some of them have no location information and/or the actual elevation provided is not considered reliable. For the 38 selected stations, daily rainfall is available in the 2010 study period. Monthly rainfall amounts for selected stations are given in Figure 2-2. Long-term annual average rainfall varies between 830 mm and 2500 mm/year from 1994 to 2008. Approximately eighty six percent of the annual rainfall falls between June and September.

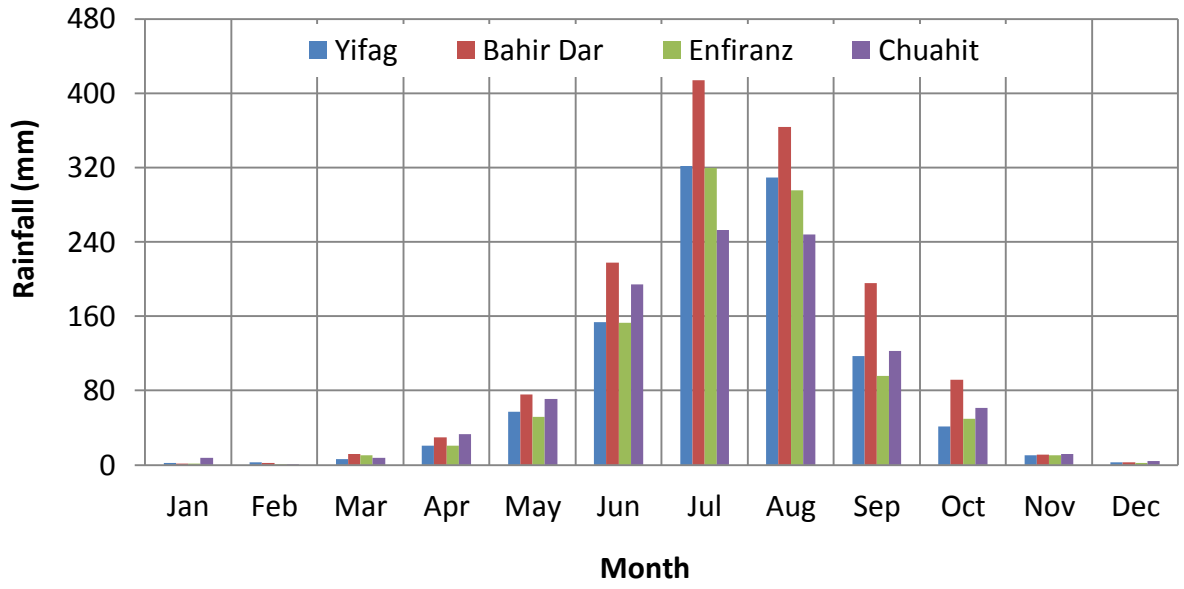

Figure 2-2: Averaged monthly gauged rainfall distribution of selected stations in the Lake Tana basin (from 1994 to 2008).

2.2.2 Statistical measures

Three statistical measures were used to compare the satellite rainfall estimates with the ground rainfall observations consisting of the coefficient of determination (R^2), multiplicative bias (Bias) and root mean square error (RMSE).

The coefficient of determination (R^2) is used to evaluate the goodness of fit of the relation. R-Square address the question of how well the satellite rainfall estimates correspond to the ground rainfall observations: it is the degree of linear association between the two terms; see Eq. (1).

$$R^2 = \left(\frac{n\sum(G_i S_i) - (\sum G_i)(\sum S_i)}{\sqrt{(n(\sum {G_i}^2) - (\sum G_i)^2)(n(\sum {S_i}^2) - (\sum S_i)^2)}} \right)^2 \qquad \text{Eq. (1)}$$

Where: R^2 is coefficient of determination, Gi the ground rainfall measurements, Si the satellite rainfall estimates, and n the number of data pairs.

Root mean square error (RMSE) measures the difference between the distributions of the ground-observed rainfall and the distribution of satellite rainfall estimation, and calculates a weighted average error, weighted according to the square of the error. RMSE is givers a higher weight for a larger errors. The lower the RMSE score, the closer the satellite rainfall estimation represents the observed ground rainfall measurement; see Eq. (2).

$$RMSE = \sqrt{\frac{\sum(G_i - S_i)^2}{n}} \qquad \text{Eq. (2)}$$

Where: RMSE is root mean square error, Gi the ground rainfall measurements, Si the satellite rainfall estimates, and n is the number of data pairs.

Bias is a measure of how the average satellite rainfall magnitude compares to the ground rainfall observation. It is simply the ratio of the mean satellite rainfall estimation value to the mean of the ground rainfall observed value. A bias of 1.1 means the satellite rainfall is 10 percent higher than the average ground rainfall observations; see Eq. (3).

$$\text{Bias} = \frac{\sum S_i}{\sum G_i} \qquad \text{Eq. (3)}$$

Where: Gi = ground rainfall measurements and Si = satellite rainfall estimates.

2.3 Result and Discussion

The long-term annual average rainfall from 1994 to 2008 is plotted against station elevation to see the rainfall-elevation relation (Figure 2-3a). Two clear relationships can be observed; the first one shows a 50 mm of rainfall increase for every 100 m elevation increase and the second trend observed was a 125 mm rainfall increase for every 100 m elevation increase. These two relations can be explained by stations likely affected by convective rainfall only (rectangles) and those very much affected by a combination of orographic and convective precipitation (in circles) in Figure 2-3b.

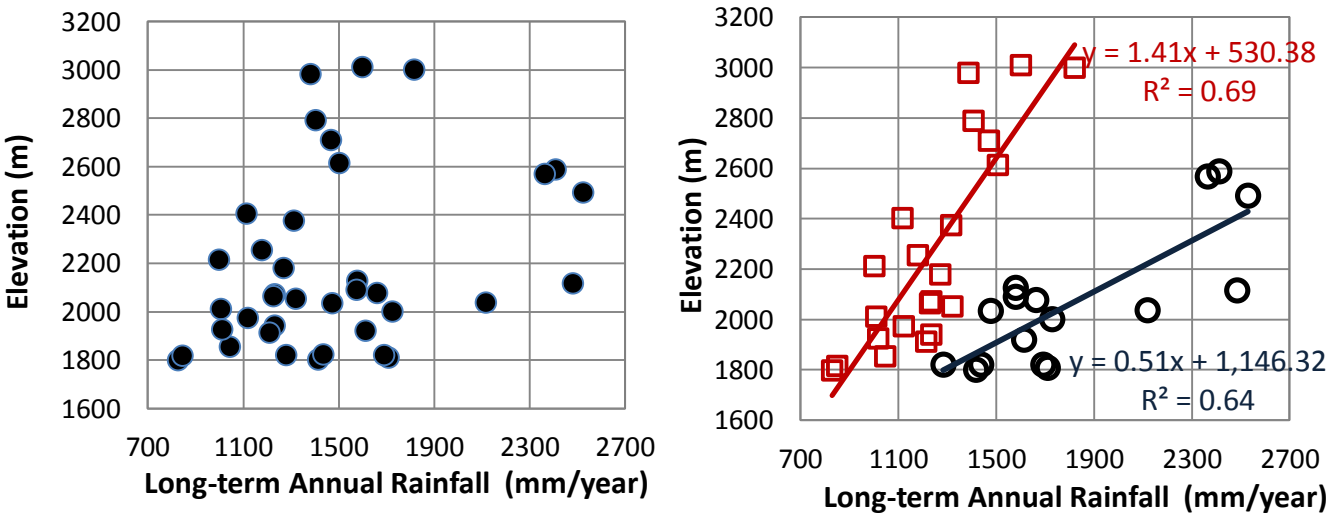

(a.) (b.)

Figure 2-3: (a.) Elevation vs. long-term annual average rainfall relations in the Lake Tana basin (38 stations from 1984 to 2008) and (b.) two clear relationships: the first one shows a 50 mm

rainfall increase for every 100 m elevation increase, and the second trend observed was a 125 mm rainfall increase for every 100 m elevation increase.

2.3.1 Point to grid comparison

The satellite rainfall estimates are aggregated to monthly temporal intervals, and the monthly satellite rainfall estimation was extracted for the 38 station locations. The observed ground rainfall and the extracted satellite rainfall for all 38 stations are depicted for the three standard statistical techniques in Figure 2-4 a, b and c.

As shown in Figure 2-4a, the monthly MPEG and CFSR have strong correlation with the ground rainfall observations stations (GROS). For MPEG, the coefficient of determination ranges from a maximum of 0.99 (Enfranz station) to a minimum value of 0.58 (Aykel station). On average, 78% of the total observed rainfall variation is explained by the MPEG satellite rainfall estimate. The CFSR has a coefficient of determination ranging from 0.63 to 0.99 for Shembekit and Gassay respectively; on average, 86% of the total observed rainfall variation is explained by CFSR rainfall data for the 38 stations. The correlation between TRMM and GROS on a monthly basis is weak, with a maximum coefficient of determination of 0.29 (Addis Zemen station) and a minimum value of 0.00. Multiple stations did not show a correlation with TRMM data. On average, only 7% of the total observed rainfall variation is explained by the TRMM satellite rainfall estimates. The root mean square error in Figure 2-4b gives very much the same trends as in Figure 2-4a. The MPEG and CFSR have a much better RMSE (ranging from 0.63 to 9.5 mm/day), while TRMM has a RMSE ranging from 3.8 to 11.8 mm/day.

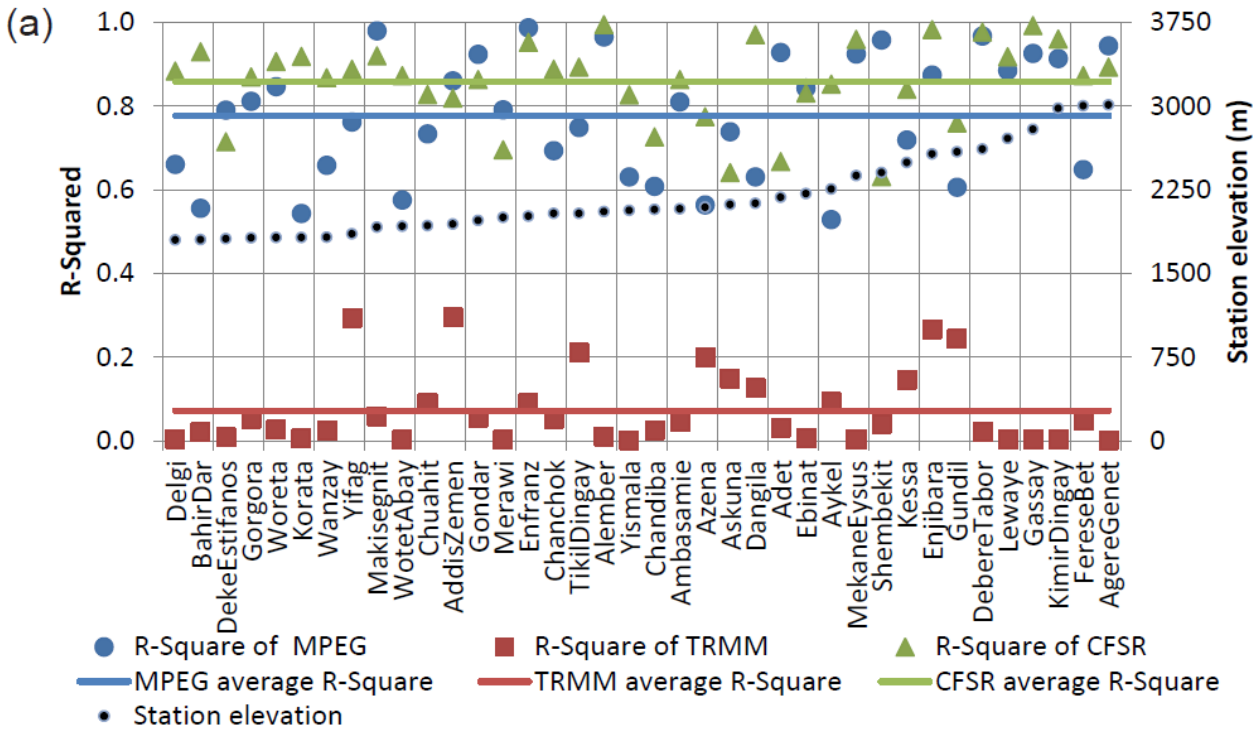
(a)
R-Squared
Station elevation (m)
1.0
0.8
0.6
0.4
0.2
0.0
3750
3000
2250
1500
750
0
Delgi
BahirDar
DekeEstifanos
Gorgora
Woreta
Korata
Wanzay
Yifag
Makisegnit
WotetAbay
Chuahit
AddisZemen
Gondar
Merawi
Enfranz
Chanchok
TikilDingay
Alember
Yismala
Chandiba
Ambasamie
Azena
Askuna
Dangila
Adet
Ebinat
Aykel
MekaneEysus
Shembekit
Kessa
Enjibara
Gundil
DebereTabor
Lewaye
Gassay
KimirDingay
FereseBet
AgereGenet
R-Square of MPEG
R-Square of TRMM
R-Square of CFSR
MPEG average R-Square
TRMM average R-Square
CFSR average R-Square
Station elevation

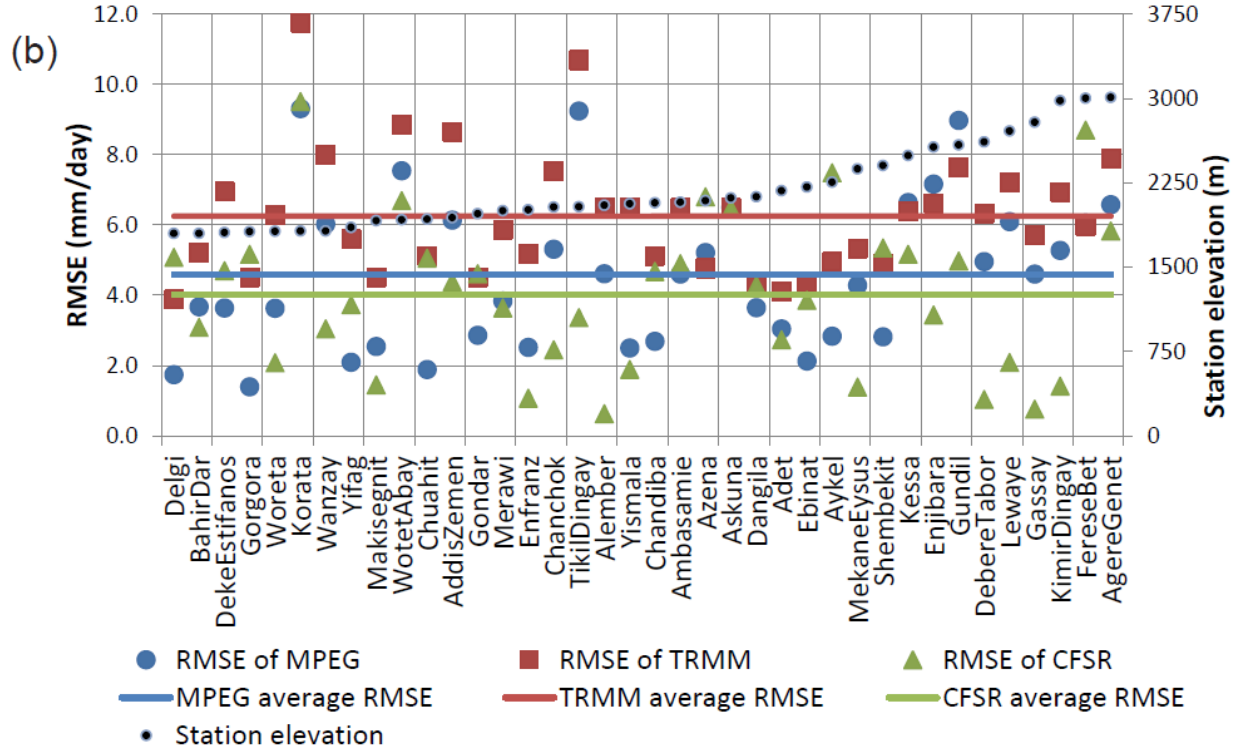
(b)
RMSE (mm/day)
Station elevation (m)
12.0
10.0
8.0
6.0
4.0
2.0
0.0
3750
3000
2250
1500
750
0
Delgi
BahirDar
DekeEstifanos
Gorgora
Woreta
Korata
Wanzay
Yifag
Makisegnit
WotetAbay
Chuahit
AddisZemen
Gondar
Merawi
Enfranz
Chanchok
TikilDingay
Alember
Yismala
Chandiba
Ambasamie
Azena
Askuna
Dangila
Adet
Ebinat
Aykel
MekaneEysus
Shembekit
Kessa
Enjibara
Gundil
DebereTabor
Lewaye
Gassay
KimirDingay
FereseBet
AgereGenet
RMSE of MPEG
RMSE of TRMM
RMSE of CFSR
MPEG average RMSE
TRMM average RMSE
CFSR average RMSE
Station elevation

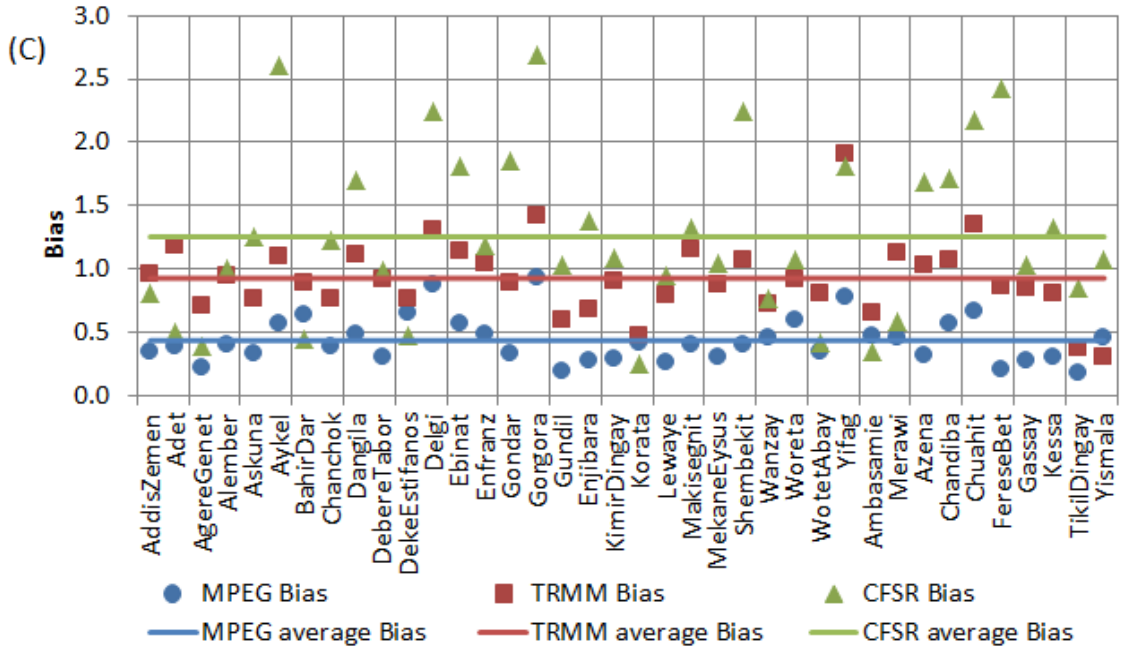

Figure 2-4: (a) R2 of MPEG, TRMM and CFSR compared with 38 ground rainfall observation stations (GROS) in the Lake Tana basin, sorted according to increasing station elevation. (b) RMSE of MPEG, TRMM and CFSR compared with the 38 ground rainfall observation stations in the Lake Tana basin, sorted according to increasing station elevation. (c) Bias of MPEG, TRMM and CFSR compared with 38 ground rainfall observation stations in the Lake Tana basin.

Thus, MPEG and CFSR rainfall estimates are clearly better related to gauged rainfall than TRMM. This is in agreement with the findings of Dinku et al. (2008), where, on average, TRMM-3B42 captures only 15% of the rainfall variability for the whole of Ethiopia.

Finally, if we look at the rainfall distribution throughout the year, we found that the rainfall estimates of MPEG and CFSR agree with the ground-based observation of 84 to 86 % of the annual rainfall that occurs in the rainy monsoon phase from June to September, as exemplified in Figure 2-5 for Gorgara and Agre Genet stations. In contrast, TRMM finds that only 30 % of

rainfall is during the rainy season. Figure 2-6 shows the spatial distribution of total rainfall for the year 2010 from MPEG, CFSR and TRMM.

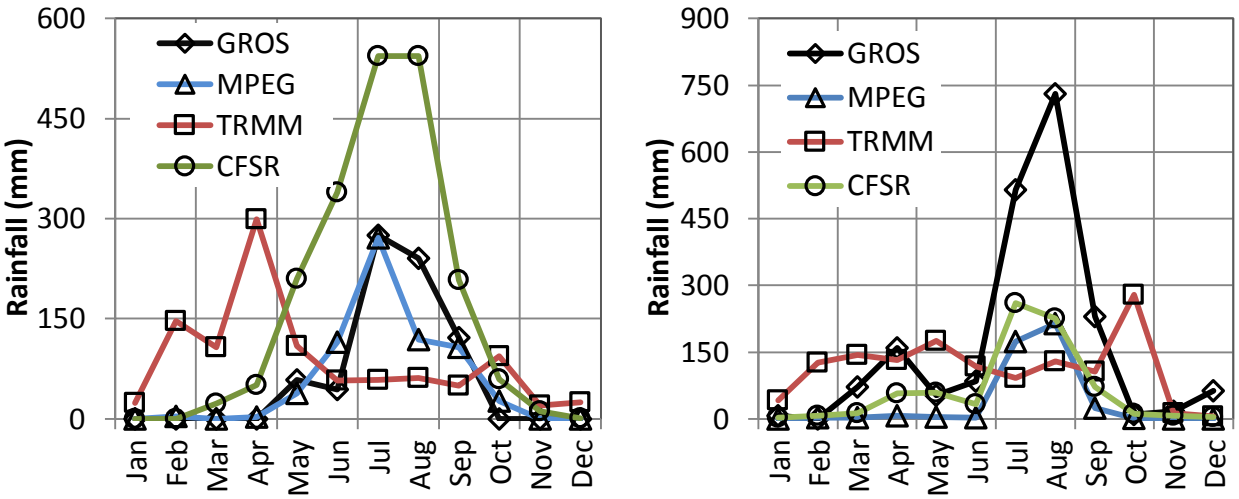

(A) Gorgara station

(B) Agre Genet station

Figure 2-5: Temporal distribution of gauged rainfall and satellite rainfall estimation from Tropical Rainfall Measuring Mission's (TRMM), Multi-Sensor Precipitation Estimate-Geostationary (MPEG) and Climate Forecast System Reanalysis (CFSR) for Gorgara and Agre Genet stations (year 2010).

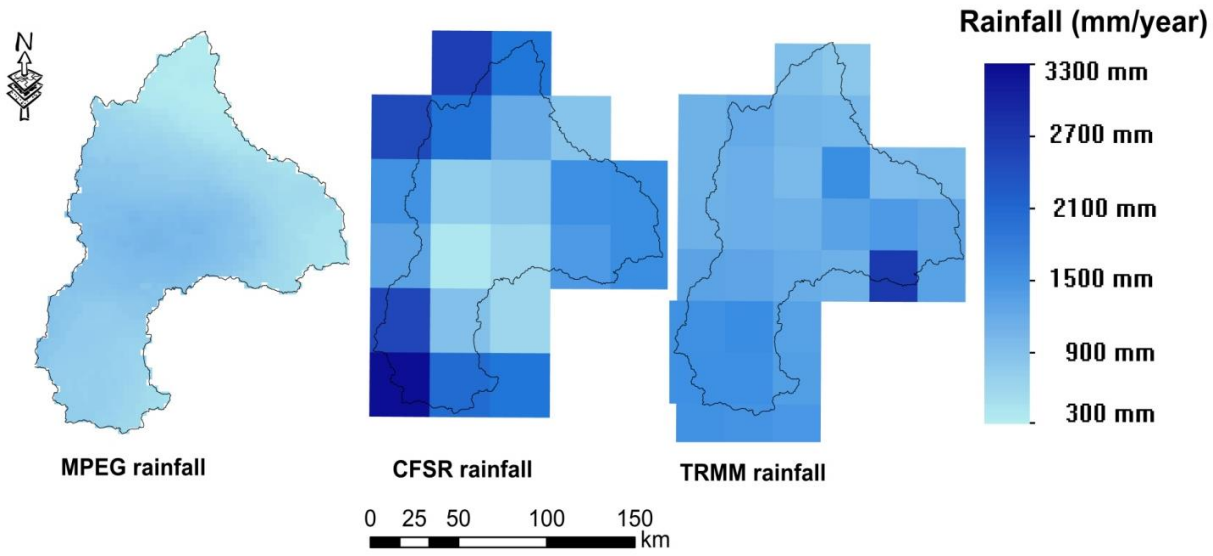

Figure 2-6: Spatial distribution of annual rainfall estimate for year 2010 from MPEG, CFSR and TRMM data.

The bias calculated (Figure 2-4c) for MPEG, TRMM and CFSR ranges from 0.2 to 0.9, 0.5 to 1.9 and 0.24 to 2.69, with an average values of 0.43, 1.0 and 1.3, respectively. The MPEG is consistent in under-predicting the observed rainfall; on average, it underestimates by 57 %. The TRMM overestimates for 15 stations, and it underestimates for the remainder. The CFSR also overestimates for 24 stations and it has the largest standard deviation of bias indicating the spread of the bias between stations.

Stations likely affected by convective rainfall (22 stations, marked in rectangles in Figure 2-3b) have a better correlation coefficient and a smaller RMSE than the stations likely affected by a combination of orographic and convective precipitation (16 station, marked in circle in Figure 2-3b). The bias also indicated that stations likely affected by both convective and orographic rainfall will have a higher bias than the likely stations affected by convective rain only. This is quite reasonable, because orographic lifting of the moist air will lead to precipitation, while the

cloud-top temperature is still relatively warm. Satellite rainfall products may not detect the rainfall from the warm clouds, as the cloud-top temperature would be too warm for TIR thresholds (Dinku et al., 2008), and there will not be much ice aloft to be determined by PM sensors, but, both sensors can detect the rainfall from the deep convection (Tsidu, 2012).

2.3.2 Areal comparison

Stations likely affected by convective rainfall are interpolated using the Thiessen polygon method, and their weights on areal rainfall for the major watersheds are determined. Gilgel Abay watershed has two stations likely affected by convective rainfall; Megech has three, Gumara six and Ribb seven stations. The areal observed rainfall is compared with the areal satellite rainfall estimation for the major gauged river basins in the Lake Tana. Figure 2-7 shows the correlation and RMSE of areal ground rainfall observation station (GROS) vs. MPEG, areal GROS vs. TRMM and areal GROS vs. CFSR for the major river basins of Lake Tana. Figure 2-8 shows the bias of satellite rainfall estimation compared with the ground observation stations.

The areal MPEG and CFSR satellite rainfall estimations have a very high coefficient of determination above 0.8; on average, both MPEG and CFSR captured 93 percent of the areal observed rainfall variability in the major river sub-basins of Lake Tana (Figure 2-7). Overall, the areal satellite rainfall estimates for the major river basins have a smaller RMSE and a higher R^2 compared to the results of point-to-grid comparison. This is because the stations used for areal observed rainfall estimations are the stations likely affected by convective rainfall only, and the satellite observation data are average value over the grid area. The areal bias computed (Figure 2-8) indicated that the MPEG rainfall consistently underestimates the observed rainfall by an average of 60 percent, while the areal CFSR overestimates for Gilgel Abay and Ribb (on average

by 40%) and underestimates for Megech and Gumara (on average by 5%). The areal RMSE of MPEG is smaller than areal CFSR estimation. The areal TRMM rainfall indicated a very small R-squared and a very high RMSE. The bias for TRMM rainfall estimation is not constant; it overestimates for Gilgel Abay and Gumara by 40 and 10 %, respectively and underestimates for Ribb and Megech watersheds by 10%. Thus, the consistence bias with an excellent correlation for MPEG rainfall estimate means there is a possibility to use scaling factors for the rainfall bias correction.

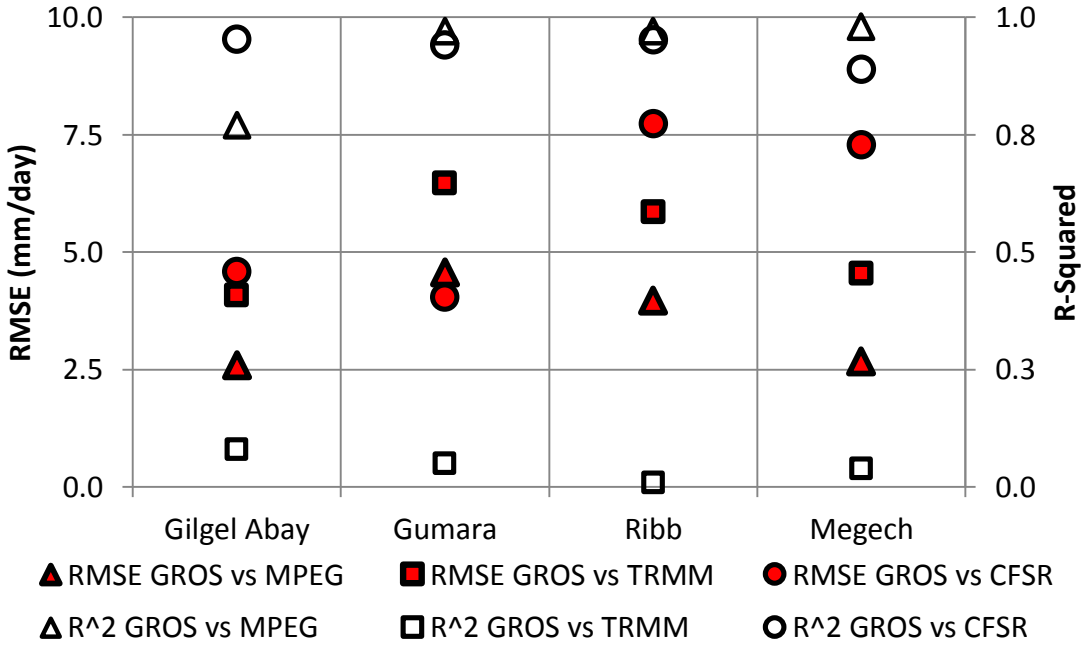

Figure 2-7: R-Squared and RMSE of areal ground observed rainfall vs. the satellite rainfall estimate for the major river basins in Lake Tana.

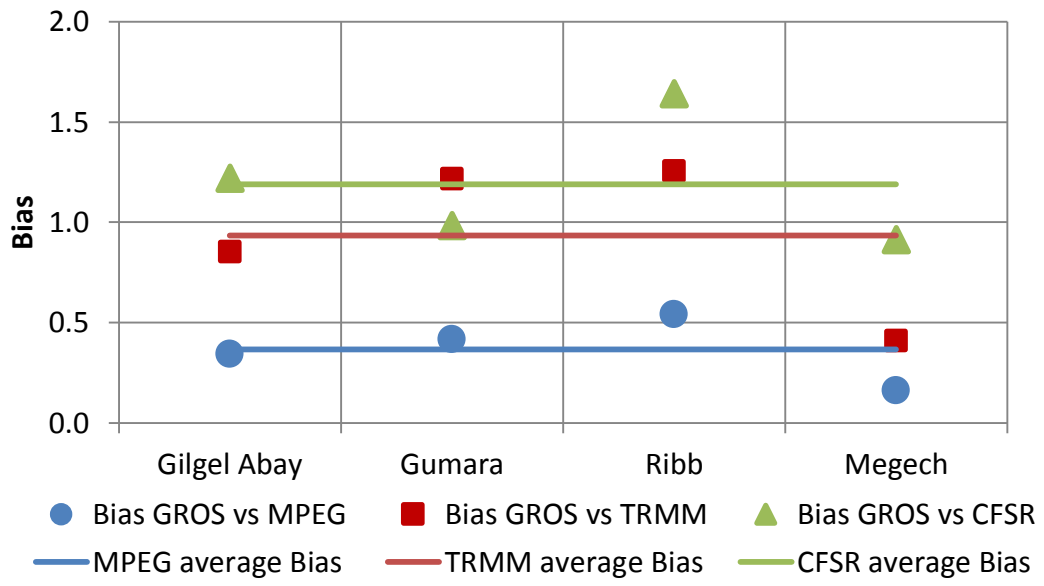

Figure 2-8: Bias of areal ground observed rainfall versus satellite rainfall estimate for the major river basins in the Lake Tana.

2.4 Conclusions

This study evaluated EUMETSAT's MPEF Multi-Sensor Precipitation Estimate-Geostationary (MPEG), Tropical Rainfall Measuring Mission (TRMM) Multi-satellite precipitation analysis TRMM 3B42 data version 7 and Climate Forecast System Reanalysis (CFSR) rainfall estimation, using 38 ground rainfall observation stations in and around the Lake Tana basin for 2010. Two approaches were used in the evaluation: the precipitation of the point-gauged data was compared to satellite-predicted rainfall for the grid in which the rainfall station was located; and all satellite grid-based prediction was compared with the areal interpolated observed rainfall stations that were only influenced by convective rainfall. The performance of MPEG and CFSR satellite rainfall estimates for both point-to-grid and areal comparisons were better than for the TRMM satellite rainfall amounts. Although the MPEG satellite rainfall underestimated

consistently the ground-observed rainfall by an average of 60%, it captured the rainfall pattern well. CFSR satellite rainfall also captured the observed rainfall pattern, but it overestimated for some and underestimated for the other stations. TRMM rainfall was not consistent in estimating the ground rainfall observation for both point-to-grid and areal comparison, and did not capture the observed rainfall pattern at all.

The ground observation data indicated that 86 % of the annual rainfall occurred from June to September, and the MPEG and CFSR indicated approximately the same percentage. The TRMM indicated that only 30% of the annual rainfall to occurred during the rainy season of June to September. Although the TRMM 3B42 bias is adjusted with monthly gauged rainfall data and has performed well in many parts of the world (Javanmard et al., 2010; Ouma et al., 2012), such an adjustment was not made for the Ethiopian highlands, because observed rainfall data were not made available to the TMPA research team (Haile et al., 2013). Based on the study period for the study area, MPEG has performed better in capturing the spatial and temporal patterns of observed rainfall. The result suggested that there should be a further calibration for the TRMM 3B42 rainfall product to capture the temporal variation of rainfall, and MPEG can easily be calibrated by a correction factor to capture the observed rainfall.

References

Baveye, P. C.: Hydrology and the looming water crisis: It is time to think, and act, outside the box, Journal of Hydrology and Hydromechanics, 61, 89-96, 2013.

Camberlin, P.: Rainfall anomalies in the source region of the Nile and their connection with the Indian summer monsoon, Journal of Climate, 10, 1380-1392, 1997.

Chaubey, I., Haan, C., Grunwald, S., and Salisbury, J.: Uncertainty in the model parameters due to spatial variability of rainfall, Journal of Hydrology, 220, 48-61, 1999.

Creutin, J. D., and Borga, M.: Radar hydrology modifies the monitoring of flash-flood hazard, Hydrological processes, 17, 1453-1456, 2003.

Dinku, T., Chidzambwa, S., Ceccato, P., Connor, S., and Ropelewski, C.: Validation of high-resolution satellite rainfall products over complex terrain, International Journal of Remote Sensing, 29, 4097-4110, 2008.

Dinku, T., Connor, S. J., and Ceccato, P.: Comparison of CMORPH and TRMM-3B42 over mountainous regions of Africa and South America, in: Satellite Rainfall Applications for Surface Hydrology, Springer Netherlands, 193-204, 2010.

Dinku, T., Ceccato, P., and Connor, S. J.: Challenges of satellite rainfall estimation over mountainous and arid parts of east Africa, International Journal of Remote Sensing, 32, 5965-5979, 2011.

EUMETSAT: MSG Meteorological Products Extraction Facility Algorithm Specification Document, Darmstadt, Germany 2008

Ferraro, R. R.: Special sensor microwave imager derived global rainfall estimates for climatological applications, Journal of Geophysical Research: Atmospheres (1984–2012), 102, 16715-16735, 1997.

Haile, A. T., Rientjes, T., Gieske, A., and Gebremichael, M.: Multispectral remote sensing for rainfall detection and estimation at the source of the Blue Nile River, International Journal of Applied Earth Observation and Geoinformation, 12, S76-S82, 2010.

Haile, A. T., Habib, E., Elsaadani, M., and Rientjes, T.: Inter-comparison of satellite rainfall products for representing rainfall diurnal cycle over the Nile basin, International journal of applied earth observation and geoinformation, 21, 230-240, 2013.

Heinemann, T., Latanzio, A., and Roveda, F.: The Eumetsat multi-sensor precipitation estimate (MPE), Second International Precipitation Working group (IPWG) Meeting, 23–27 September 2002, Madrid, Spain, 2002,

Heinemann, T., and Kerényi, J.: The EUMETSAT multi sensor precipitation estimate (MPE): Concept and validation, EUMETSAT Users Conf., Weimar, Germany, 2003,

Huffman, G. J., Bolvin, D. T., Nelkin, E. J., Wolff, D. B., Adler, R. F., Gu, G., Hong, Y., Bowman, K. P., and Stocker, E. F.: The TRMM multisatellite precipitation analysis (TMPA): Quasi-global, multiyear, combined-sensor precipitation estimates at fine scales. , Journal of Hydrometeorology, 8, 38-55, 2007.

Javanmard, S., Yatagai, A., Nodzu, M., BodaghJamali, J., and Kawamoto, H.: Comparing high-resolution gridded precipitation data with satellite rainfall estimates of TRMM_3B42 over Iran, Advances in Geosciences, 25, 119-125, 2010.

Joyce, R. J., Janowiak, J. E., Arkin, P. A., and Xie, P.: CMORPH: A method that produces global precipitation estimates from passive microwave and infrared data at high spatial and temporal resolution, Journal of Hydrometeorology, 5, 487-503, 2004.

Kaba, E., Philpot, W., and Steenhuis, T.: Evaluating suitability of MODIS-Terra images for reproducing historic sediment concentrations in water bodies: Lake Tana, Ethiopia, International Journal of Applied Earth Observation and Geoinformation, 26, 286-297, 2014.

Kebede, S., Travi, Y., Alemayehu, T., and Marc, V.: Water balance of Lake Tana and its sensitivity to fluctuations in rainfall, Blue Nile basin, Ethiopia, Journal of hydrology, 316, 233-247, 2006.

Kidd, C.: Satellite rainfall climatology: a review, International Journal of Climatology, 21, 1041-1066, 2001.

Kidd, C., Kniveton, D. R., Todd, M. C., and Bellerby, T. J.: Satellite rainfall estimation using combined passive microwave and infrared algorithms, Journal of Hydrometeorology, 4, 1088-1104, 2003.

NASDA: TRMM Data Users Handbook, National Space Development Agency of Japan, Japan, 2001.

Negri, A. J., Adler, R. F., and Wetzel, P. J.: Rain estimation from satellites: An examination of the Griffith-Woodley technique, Journal of climate and applied meteorology, 23, 102-116, 1984.

NMSA: Climatic and Agroclimatic Resources of Ethiopia. , National Meteorology Service Agency of Ethiopia, Addis Ababa, Ethiopia, 137 pp., 1996.

Ouma, Y. O., Owiti, T., Kipkorir, E., Kibiiy, J., and Tateishi, R.: Multitemporal comparative analysis of TRMM-3B42 satellite-estimated rainfall with surface gauge data at basin scales: daily, decadal and monthly evaluations, International Journal of Remote Sensing, 33, 7662-7684, 2012.

Pardo-Igúzquiza, E.: Optimal selection of number and location of rainfall gauges for areal rainfall estimation using geostatistics and simulated annealing, Journal of Hydrology, 210, 206-220, 1998.

Ramakrishna, S., and Nasreen, S. A. A. N.: An overview on water resources: pollution and nanomaterials, 2013.

Saha, S., Moorthi, S., Wu, X., Wang, J., Nadiga, S., Tripp, P., Behringer, D., Hou, Y.-T., Chuang, H.-y., and Iredell, M.: The NCEP climate forecast system version 2, Journal of Climate, 27, 2185-2208, 2014.

Seleshi, Y., and Demaree, G.: Rainfall variability in the Ethiopian and Eritrean highlands and its links with the Southern Oscillation Index, Journal of Biogeography, 945-952, 1995.

Seleshi, Y., and Zanke, U.: Recent changes in rainfall and rainy days in Ethiopia, International Journal of Climatology, 24, 973-983, 2004.

Simpson, J., Adler, R. F., and North, G. R.: A proposed tropical rainfall measuring mission (TRMM) satellite, Bulletin of the American Meteorological Society, 69, 278-295, 1988.

Todd, M. C., Kidd, C., Kniveton, D., and Bellerby, T. J.: A combined satellite infrared and passive microwave technique for estimation of small-scale rainfall, Journal of Atmospheric and Oceanic Technology, 18, 742-755, 2001.

Tsidu, G. M.: High-Resolution Monthly Rainfall Database for Ethiopia: Homogenization, Reconstruction, and Gridding, Journal of Climate, 25, 8422-8443, 2012.

Turk, F. J., Rohaly, G. D., Hawkins, J., Smith, E. A., Marzano, F. S., Mugnai, A., and Levizzani, V.: Meteorological applications of precipitation estimation from combined SSM/I, TRMM and infrared geostationary satellite data, Microwave Radiometry and Remote Sensing of the Earth's Surface and Atmosphere, VSP BV, the Netherlands, 353-363, 1999.

Wale, A.: Hydrological balance of Lake Tana, M.Sc Thesis, International Institute for Geo-Information Science and Earth Observation (ITC), the Netherlands, 2008.

Wale, A., Kaba, E., Mengeste, A., Workaferahu, A., Mulken, M., and Aemro, B.: Opportunities of the Low-Cost Satellite Image Reception Station Established at GIS & RS Center of Bahir Dar University, Institute of Technology, 2nd Symposium on biodiversity and Natural Conservation at Arba Minch University, Ethiopia (June 03-05, 2010), June 03-05, 2010, 2011.

Wang, W., Xie, P., Yoo, S.-H., Xue, Y., Kumar, A., and Wu, X.: An assessment of the surface climate in the NCEP climate forecast system reanalysis, Climate dynamics, 37, 1601-1620, 2011.

WMO: World Meteorological Organization, Guide to Hydrological Practices: : Data Acquisition and Processing, Analysis, Forecasting and other Applications. WMO-No. 168., WMO, Geneva, 770, 1994.

Xu, L., and Zhang, W.-J.: Comparison of different methods for variable selection, Analytica Chimica Acta, 446, 475-481, 2001.

CHAPTER 3: COMPARING TRMM 3B42, CFSR AND GROUND-BASED RAINFALL ESTIMATES AS INPUT FOR HYDROLOGICAL MODELS, IN DATA SCARCE REGIONS: THE UPPER BLUE NILE BASIN, ETHIOPIA[3]

Abstract

Accurate prediction of hydrological models requires accurate spatial and temporal distribution of rainfall observation network. In developing countries rainfall observation station network are sparse and unevenly distributed. Satellite-based products have the potential to overcome these shortcomings. The objective of this study is to compare the advantages and the limitation of commonly used high-resolution satellite rainfall products as input to hydrological models as compared to sparsely populated network of rain gauges. For this comparison we used two semi-distributed hydrological models Hydrologiska Byråns Vattenbalansavdelning (HBV) and Parameter Efficient Distributed (PED) that performed well in Ethiopian highlands in two watersheds: the Gilgel Abay with relatively dense network and Main Beles with relatively scarce rain gauge stations. Both are located in the Upper Blue Nile Basin. The two models are calibrated with the observed discharge from 1994 to 2003 and validated from 2004 to 2006. Satellite rainfall estimates used includes Climate Forecast System Reanalysis (CFSR), Tropical Rainfall Measuring Mission (TRMM) 3B42 version 7 and ground rainfall measurements. The rainfall estimates are also validated for their prediction capacity using the calibrated and

[3] Worqlul, A., Collick, A., Tilahun, S., Langan, S., Rientjes, T., and Steenhuis, T.: Comparing TRMM 3B42, CFSR and ground-based rainfall estimates as input for hydrological models, in data scarce regions: the Upper Blue Nile Basin, Ethiopia, Hydrology and Earth System Sciences Discussions, 12, 2081-2112, 2015a.

validated model parameter sets of gauged rainfall. The results indicated that both the gauged and the CFSR precipitation estimates were able to reproduce the stream flow well for both models and both watershed, although care should be taken to further use the model parameters of CFSR data. TRMM 3B42 was not be able to capture the gauged rainfall temporal variation. CFSR data performed will when validated with gauged rainfall calibrated model parameter in Gilgel Abay and had a poor performance over Main Beles. As expected the HBV model performed slightly better than the PED model, because HBV divides the watershed into sub-basins resulting in a greater number of calibration parameters. The simulated discharge for the Gilgel Abay was better than for the less well endowed (rain gauge wise) Main Beles.

3.1 Introduction

Sound predictions of hydrological models need accurate spatial and temporal distribution of precipitation (Sharma et al., 2012). However, in developing countries ground rainfall observation stations are often unevenly and sparsely distributed and unlikely to improve soon (Worqlul et al., 2014). According to the World Meteorological Organization (WMO, 1994) the minimum rainfall station network density for tropical regions are 600 to 900 km^2 per station for flat areas and 100 to 250 km^2 per station for mountainous regions. But, in developing countries such a dense network is not available (Taye and Willems, 2012;Conway, 2000). Recently, the availability of satellite rainfall estimation where there is limited or no conventional ground rainfall observation stations has attracted the interest of hydrologists (Collischonn et al., 2008;Yilmaz et al., 2005;Hong et al., 2007). Satellite rainfall estimates have the advantage of high temporal resolution and spatial coverage, even over mountainous regions and sparsely populated areas.

Rainfall products, the Climate Forecast System Reanalysis (CFSR) and Tropical Rainfall Measuring Mission (TRMM) 3B42 version 7 (hereafter, simply "TRMM"), besides being widely used and freely available in Africa, have a relatively high spatial resolution, global coverage and high temporal resolution. The product TRMM 3B42 has been available since 1998 in a spatial resolution of 0.25^{o} by 0.25^{o} grid (≈27 km at the equator) at a 3-hourly temporal resolution in a global belt extending from 50^{o} N to 50^{o} S. The performance of TRMM 3B42 version 6 has been evaluated over Iran by Javanmard et al. (2010), over Nzoia River Bain in Kenya by Ouma et al. (2012), over USA by Tian et al. (2007) and over Ethiopia by (Dinku et al., 2007) among others, and the result indicated the importance of TRMM rainfall estimate in rainfall data scares regions. The improved version 7 of TRMM 3B42RT which is near-real time and the research version 3B42 adjusted for monthly rain gauged data (Moazami et al., 2014;Xue et al., 2013;Chen et al., 2013) has also performed well in capturing the gauged rainfall amounts and pattern. According to Romilly and Gebremichael (2011) the near-real time version 3B42RT has performed well in capturing the five year averaged gauged rainfall in Ethiopia compared to Precipitation Estimation from Remotely Sensed Information Using Neural Networks (PERSIANN) and Climate Prediction Center morphing method (CMORPH) rainfall estimates. Chen et al. (2013) after comparing the real-time and research products with gauged rainfall data in the Mainland China indicated that, the research version 3B42 has much better performance than the real-time product 3B42RT. The CFSR global atmosphere data has a spatial resolution of approximately 38 km and the data is available since 1979 (Saha et al., 2010). Detail information on TRMM and CFSR data can be found in (Worqlul et al., 2014;Wang et al., 2011;Saha et al., 2010;Huffman et al., 2007).

The validation of satellite rainfall products can be achieved by direct comparison with the ground observation station network (Dinku et al., 2008; Bitew et al., 2012; Worqlul et al., 2014) or by

their ability to predict stream flow using hydrological models (Bitew et al., 2012;Fuka et al., 2013). A variety of hydrology models applied in the Ethiopian highlands, such as the Agricultural Non-Point Source Pollution (AGNPS) (Haregeweyn and Yohannes, 2003; Mohammed et al., 2004), Water Erosion Prediction Project (WEPP) (Zeleke, 2000) and the Soil and Water Assessment Tool (SWAT) (Setegn et al., 2008, 2009, 2010; Betrie et al., 2011), had limitations in capturing the daily runoff dynamics because the underlying runoff mechanism in these models is based on infiltration excess although experimentally it has been shown that saturation excess is the dominant mechanism of generating overland flow (Bayabil et al., 2010;Tilahun et al., 2013a;Tilahun et al., 2013b). Water balance models, in particular the Parameter Efficient Distributed (PED) (Steenhuis et al., 2009) and the Hydrologiska Byråns Vattenbalansavdelning (HBV) (Lindström et al., 1997), which include saturation excess processing and are not input data intensive, could represent the runoff better in monsoon climates than infiltration excess runoff models for scales ranging from 100 ha basin to the whole Blue Nile basin (Tilahun et al., 2013 a, b, c; 2014; Steenhuis et al., 2015; Abdo et al., 2009; Wale et al., 2009).

Therefore, using the PED and HBV models to simulate stream flow, we assessed the suitability (performance) and the limitations of state-of-the-art high-resolution satellite rainfall products readily available in Africa in two watersheds, Gilgel Abay and Main Beles, located in the upper Blue Nile Basin, Ethiopia. Gilgel Abay basin has high quality discharge data and a relatively well distributed network of ground rainfall observation station, and Main Beles basin also has good quality discharge data, but a less well-endowed network of ground rainfall stations with a long period daily record data.

3.2 Methodology

3.2.1 Study Area Description

The study watersheds, Gilgel Abay and Main Beles, are located in the Blue Nile Basin, in the western part of the Ethiopian highland. The Gilgel Abay watershed is located in the Tana basin, between 10°56’ to 11°58’N latitude and 36°44’ to 37°34’E longitudes. Gilgel Abay River is the source of Lake Tana; it originates from a small spring located near Gish Abay Mountain at elevation of 3000 m amsl. The Main Beles watershed is located in the Beles basin, geographically it extends from 10º56’ to 12º N latitude and 35º12’ to 37º E longitude. The watershed areas of the Gilgel Abay and Main Beles at their gauging sites are approximately 1,650 km^2 and 3,212 km^2, respectively, extracted from the 90 m resolution Shuttle Radar Topographic Mission (SRTM) Digital Elevation Model (DEM). In Figure 3-1, the location of meteorological stations and drainage pattern of the Gilgel Abay and Main Beles sub-basins are depicted.

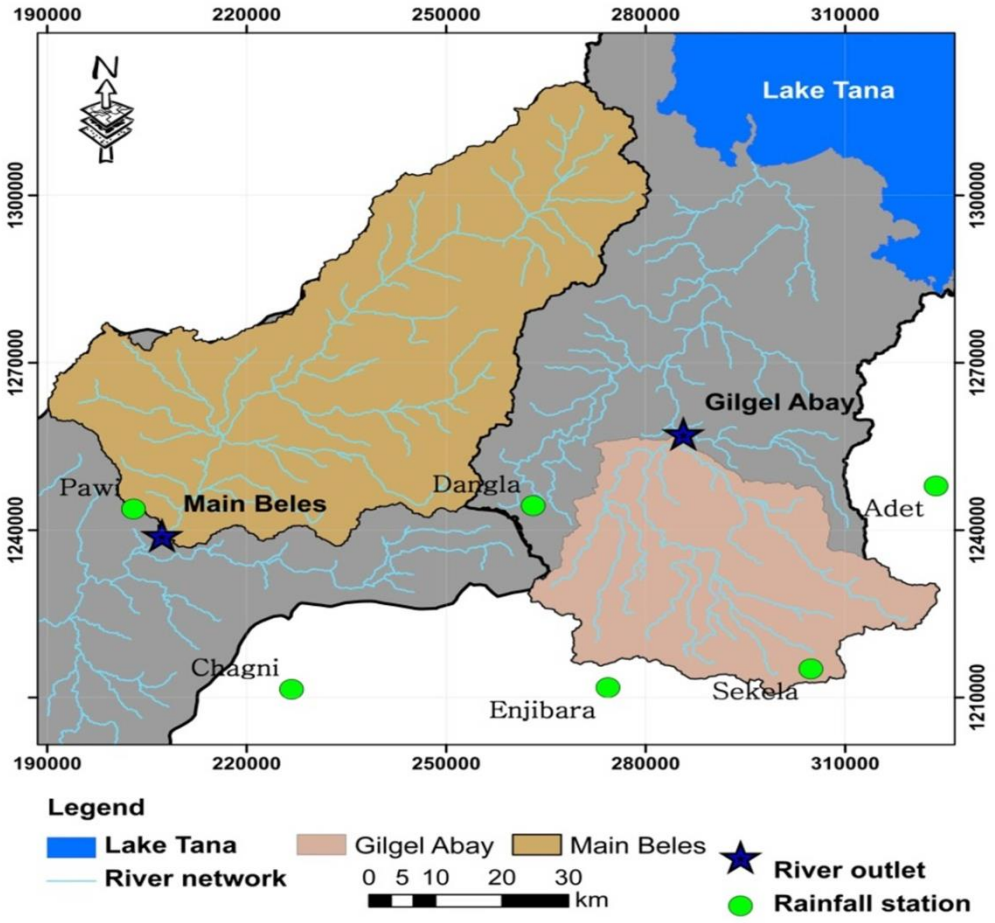

Figure 3-1: Drainage Pattern and meteorological station network of the Gilgel Abay and Main Beles basins.

Gilgel Abay and Main Beles basins have a complex topography with a significant elevation variation ranging from 1890 to 3530 and 990 to 2725 m, respectively. The slope of the watersheds varies from zero to 140%, with an average slope of 12% for Gilgel Abay and 14% for Main Beles basins. Approximately 50 percent of the watersheds have a slope less than 8%. Gilgel Abay and Main Beles basins have an average annual rainfall of 1860 and 1550 mm, respectively. The main rainfall season is from June to September and accounts for 70 to 90% of the annual rainfall (Kebede et al., 2006;Tarekegn and Tadege, 2006).

3.2.2 Climatological and Discharge Data

Daily precipitation is collected from Ethiopian Meteorological Agency (EMA) for multiple stations. Daily data from 1994 to 2006 is obtained from Dangila, Adet, Sekela and Enjibara stations and the data collected from Chagni and Pawi was from 1998 to 2006. In addition, the only data needed to estimate potential evaporation such as maximum and minimum temperature, daily sunshine hour; maximum and minimum humidity and wind speed was available at the Dangila station. Daily discharge data for Gilgel Abay and Main Beles at the outlet stations from 1994 to 2006 was obtained from Ethiopian Ministry of Water, Irrigation and Energy. The daily gridded satellite rainfall estimation data TRMM product (3B42) Version 7 was downloaded from the ftp server at ftp://disc2.nascom.nasa.gov/data/s4pa/TRMM_L3/TRMM_3B42 daily/ and CFSR at http://rda.ucar.edu/datasets/ds094.1/ .

3.2.3 Satellite data

The two satellite rainfall estimates used in this study are TRMM product 3B42 version 7 and CFSR. The TRMM-3B42 estimates are produced in four steps (Dinku et al., 2010;Huffman et al., 2007): (i) the PM estimates are adjusted and combined, (ii) TIR precipitation estimates are created using the PM estimates for calibration, (iii) PM and TIR estimates are combined, and (iv) the data is rescaled to monthly totals where by gauge observations are used indirectly to adjust the satellite product (Huffman et al., 2007). The near-real time version 3B42RT is produced at the end of the third procedure, this data does not include gauge information (Ouma et al., 2012;Huffman and Bolvin, 2013). The product TRMM 3B42 has been available since 1998 with a spatial resolution of approximately 27 km at the equator and with a temporal resolution of 3 hour. The CFSR was designed and executed as a global, high-resolution coupled atmosphere–

ocean-land surface-sea ice system to provide the best estimate of the state of these coupled domains for the study period (Saha et al., 2014). The new feature in CFSR includes: the first reanalysis system in which the guess fields are taken as the 6-h forecast from a coupled atmosphere-ocean climate system with an interactive sea ice component; and it assimilates satellite radiances and humidity values (Wang et al., 2011). The CFSR global atmosphere data has a spatial resolution of approximately 38 km and the data is available from 1979 (Saha et al., 2010).

3.2.4 Methods

The study comprises of two parts, in the first part, the satellite rainfall estimates (TRMM and CFSR) are compared with gauged rainfall data within the satellite grid box. Then a monthly comparison is done using a standard statistics (i.e., coefficient of determination and bias). The areal rainfall of the gauged data and satellite grids are estimate by using inverse distance interpolation. Next, the high-resolution satellite rainfall products (CFSR and TRMM) and gauged rainfall daily data are used as an input to two watershed models HBV-IHMS and PED for daily stream flow simulation in the Gilgel Abay and Main Beles basins. The model parameters are used to fit the observed flow through model calibration. The model calibration period ranges from 1994 to 2003 and the model is validated from 2004 to 2006 for gauged rainfall, CFSR and TRMM data. The performance of the calibrated model is evaluated by the Nash-Sutcliffe Coefficient (NSE), percent bias (PBIAS), and coefficient of determination (R2). In addition, the calibrated and validated model parameter sets of the gauged rainfall are used to evaluate the performance of CFSR and TRMM rainfall estimate in capturing the observed flow. The hydrological models HBV and PED are described below:

3.2.4.1 HBV-IHMS model:

The HBV (Hydrologiska Byråns Vattenbalansavdelning) model (Lindström et al., 1997) is a conceptual rainfall-runoff model for continuous daily simulation of catchment runoff. In HBV, the watershed is divided into sub-watersheds and further divided into elevation and land use zones. The model simulates daily runoff using daily rainfall, temperature, long-term average monthly potential evaporation, geographical information of the catchment which is sliced elevation crossed with land use and observed runoff data for calibration. The general water balance is described in Eq. (1):

$$P - E - Q = \frac{d}{dt}[SP + SM + UZ + LZ + L] \qquad \text{Eq. (1)}$$

where P is the precipitation, E is evapotranspiration, Q is runoff, SP is snow pack, SM is soil moisture, UZ is upper ground zone, LZ is lower ground zone, and L is the lake volume.

The model consists of subroutines for precipitation, soil moisture, response, transformation function and simple routing procedure. The soil moisture accounting routine is based on three parameters, Beta (β), FC and LP. β controls the contribution to the response function from each millimeter of rainfall. FC is the maximum soil moisture storage. As the soil moisture exceeds the limit for potential evaporation (LP), water will evaporate at a potential rate. The response routine is described by an upper non-linear reservoir and a linear lower response routine connected with Percolation (PERC) parameter. Khq and K4 are recession coefficient parameters for the upper and lower response parameters. The non-linearity of the upper reservoir is controlled by the parameter Alpha (α). The higher α, the higher the peaks and the quicker the recession (SHMI, 2006). A complete description of the HBV model can be found in Lindström et al. (1997), SMHI

(2006) and Wale et al. (2009) among others. Input for HBV includes: long-term monthly potential evaporation is estimated by the Penman-combination equation using Dangila meteorological station. A digital elevation model (DEM) from SRTM DEM (Jarvis et al., 2008) is used to extract the drainage area of the watersheds and to divide each watershed into three different sub-basins and elevations zones. Land use data is collected from Ethiopia Ministry of Water, Irrigation and Energy.

3.2.4.2 PED model:

The PED (Parameter Efficient Distributed) model (Steenhuis et al., 2009) is a conceptual semi-distributed rainfall-runoff model for continuous daily simulation of catchment runoff. In PED the watershed is subdivided into three sub-regions distinguished as the bottom lands that potentially saturate in the rainy monsoon phase, degraded hillslope/exposed rock with little or no soil cover and permeable hillslopes (infiltration zones). In the PED model various portions of the watershed become hydrologically active when threshold moisture content is exceeded (Steenhuis et al., 2013). The permeable hillslopes/infiltration zones contribute to the rapid subsurface flow (called interflow) characterized by flow decreasing as a linear function of time, and baseflow is characterized by an exponentially decreasing flow in time Steenhuis et al. (2013). Overland flow is generated from saturated areas in the relatively flatter areas in the landscape and areas where bed rock is exposed Steenhuis et al. (2009). For each of the three regions, the water balance calculation is based on Thornthwaite and Mather (1955) procedure. The general water balance equation for the sub-regions is described under Eq. (2):

$$S_t = S_{t-\Delta t} + (P - AET - R - Perc)\Delta t \qquad \text{Eq. (2)}$$

where St is water stored in the topmost layer, St-Δt is the previous time step storage (mm), P is precipitation (mm day-1), AET is the actual evapotranspiration, R is the saturation excess runoff (mm day-1), Perc is the percolation to the subsoil (mm day-1), and Δt is the time step (day).

The model simulates the daily runoff using daily rainfall, potential evaporation and daily runoff data for calibration. Input for PED: potential evaporation is estimated by the Penman-combination equation. Landscape parameters for the model, the relative areas of three regions are used as a model calibration parameter with their respective maximum soil moisture storage capacity. Subsurface flow is simulated using a linear reservoir with a half-life (t1/2) and interflow employing a zero order reservoir calibration parameter τ* is the duration of the period after a single rainstorm until interflow ceases. A complete description of the PED model can be found in Steenhuis et al. (2009), Tesemma et al. (2010), and Tilahun et al. (2013b).

3.2.4.3 Model Calibration and Validation

The two simulation models were calibrated manually, first by fitting the runoff volumes followed by calibrating the shape of the hydrograph from 1994 to 2003 for gauged rainfall and CFSR data. The TRMM data is calibrated from 1998 to 2003. The calibrated model is validated from 2004 to 2006 in all cases. In addition the CFSR data is validated with the calibrated and validated model parameter sets of gauged rainfall parameter in capturing the observed flow.

The model performance is evaluated by three objective functions consisting of the Nash-Sutcliffe Efficiency (NSE) (Nash and Sutcliffe (1970), percent bias (PBIAS), and coefficient of determination (R2). NSE is a normalized statistic that determines the relative magnitude of the residual variance compared to the measured observed flow variance. NSE ranges from negative infinite to 1. Generally, NSE value between 0.6 and 0.8 indicates fair to good performance and a

model is said to be very good when NSE is above 0.8 (Moriasi et al., 2007). PBIAS is the relative difference between the observed and simulated flows. PBIAS measures the tendency of the average simulated flow to be larger or smaller than the observed flow (Gupta et al., 1999). R^2 is used to evaluate the goodness of fit of the relations. R^2 examines the degree of linear association between the observed and simulated flows.

3.3 Results and Discussion

3.3.1 Comparison of areal gauged rainfall with TRMM and CFSR rainfall estimates

The satellite rainfall estimate of TRMM and CFSR data are compared with the gauged rainfall data station located inside the satellite grid box. Figure 3-2 shows the correlation coefficient and bias of gauged rainfall vs. TRMM and CFSR data. The results indicate that CFSR data capturing 89 to 92% of the gauged rainfall pattern and TRMM captured 28 to 55% of the gauged rainfall pattern. The bias calculated as a ratio of annual mean of satellite rainfall estimate to the gauged data was 0.97 and 1.16 for TRMM and CFSR data respectively.

The areal rainfall of the gauged rainfall and satellite data is estimated by the inverse distance interpolation method. Figure 3-3 indicates the satellite rainfall observation grid generated from TRMM and CFSR data for Gilgel Abay and Main Beles basins. The long-term monthly areal average ground observed rainfall; TRMM and CFSR for the Gilgel Abay and Main Beles basins are depicted in Figure 3-4. The CFSR satellite rainfall and gauged data are averaged over the period from 1994 to 2006 and TRMM over the period from 1998 to 2006 for the Gilgel Abay and Main Beles basins.

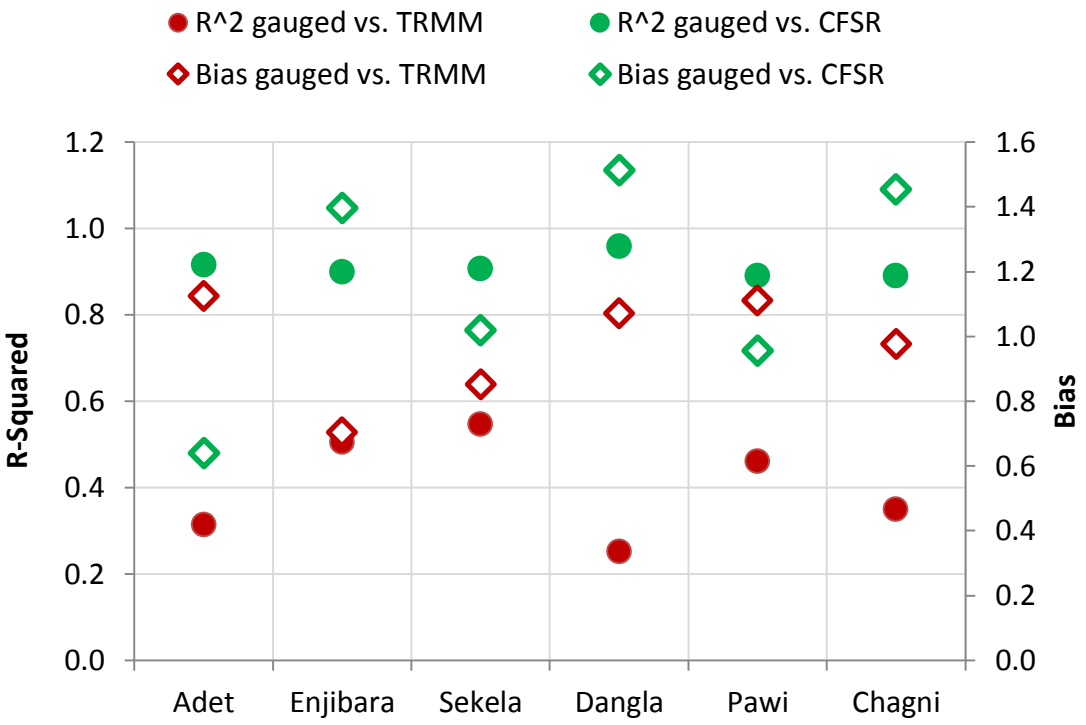

Figure 3-2: Long-term average monthly R-square and Bias of TRMM and CFSR rainfall estimate vs. ground rainfall observation stations within the satellite grid box

Table 3-1: Coefficient of Determination (R^2) areal gauged and satellite rainfall estimates for Gilgel Abay and Main Beles basins.

		Main Beles			Gilgel Abay		
Basins		TRMM	CFSR	Gauged	TRMM	CFSR	Gauged
Main Beles	TRMM	1.00					
	CFSR	0.10	1.00				
	Gauged	0.15	0.93	1.00			
Gilgel Abay	TRMM	0.87	0.26	0.37	1.00		
	CFSR	0.11	0.99	0.90	0.26	1.00	
	Gauged	0.16	0.94	0.99	0.38	0.93	1.00

Gilgel Abay and Main Beles watersheds have similar areal rainfall patterns according to both gauged and CFSR rainfall data with a goodness of fit, R^2, of 0.99 for each (Table 3-1). Areal

TRMM rainfall estimates for Gilgel Abay and Main Beles have a similar pattern indicated by R^2, of 0.87. CFSR also has captured the gauged rainfall for Gilgel Abay and Main Beles with R^2 values of 0.94 and 0.93, respectively. The fit between TRMM and gauged data is poor, 0.38 and 0.15 for Gilgel Abay and Main Beles, respectively. TRMM average annual areal rainfall volume estimates underpredict by 10% and 6% for Gilgel Abay and Main Beles, respectively, while CFSR data overpredicts by 16% and 37%, respectively. Seventy five percent of the gauged areal rainfall occurs during the rainy season from June through September compared to eighty percent for CFSR and only 39% for TRMM.

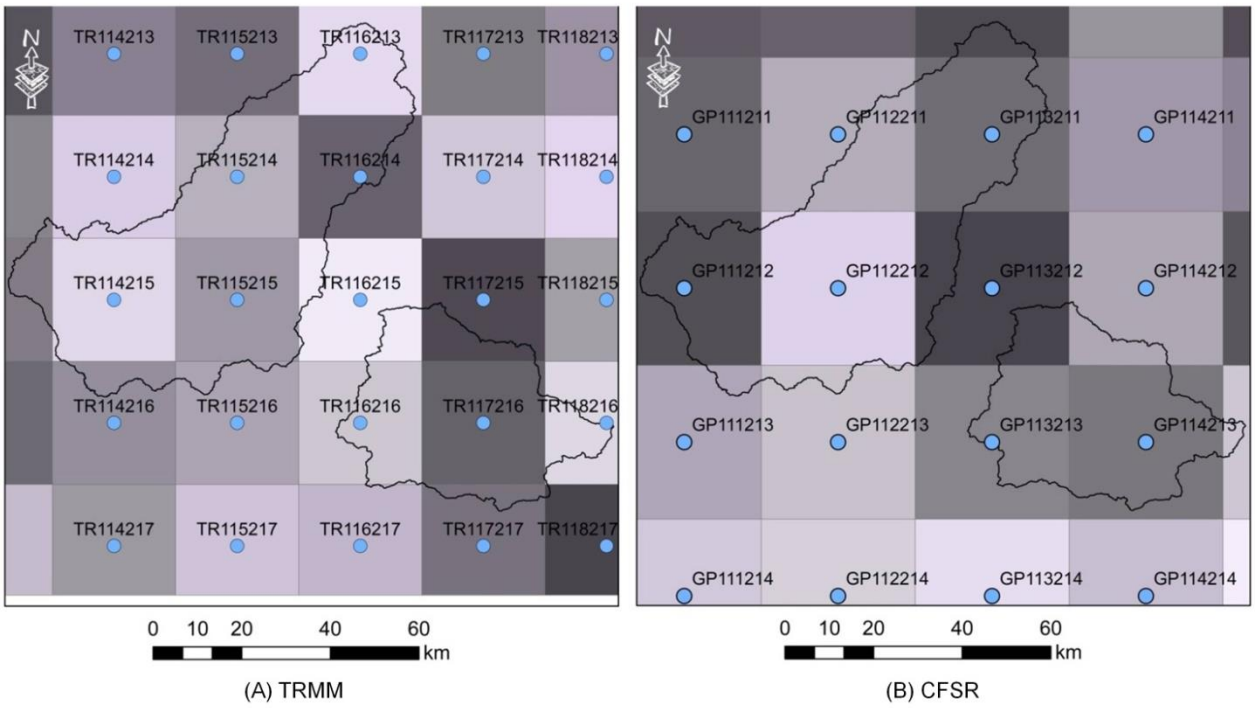

Figure 3-3: Satellite rainfall observation grid of (A) TRMM and (B) CFSR for Gilgel Abay and Main Beles basins. Grid size is approximately 27 km and 38 km for TRMM and CFSR, respectively.

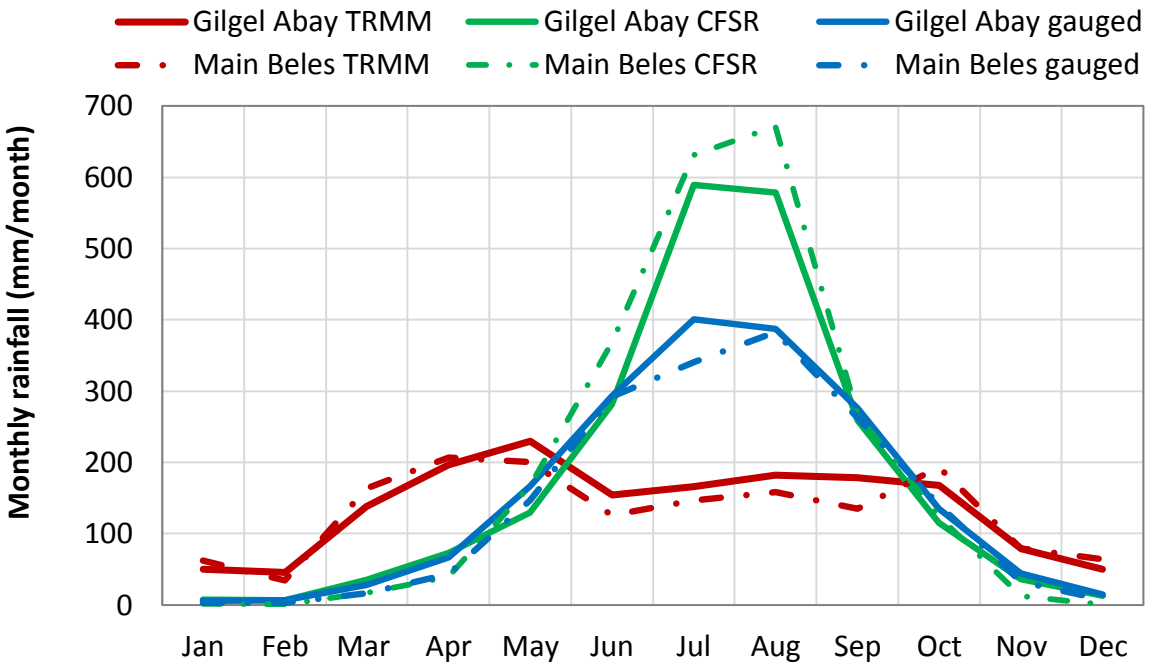

Figure 3-4: Long-term monthly average areal rainfall of gauged rainfall, CFSR data (from 1994 to 2003) and TRMM (from 1998 to 2003) for Gilgel Abay and Main Beles basins.

Thus the TRMM 3B42 satellite rainfall data does not capture the temporal variation of rainfall well for either point to grid or areal comparison. The poor seasonal rainfall predictions will cause the misrepresentation of watershed discharge, with nearly 82% and 83% of annual discharge occurring between June through September for Gilgel Abay and Main Beles, respectively. Apparently, the TRMM 3B42 bias is adjusted with monthly gauged rainfall data, and as a result, has performed well in many parts of the world (Ouma et al., 2012;Javanmard et al., 2010). But, Dinku et al. (2008) and Haile et al. (2013), in the Ethiopian highlands, have indicated a consistent result with our study. Haile et al. (2013) after personal communication with TMPA research team indicated that gauged rainfall data of the Upper Blue Nile Basin was not made available to them when the bias adjustment was conducted; therefore, further adjustment has to be done to use TRMM 3B42 rainfall products in the Blue Nile Basin. Likely, the additional adjustments will correct the seasonal distribution of rainfall in the Gilgel and Main Beles

watersheds. A study by Romilly and Gebremichael (2011) indicated that, the near-real time product 3B42RT performed better than PERSIANN rainfall estimate in capturing the gauged rainfall with an average bias ratio of 1.05 for Ethiopia. Bitew et al. (2012) also indicated that, 3B42RT rainfall estimate has a smaller bias compared to the PERSIANN and 3B42 rainfall estimates. Likely, the additional adjustment of 3B42RT with gauged data seems not working for our study site. Since TRMM 3B42 data did not capture the temporal pattern of the gauged rainfall, TRMM data is not used to capture the observed flow though model calibration.

3.3.2 Simulated runoff using PED and HBV models

3.3.2.1 Simulation of stream discharge with PED model

The calibrated PED models using gauged rainfall or CFSR rainfall could represent the observed daily stream flow reasonably well for both the calibration and validation periods for the Gilgel Abay basin (0.80 > NSE > 0.60) and the Main Beles (0.80 > NSE > 0.60), see Table 3-2 and Figure 3-5. For both basins, as demonstrated in Figure 3-6 in which the average monthly values are depicted and Table 3-2, the gauged rainfall gave slightly better results than the CFSR data (Figure 3-7 a and b). For the daily values the same trend is observed in which the regression coefficient indicated that during the validation period of the Gilgel Abay basin, the gauged rainfall could explain 76% of the observed runoff variation and CFSR data could capture 68% of the flow variation (Table 3-2).

We found that the PED model parameters of the fractional areas, the half-life of the baseflow and the duration of the interflow after a rainstorm are sensitive for the prediction of stream discharge using either of the two rainfall records similar to (Tilahun et al., 2013b). The model is insensitive to the maximum soil moisture storage for any of three regions (periodically saturated bottom

lands, degraded soils, and permeable hillside). The reason is that, for a monsoon climate during the rainy phase, the soil does not dry out once wet, only during the first rains the discharge is affected by the amount of the water that can be stored in the soils. Therefore we kept, maximum water storages remained the same for all simulation.

Table 3-2: Optimized model parameter set of PED and model performance for gauged rainfall and CFSR data for Gilgel Abay and Main Beles.

Description		Gilgel Abay		Main Beles	
		Gauged rainfall	CFSR	Gauged rainfall	CFSR
Fraction of saturated area (%)		0.07	0.06	0.02	0.02
Fraction of degraded area (%)		0.05	0.05	0.05	0.02
Fraction of hillside area (%)		0.86	0.57	0.73	0.35
$t_{1/2}$ (days)		45	45	18	20
τ^* (days)		40	40	46	66
Calibration Period (1994 to 2003)	PBIAS (%)	10	7.6	-8.0	4.9
	NSE	0.74	0.73	0.61	0.63
	R^2	0.75	0.74	0.63	0.65
Validation period (2004 to 2006)	PBIAS (%)	-9.2	-5.9	-9.0	6.2
	NSE	0.65	0.63	0.68	0.66
	R^2	0.76	0.68	0.69	0.72

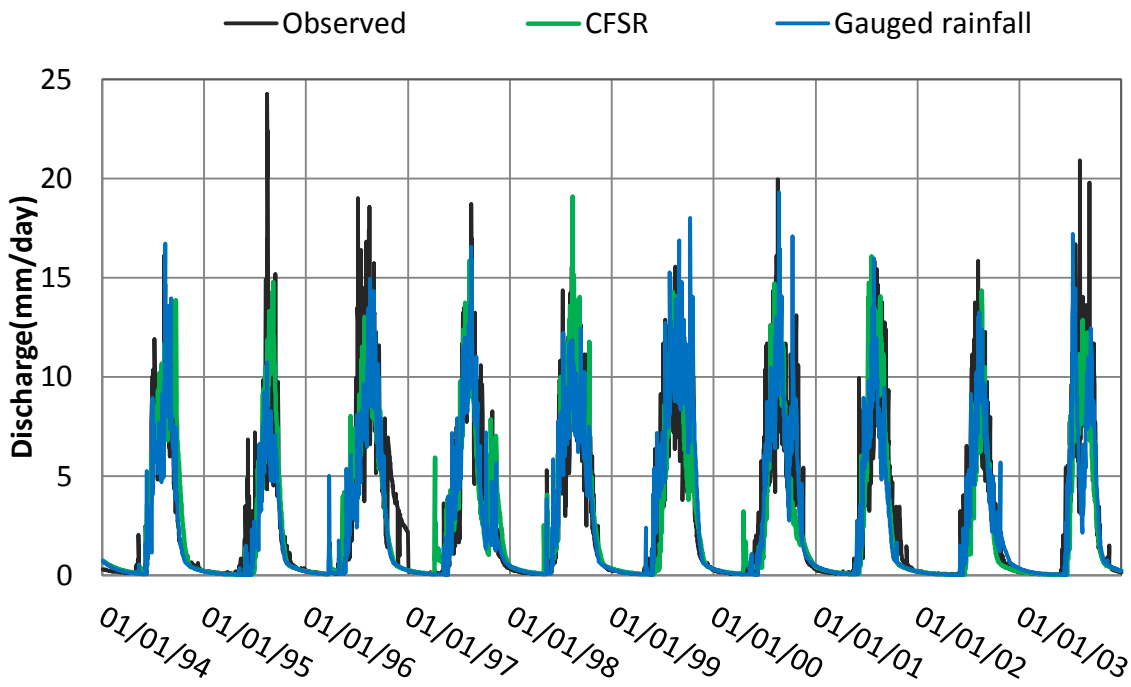

Figure 3-5: Simulated flow of PED model by gauged rainfall and CFSR data plotted with observed flow for Gilgel Abay basin.

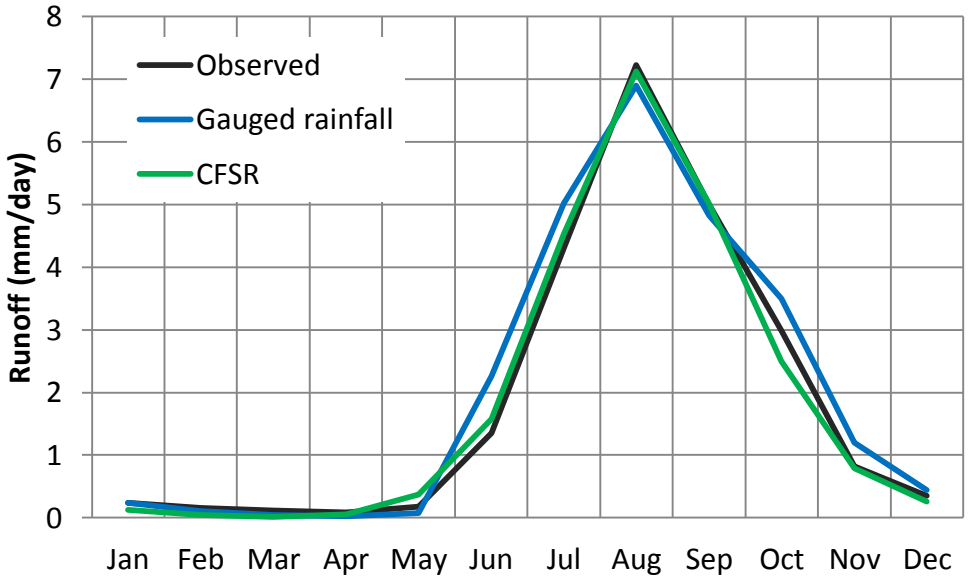

Figure 3-6: Comparison of long-term average monthly Gilgel Abay observed flow and PED simulation for gauged rainfall, CFSR (from 1994 to 2003) and TRMM rainfall estimate (from 1998 to 2003).

Table 3-2 lists the optimized PED model parameter sets for the gauged and CFSR rainfall estimate for Gilgel Abay and Main Beles basins. The calibrated model parameters for the subsurface flow represented by the half-life ($t_{1/2}$) and interflow calibration parameter τ^* for the different rainfall input data are almost the same for all simulations as expected and consistent with values used in simulation of Anjeni and Blue Nile Basins (Tilahun et al., 2013a). The fractional regions contributing to rapid subsurface and overland flow have different values for the gauged rainfall and CFSR rainfall data simulation. The total contributing area for the gauged rainfall adds up to 98% for Gilgel Abay and 80% for Main Beles. It is also consistent with earlier studies of PED simulation for a wide scale of watersheds study areas Tilahun et al. (2013b) indicated that the fractional area's for a 180,000 km^2 Blue Nile Basin adds up to 100 % while the smaller watershed of less than 5 km^2 are in the order of 60%. So, for a mid-range watershed area in a range of 1000 km^2 the fraction area up to 80 to 97% would be realistic. Using the CFSR the fractional area adds up to 68% for the Gilgel Abay and 39% for the Main Beles. A fractional area of 1 would mean that all rainwater minus evaporation over the long-term becomes discharge at the outlet. The result of CFSR simulation indicates there should be a caution when calibrating a hydrologic model directly with a rainfall estimate. Some of the caution taken should be validation and adjusting of the bias of the satellite rainfall estimate using dense in situ measurements. Otherwise, the poor prediction of satellite rainfall can be compensated by the model parameters.

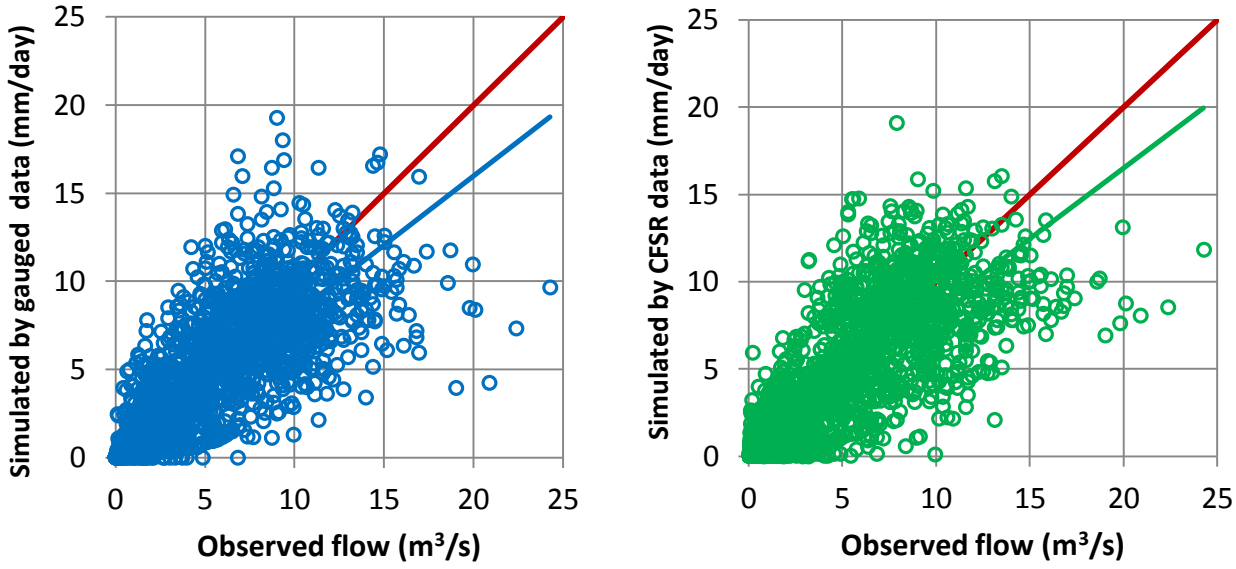

(a) Observed flow vs. flow simulated by gauged rainfall (b) Observed flow vs. flow simulated by CFSR data

Figure 3-7: Correlation between observed flow and simulated flow for the calibration period using (a) gauged rainfall and (b) CFSR data for the Gilgel Abay Basin using PED model.

3.3.2.2 Simulation of stream discharge with HBV model

The semi-distributed HBV model has seven parameters controlling the total volume and shape of the hydrograph; there level of model parameter sensitivity is documented in Wale et al. (2009). The model is calibrated manually first by volume controlling parameters (FC, LP and Beta) followed by calibrating the shape controlling parameters (Alpha, PERC, K4 and K). The optimized model parameter sets of both watersheds and simulated discharge versus observed runoff for gauged rainfall, and CFSR data of Gilgel Abay is shown in Table 3-3 and Figure 3-8 respectively.

Table 3-3: Optimized model parameter set of HBV model and its performance for gauged rainfall and CFSR data.

Description		Gilgel Abay		Main Beles	
		Gauged rainfall	CFSR	Gauged rainfall	CFSR
Alpha		0.50	0.50	0.80	0.50
Beta		1.00	1.00	1.30	1.00
FC		245	1200	650	1400
LP		0.99	0.99	0.70	0.40
PERC		1.30	0.08	0.70	0.60
K4		0.04	0.04	0.002	0.002
Khq		0.10	0.08	0.13	0.08
Calibration Period (1994 to 2003)	PBIAS (%)	3.02	6.81	-3.12	2.82
	NSE	0.78	0.72	0.63	0.62
	R^2	0.79	0.73	0.65	0.63
Validation period (2004 to 2006)	PBIAS (%)	10.0	0.19	9.2	9.6
	NSE	0.71	0.62	0.61	0.60
	R^2	0.81	0.68	0.63	0.61

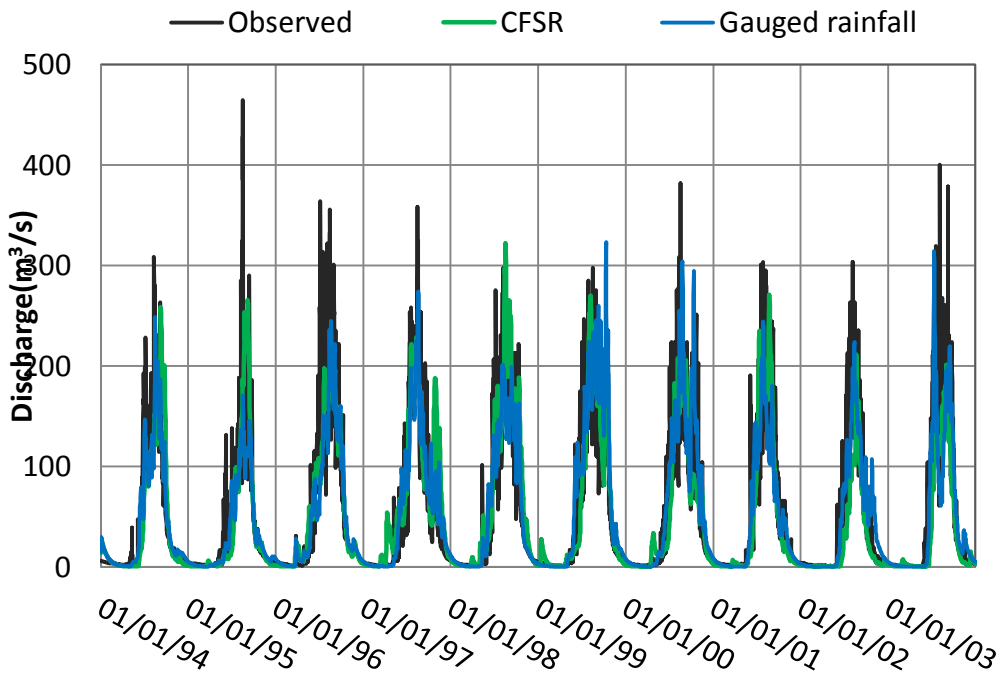

Figure 3-8: Simulated flow of HBV model by gauged rainfall and CFSR data plotted with observed flow for Gilgel Abay basin (1994-2003).

The simulated data for the calibration period using the gauged rainfall and CFSR indicated a fair to good performance with a daily NSE performance indicator equals to 0.78 and 0.72 for Gilgel Abay and 0.63 and 0.62 for Main Beles, respectively, and with a reasonable R^2 and PBIAS (Table 3-3, Figure 3-10 a and b). The simulation for both gauged rainfall and CFSR data captured well the base flow, the rising and recession limb of the hydrograph. Figure 3-10 depicts the long-term monthly average observed flow and simulated flow for gauged rainfall and CFSR rainfall estimate of Gilgel Abay and Main Beles basins.

The peak flow is better captured by the CFSR data than the gauged rainfall although both simulation by gauged and CFSR rainfall underestimate very high single peaks that are commonly caused by extreme high rainfall events. For the study period, in the Gilgel Abay watershed there are 505 days with observed flow above 200 m^3/s, the simulation by the CFSR rainfall estimate has captured 340 events and the gauged rainfall has captured 235 events. The optimized model parameters of the gauged rainfall and CFSR data have similar values except for FC and PERC in both watersheds (Table 3-3). Field capacity (FC) of the calibrated model using CFSR data is significantly higher than the FC value of model calibrated by gauged rainfall (1200 and 245 mm for Gilgel Abay and 1400 and 650 mm for Main Beles). The FC value for the CFSR model simulation indicated that the soil retained greater quantities of water and released it afterwards by evapotranspiration and base flow compared to the gauged flow simulation, and it is the models way to deal with the greater amounts of rainfall in the CFSR data compared to the gauged. The increase FC will cause an increase in baseflow, and this has a counter effect on the percolation parameter (PERC). The optimized model parameter set is tested for independent data from 2004 to 2006 and the result is acceptable for both gauged rainfall and CFSR data for the study watersheds.

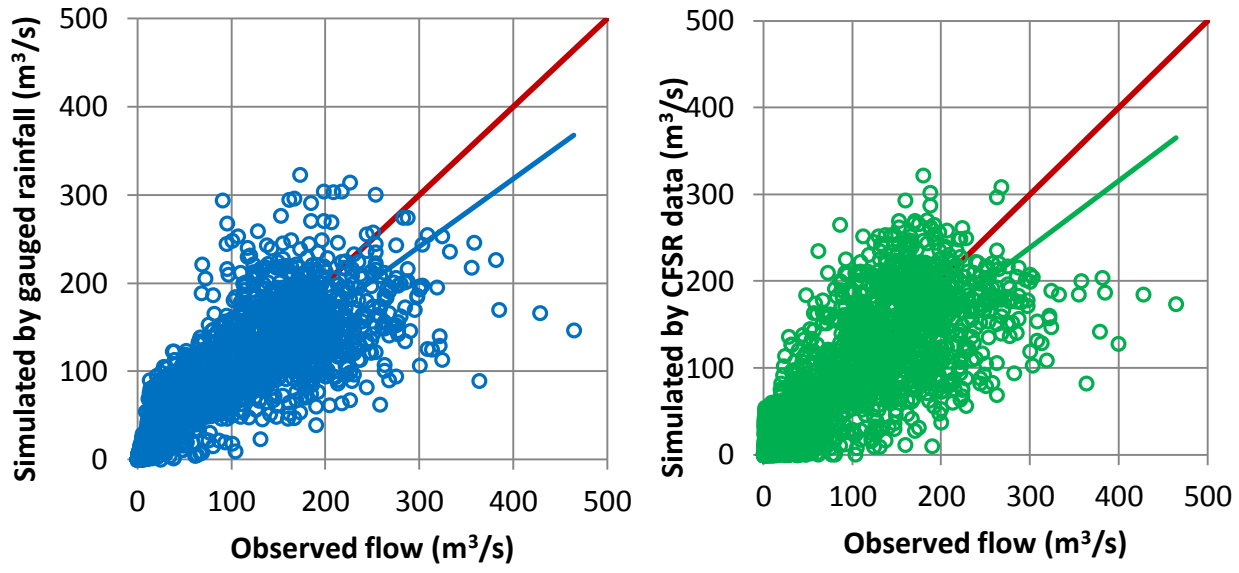

(a) Observed flow vs. flow simulated by gauged rainfall (b) Observed flow vs. flow simulated by CFSR data

Figure 3-9: Correlation between observed flow and simulated flow for the calibration period using (a) gauged rainfall and (b) CFSR data for the Gilgel Abay Basin using HBV model.

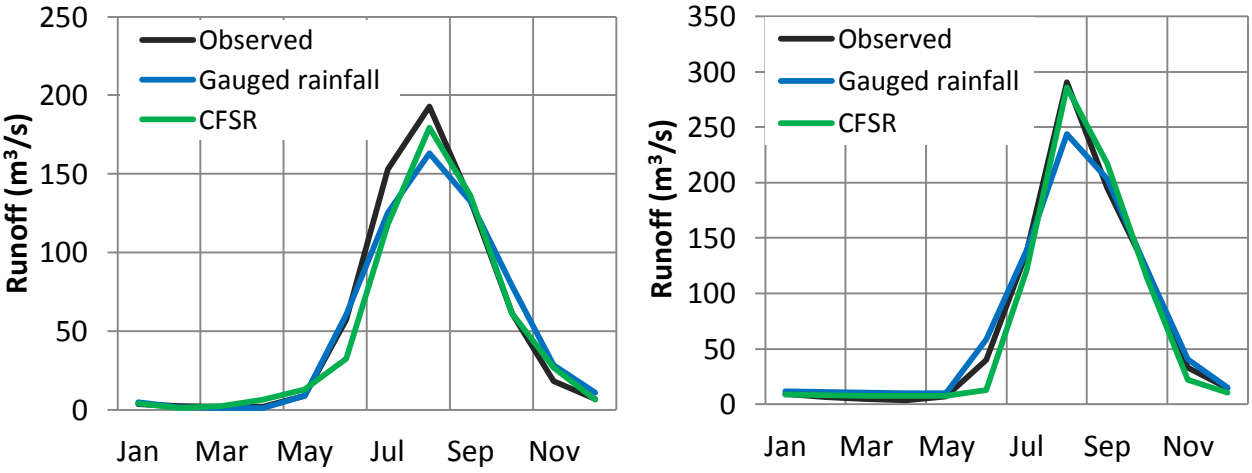

(a) Gilgel Abay (b) Main Beles

Figure 3-10: Comparison of long-term average monthly observed flow and HBV simulation for gauged rainfall, TRMM and CFSR rainfall estimate of (a) Gilgel Abay and (b) Main Beles basins.

3.3.2.3 Validation of CFSR rainfall estimate by gauged rainfall calibrated and validated parameters

The optimized model parameter sets of the gauged rainfall are used to validate the performance of CFSR rainfall estimate by predicting the observed flow of both watersheds. This is achieved by rerunning the calibrated and validated gauged rainfall model by CFSR rainfall estimate, while keeping the optimized gauged rainfall model parameters. The performance of the simulated flow has captured the observed flow pattern with R-square in between 0.6 and 0.74 for both watersheds and both models but there are a larger volume difference between the simulated and observed flow. The NSH value ranges between 0.4 and 0.5 for Gilgel Abay simulated by PED and HBV model and it ranges between 0.0 and 0.2 when Main Beles is simulated by PED and HBV. The performance of CFSR data for Gilgel Abay was better than the result of Main Beles, this is associated with the quality of gauged rainfall data in the Gilgel Abay watershed which lead to a reliable calibrated model parameter sets. Main Beles which has scarce gauged rainfall observations the calibration model parameters seems not quite representative of the watershed and leads to poor performance of CFSR data.

3.3.3 Evaluation of rainfall products using HBV and PED models

The semi-distributed hydrological models HBV and PED are considered parsimonious models since they have a limited number of model parameters, making the calibration procedure less complicated and avoiding the problem of overparamterization. Most of the time hydrologic model calibration with a large number parameters leads to over parameterization (Whittaker et al., 2010) leading to a poor prediction accuracy. Parsimonious models are preferred compared to more complex models since they often perform as well as sophisticated ones (Duan et al., 1992).

Both models have reasonably captured the observed runoff using gauged rainfall and CFSR rainfall estimate as a model input for calibration and validation period for Gilgel Abay and Main Beles. The performance of both models on Main Beles watershed using gauged rainfall and CFSR data is close compared to the case of Gilgel Abay. This is because, ground rainfall gauging stations in the Main Beles are scares compared to Gilgel Abay (Figure 3-1), and there is no rainfall observation station inside the watershed. This indicates that CFSR data can be an alternative to gauged rainfall as input to hydrological modelling when the rainfall station network is less dense. But, caution should be taken when calibrating runoff using satellite rainfall estimate, the data has to be corrected for bias otherwise the calibrated model parameters might not be representative of the watershed characteristics. The peak flow for both models is better captured by the CFSR rainfall data than the gauged rainfall for obvious reason of 20 % and 36% additional rainfall for Gilgel Abay and Main Beles respectively. The simulation by the gauged rainfall underestimates very high single peaks that are commonly caused by extreme high rainfall events.

3.4 Conclusion

This study has assessed the performance of commonly used high-resolution satellite rainfall products Climate Forecast System Reanalysis (CFSR) and Tropical Rainfall Measuring Mission (TRMM) 3B42 version 7 compared to in situ measurements. In addition the CFSR data performance is evaluated by its prediction capacity of the observed flow as input to semi-distributed hydrological models HBV and PED in the Gilgel Abay and Main Beles basins, Ethiopia. The simulation is also done for the gauged rainfall to capture the observed flow through model parameter calibration and the calibrated model parameters are used to validate the

performance of CFSR data. The gauged rainfall has performed well for both calibration and validation period with a fair to good NSE and on average the simulation has explained approximately 70% of the observed flow variation through model calibration for both models. Rainfall estimate from the CFSR has also captured the observed flow though model calibration with a fair to good NSE and on average the CFSR runoff simulation has captured approximately 69% of the variation of the observed flow for both models through model calibration. PED and HBV models through model calibration have responded for the extra rainfall of CFSR satellite rainfall estimate it has compared to the gauged rainfall. In HBV model, the maximum soil moisture storage parameter (FC) was too large indicating a deeper hydraulically active soil increasing the storage capacity of the soil. In PED model the fractional contributing area for CFSR rainfall estimate adds up to 68% for Gilgel Abay and 39% for Main Beles respectively, while the fractional contribution area for the gauged rainfall is 98% and 80% for Gilgel Abay and Main Beles.

The TRMM data was not used to capture the observed flow since it was unable to capture the gauged rainfall amount and pattern. We suggest further calibration of TRMM 3B42 rainfall product for the Blue Nile area before the data is used for any application. The performance of CFSR data was tested with the calibrated and validated model parameter sets of gauged rainfall data. CFSR data performed better for the Gilgel Abay compared to the Main Beles watershed in capturing the observed flow. This is possibly caused by the gauged rainfall data quality of Gilgel Abay which is representative of the area. The gauged rainfall data used to simulate Main Beles are outside of the watershed and they do not represent the upper catchment of the watershed.

Although only one station is available in the Gilgel Abay watershed and no rainfall station in the Main Beles basin, the performance of the gauged rainfall in capturing the observed runoff is

better than both CFSR rainfall estimates for calibration as well as validation periods. This indicates that gauged rainfall has its merit, but for remote regions with few or no observation stations in the Blue Nile area, CFSR rainfall estimate can be used to complement gauged rainfall data scarcity. The fractional saturated and degraded area of the PED model can be validated through satellite imagery by supervised land use classification. The simulation by the CFSR data for both HBV and PED models was able to capture the peak flows better than the runoff simulation by the gauged rainfall. So, the CFSR data might be more suitable to predict extreme events when using either PED or HBV models.

References

Baveye, P. C.: Hydrology and the looming water crisis: It is time to think, and act, outside the box, Journal of Hydrology and Hydromechanics, 61, 89-96, 2013.

Camberlin, P.: Rainfall anomalies in the source region of the Nile and their connection with the Indian summer monsoon, Journal of Climate, 10, 1380-1392, 1997.

Chaubey, I., Haan, C., Grunwald, S., and Salisbury, J.: Uncertainty in the model parameters due to spatial variability of rainfall, Journal of Hydrology, 220, 48-61, 1999.

Creutin, J. D. and Borga, M.: Radar hydrology modifies the monitoring of flash-flood hazard, Hydrological processes, 17, 1453-1456, 2003.

Dinku, T., Ceccato, P., and Connor, S. J.: Challenges of satellite rainfall estimation over mountainous and arid parts of east Africa, International Journal of Remote Sensing, 32, 5965-5979, 2011.

Dinku, T., Chidzambwa, S., Ceccato, P., Connor, S., and Ropelewski, C.: Validation of high-resolution satellite rainfall products over complex terrain, International Journal of Remote Sensing, 29, 4097-4110, 2008.

Dinku, T., Connor, S. J., and Ceccato, P.: Comparison of CMORPH and TRMM-3B42 over mountainous regions of Africa and South America. In: Satellite Rainfall Applications for Surface Hydrology, Springer Netherlands, 2010.

EUMETSAT: MSG Meteorological Products Extraction Facility Algorithm Specification Document, Darmstadt, Germany 2008

Ferraro, R. R.: Special sensor microwave imager derived global rainfall estimates for climatological applications, Journal of Geophysical Research: Atmospheres (1984–2012), 102, 16715-16735, 1997.

Haile, A. T., Habib, E., Elsaadani, M., and Rientjes, T.: Inter-comparison of satellite rainfall products for representing rainfall diurnal cycle over the Nile basin, International journal of applied earth observation and geoinformation, 21, 230-240, 2013.

Haile, A. T., Rientjes, T., Gieske, A., and Gebremichael, M.: Multispectral remote sensing for rainfall detection and estimation at the source of the Blue Nile River, International Journal of Applied Earth Observation and Geoinformation, 12, S76-S82, 2010.

Heinemann, T. and Kerényi, J.: The EUMETSAT multi sensor precipitation estimate (MPE): Concept and validation, 2003.

Heinemann, T., Latanzio, A., and Roveda, F.: The Eumetsat multi-sensor precipitation estimate (MPE), 23–27 September 2002, Madrid, Spain2002.

Huffman, G. J., Bolvin, D. T., Nelkin, E. J., Wolff, D. B., Adler, R. F., Gu, G., Hong, Y., Bowman, K. P., and Stocker, E. F.: The TRMM multisatellite precipitation analysis (TMPA): Quasi-global, multiyear, combined-sensor precipitation estimates at fine scales. , Journal of Hydrometeorology, 8, 38-55, 2007.

Javanmard, S., Yatagai, A., Nodzu, M., BodaghJamali, J., and Kawamoto, H.: Comparing high-resolution gridded precipitation data with satellite rainfall estimates of TRMM_3B42 over Iran, Advances in Geosciences, 25, 119-125, 2010.

Joyce, R. J., Janowiak, J. E., Arkin, P. A., and Xie, P.: CMORPH: A method that produces global precipitation estimates from passive microwave and infrared data at high spatial and temporal resolution, Journal of Hydrometeorology, 5, 487-503, 2004.

Kaba, E., Philpot, W., and Steenhuis, T.: Evaluating suitability of MODIS-Terra images for reproducing historic sediment concentrations in water bodies: Lake Tana, Ethiopia, International Journal of Applied Earth Observation and Geoinformation, 26, 286-297, 2014.

Kebede, S., Travi, Y., Alemayehu, T., and Marc, V.: Water balance of Lake Tana and its sensitivity to fluctuations in rainfall, Blue Nile basin, Ethiopia, Journal of hydrology, 316, 233-247, 2006.

Kidd, C.: Satellite rainfall climatology: a review, International Journal of Climatology, 21, 1041-1066, 2001.

Kidd, C., Kniveton, D. R., Todd, M. C., and Bellerby, T. J.: Satellite rainfall estimation using combined passive microwave and infrared algorithms, Journal of Hydrometeorology, 4, 1088-1104, 2003.

NASDA: TRMM Data Users Handbook, National Space Development Agency of Japan, Japan, 2001.

Negri, A. J., Adler, R. F., and Wetzel, P. J.: Rain estimation from satellites: An examination of the Griffith-Woodley technique, Journal of climate and applied meteorology, 23, 102-116, 1984.

NMSA: Climatic and Agroclimatic Resources of Ethiopia. , National Meteorology Service Agency of Ethiopia, Addis Ababa, Ethiopia, 137 pp. pp., 1996.

Ouma, Y. O., Owiti, T., Kipkorir, E., Kibiiy, J., and Tateishi, R.: Multitemporal comparative analysis of TRMM-3B42 satellite-estimated rainfall with surface gauge data at basin scales: daily, decadal and monthly evaluations, International Journal of Remote Sensing, 33, 7662-7684, 2012.

Pardo-Igúzquiza, E.: Optimal selection of number and location of rainfall gauges for areal rainfall estimation using geostatistics and simulated annealing, Journal of Hydrology, 210, 206-220, 1998.

Ramakrishna, S. and Nasreen, S. A. A. N.: An overview on water resources: pollution and nanomaterials, 2013. 2013.

Saha, S., Moorthi, S., Wu, X., Wang, J., Nadiga, S., Tripp, P., Behringer, D., Hou, Y.-T., Chuang, H.-y., and Iredell, M.: The NCEP climate forecast system version 2, Journal of Climate, 27, 2185-2208, 2014.

Seleshi, Y. and Demaree, G.: Rainfall variability in the Ethiopian and Eritrean highlands and its links with the Southern Oscillation Index, Journal of Biogeography, 1995. 945-952, 1995.

Seleshi, Y. and Zanke, U.: Recent changes in rainfall and rainy days in Ethiopia, International Journal of Climatology, 24, 973-983, 2004.

Simpson, J., Adler, R. F., and North, G. R.: A proposed tropical rainfall measuring mission (TRMM) satellite, Bulletin of the American Meteorological Society, 69, 278-295, 1988.

Todd, M. C., Kidd, C., Kniveton, D., and Bellerby, T. J.: A combined satellite infrared and passive microwave technique for estimation of small-scale rainfall, Journal of Atmospheric and Oceanic Technology, 18, 742-755, 2001.

Tsidu, G. M.: High-Resolution Monthly Rainfall Database for Ethiopia: Homogenization, Reconstruction, and Gridding, Journal of Climate, 25, 8422-8443, 2012.

Turk, F. J., Rohaly, G. D., Hawkins, J., Smith, E. A., Marzano, F. S., Mugnai, A., and Levizzani, V.: Meteorological applications of precipitation estimation from combined SSM/I, TRMM and infrared geostationary satellite data, Microwave Radiometry and Remote Sensing of the Earth's Surface and Atmosphere, 1999. VSP BV, the Netherlands, 353-363, 1999.

Wale, A.: Hydrological balance of Lake Tana, M.Sc Thesis, International Institute for Geo-Information Science and Earth Observation (ITC), the Netherlands, 2008.

Wale, A., Kaba, E., Mengeste, A., Workaferahu, A., Mulken, M., and Aemro, B.: Opportunities of the Low-Cost Satellite Image Reception Station Established at GIS & RS Center of Bahir Dar University, Institute of Technology, 2nd Symposium on biodiversity and Natural Conservation at Arba Minch University, Ethiopia (June 03-05, 2010), 2011.

Wang, W., Xie, P., Yoo, S.-H., Xue, Y., Kumar, A., and Wu, X.: An assessment of the surface climate in the NCEP climate forecast system reanalysis, Climate dynamics, 37, 1601-1620, 2011.

WMO: World Meteorological Organization, Guide to Hydrological Practices: : Data Acquisition and Processing, Analysis, Forecasting and other Applications. WMO-No. 168., WMO, Geneva, 770 pp., 1994.

Xu, L. and Zhang, W.-J.: Comparison of different methods for variable selection, Analytica Chimica Acta, 446, 475-481, 2001.

CHAPTER 4: PERFORMANCE OF BIAS CORRECTED MPEG RAINFALL ESTIMATE FOR RAINFALL-RUNOFF SIMULATION IN THE UPPER BLUE NILE BASIN, ETHIOPIA

Abstract

Spatial resolution of gauged precipitation data is poor in developing countries and often data are missing. This has led to an increasing use of satellite rainfall estimates in landscape simulation models. However satellite rainfall estimates (SRE) are prone to systematic errors. Understanding and correcting bias error is important to accurately simulate the hydrology. In this study, we corrected Multi-Sensor Precipitation Estimate-Geostationary (MPEG) data for bias and simulated the observed flow of Gilgel Abay in the Upper Blue Nile basin, Ethiopia. We found that, the MPEG satellite rainfall without bias correction captures the seasonal rainfall variation but underestimates the gauged rainfall by 60%. By adjusting the volumes for the monthly means of the MPEG by the observed means, the hydrologic model performed as well or better with the bias corrected MPEG than with the gauged rainfall in capturing the observed flow through hydrologic model calibration.

4.1 Introduction

Human ability to numerically model water resource systems has progressed greatly with advances in computational power and the understanding of processes at finer scale (Silberstein, 2006). However, water resources data collection at varying spatial and temporal scales is expensive, so that modellers often tend to conceptualize processes based on simplified views of the system (Dozier, 1992) or match the observed data even if the underlying premises are

unrealistic (Kirchner, 2006). Rainfall is one of the most sensitive model input parameter and plays an important role in the hydrologic cycle. However its accuracy as a model input has been questioned especially if gauging stations are far apart is common as in the developing countries (Fuka et al., 2013).

Recently, satellite remote sensing has received increased attention in measuring precipitation (Aonashi et al., 2009; Barrett, 1989; Ebert and McBride, 2000; Ferriday, 1994; Hong, 2003; Huffman et al., 2007; Joyce et al., 2004; Kidd, 2001; Ochoa et al., 2014; Scofield and Kuligowski, 2003; Sorooshian et al., 2000). Very few of these studies have evaluated the satellite rainfall over Africa (Ali et al., 2005; Romilly and Gebremichael, 2011; Thorne et al., 2001; Worqlul et al., 2014b). Satellite rainfall estimates (SRE) use either or the combination of thermal infrared or the passive microwave channel portions of the electromagnetic spectrum. In thermal infrared channel rainfall is estimated using a top cloud temperature threshold to discriminate between raining and non-raining clouds. The threshold can be too cold for warm orographic precipitating clouds. The rainfall estimate by passive microwave channel is a direct way of measurement, because of the strong relationship between the radiance of microwave channel and precipitation (Tian et al., 2007). Since passive microwave measurements are not available in the geostationary satellites, the associated error with the microwave channel is sampling error especially for shorter rainfall events as there is no frequent measurement in the passive microwave channel (Kidd et al., 2003). In addition, algorithm performance depends on season and local climate conditions (Dinku et al., 2007; Dinku et al., 2008; Jobard et al., 2007).

Satellite rainfall estimates can be validated either by direct comparison with the gauged data (Dinku et al., 2007; Worqlul et al., 2014a) or by transforming the satellite rainfall data to a discharge signal with a hydrological model (Bitew and Gebremichael, 2011; Cohen Liechti et al.,

2012). Translating the satellite rainfall to the discharge signal has poor predictions of rainfall can be compensated by model parameters especially if distributed models are used with many model parameters (Bitew et al., 2012). However, by using parsimonious models with few fitting parameters this drawback can be mostly avoided.

In this study, the satellite rainfall estimate produced by EUMETSAT (see section 2.3), called the Multi-sensor Precipitation Estimate Geostationary (MPEG) is validated by comparing it with the in situ rainfall measurements and, after bias correction, it is validated by its prediction capacity of the observed flow through hydrologic model calibration. In MPEG rainfall is estimated by blending rainfall rates derived from passive microwave channel from polar orbiting satellite and infrared channel from geostationary satellite (Heinemann and Kerényi, 2003). SRE are affected typically by systematic and random error (Piani et al., 2010b; Teutschbein and Seibert, 2012b). Some of the errors associated with SRE are consistent under prediction, missing seasonal variation (Worqlul et al., 2014b) and a low or higher amount of dry days (Piani et al., 2010a) are a few amongst others. Bias correction may vary from simple additive correction (Berg et al., 2012) to a more complex histogram matching that can correct multiple moments of the distribution of a variable at a time (Haerter et al., 2011; Teutschbein and Seibert, 2012a). Worqlul et al. (2014b) validated MPEG rainfall estimate using 38 rainfall gauging station in the Lake Tana sub basin indicated that MPEG rainfall estimate has a higher correlation coefficient with a consistent bias which may be corrected using a simple linear bias correction. The motivation of this research is to evaluate the usability of a bias corrected MPEG precipitation data as a forcing to a semi-distributed hydrologic model Hydrologiska Byråns Vattenbalansavdelning (HBV) (Lindström et al., 1997). HBV model is selected because, it has performed well in capturing observed stream flow of Gilgel Abay River using rainfall data from

traditional gauges (Abdo et al., 2009; Uhlenbrook et al., 2010; Wale et al., 2009; Worqlul et al., 2015a) and it has minimum number of calibration parameters.

4.2 Methodology

4.2.1 Study Area Description

Gilgel Abay watershed is located in the Blue Nile Basin, western part of Ethiopian highland in Tana sub basin between 10°56' to 11°58'N latitude and 36°44' to 37°34'E longitude. It originates from a small spring located near Gish Abay Mountain at elevation of 3000m amsl 140km away from the Lake Tana. The watershed area of the Gilgel Abay at the flow gauging site is approximately 1650 km^2 as extracted from the 90 m resolution Shuttle Radar Topographic Mission (SRTM), Digital Elevation Model (DEM). Figure 4-1 indicates drainage pattern and ground rainfall observation stations network.

The watershed has a complex topography with significant elevation variation ranging from 1890 to 3530m and slope ranges between zero to 140% with an average value of 12% (Worqlul et al., 2015a). The watershed has the largest surface irrigation potential compared to the other sub basins in the Lake Tana district (Worqlul et al., 2015b). The watershed is dominated by agricultural land; the dominant soil is Luvisols and Alisols covering approximately 56 and 40% of the watershed, respectively. Both Luvisols and Alisols have a higher clay content in the subsoil than in the topsoil (Michéli et al., 2006). Rainfall in the study area on average varies between 1300 and 2300 mm (1994 to 2013). The main rainfall season called "Kremt" from May to September accounts for up to 90% of the annual rainfall.

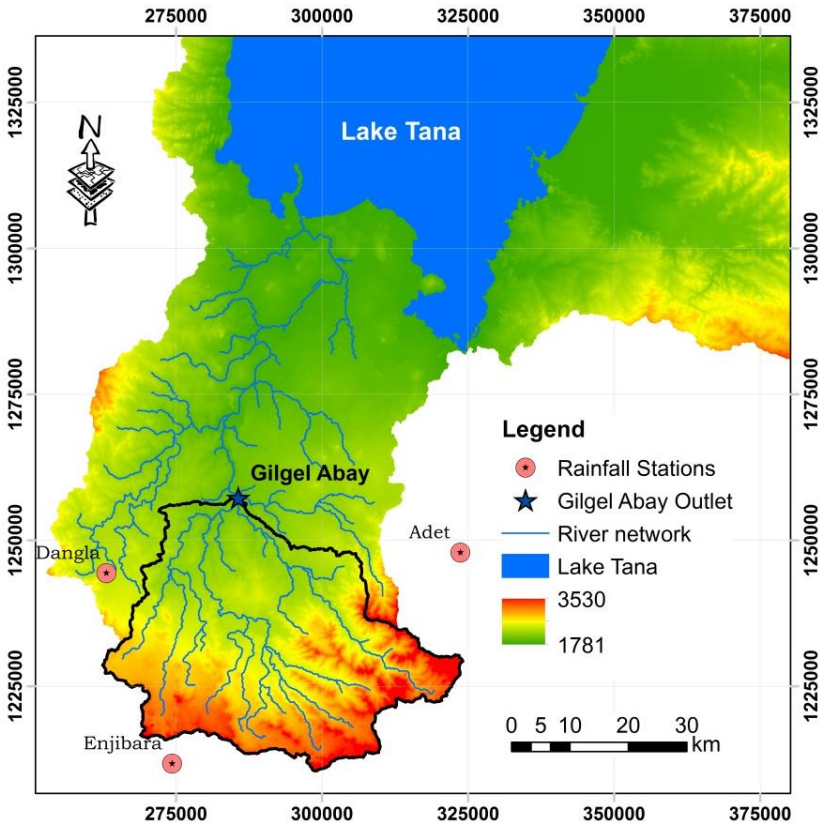

Figure 4-1: Drainage pattern and rainfall station network of Gilgel Abay basin, background a 90 m resolution digital elevation model.

4.2.2 Climate and discharge data

Meteorological and hydrological data is collected from the Ethiopian National Meteorological Agency (NMA) and Ethiopian Ministry of Water, Irrigation and Energy (EMWIE), respectively. The data is collected from 2010 where the satellite rainfall estimate from MPEG is available to end of 2013 where the meteorological and hydrological data's are available. Daily gauged rainfall data is collected from three nearby stations (Figure 4-1). Minimum and maximum temperature, relative humidity, wind speed and daily sunshine hour are available from Dangila station. Observed flow plotted for the study period indicated that, the dry season flow (January to April) has increased significantly starting from 2006. Since 2006 the dry season flow has

increased by approximately 200% when compared to the average flow of 1980 to 2005. The study by Enku et al. (2014) indicated dry season flow of Gilgel Abay has a decreasing trend since 1980 to 2000. It seems there is a problem with the rating curve especially for the dry season flow since 2006. The wet season flow did not show a significant variation compared from 1980 to 2005.

4.2.3 MPEG data

Multi-sensor precipitation estimate-geostationary (MPEG) is produced by the European Organisation for the Exploitation of Meteorological Satellites (EUMETSAT) meteorological product extraction facility (MPEF). It is produced by blending rain rates derived from Special Sensor Microwave / Imager (SSM/I) on board of the US-DMSP satellite are combined with brightness temperature from infrared channel of MTP-METOSAT satellites (Heinemann and Kerényi, 2003). The data is freely available through the GEONETCast near real time satellite based data dissemination system (Wale et al., 2011; Worqlul et al., 2014b). The MPEG data is available since 2010; it has a spatial resolution of 3 km with a 15 minute temporal resolution. The daily aggregated MPEG satellite rainfall estimate from MPEF is downloaded from the International Institute for Geo-Information Science and Earth Observation (ITC) ftp server. For this study, daily MPEG rainfall estimate of Gilgel Abay basin is constructed for the study period from 2010 to 2013.

4.2.4 Methods

The MPEG satellite rainfall estimate is used as input to a semi-distributed hydrologic model to capture the observed flow of Gilgel Abay basin through model parameter calibration. To achieve this, the methodology has three parts: first the areal MPEG satellite rainfall estimate is compared

with areal gauged rainfall data from the period of 2010 to 2013 where the MPEG and ground rainfall data is available. The comparison is done on monthly basis to see whether the MPEG rainfall is capturing the pattern and volume of gauged rainfall or not. Second: the bias associated with the MPEG data will be corrected by a multiplicative coefficient. The bias correction applied is to match the monthly mean of MPEG satellite rainfall with mean of gauged monthly rainfall amounts. To make use of the near-real-time MPEG data, the long-term average correction coefficients will be extracted. In the study site there is a minimum of one year for the collected hydrological and meteorological data to be accessible for the public use. The monthly mean of the gauged and MPEG data are calculated by aggregating the daily areal gauged rainfall interpolated by inverse distance and by aggregating the daily areal satellite grid rainfall estimate, respectively. Lastly: the gauged, original and bias corrected MPEG rainfall estimates are used as input to the hydrologic model to capture the observed flow of Gilgel Abay through HBV model parameter calibration. The hydrologic model is calibrated from the period of 2010 to 2013 and performance of the model is evaluated by using percent bias (PBIAS), coefficient of determination (R-square) and Nash-Sutcliffe coefficient (NSE) as objective functions.

In addition, the performance of bias corrected MPEG and long-term MPEG bias correction coefficients will be validated by their prediction capacity of the observed flow. In both cases the calibrated gauged rainfall parameter sets will be used as those parameters are assumed to represent the physical watershed characteristics of a watershed (Kokkonen et al., 2003; Seibert, 1999; Wale et al., 2009).

4.2.4.1 Bias correction

Some of the errors associated with SRE are consistent under prediction; missing seasonal variation (Worqlul et al., 2014b) and a low or higher amount of dry days (Piani et al., 2010a) are a few amongst others. Model parameter values obtained using biased SRE as forcing might not be taken as reliable estimate of watershed characteristics (Behrangi et al., 2011; Bitew et al., 2012). Therefore understanding the bias associated within SRE and correcting it is a necessity step. Bias correction may vary from simple additive correction (Berg et al., 2012) to a more complex histogram matching that can correct multiple moments of the distribution of a variable at a time (Haerter et al., 2011; Teutschbein and Seibert, 2012a). In this study the bias associated with MPEG, is corrected by applying a multiplication correction factor. The correction factor applied is: to match the mean of monthly MPEG rainfall estimate with mean monthly of gauged rainfall (Eq. 1).

$$P_{CorrMPEG(i)} = P_{MPEG(i)} * \frac{\overline{P_{obs_{mi}}}}{\overline{P_{MPEG_{mi}}}} \quad (1)$$

Where: $P_{CorrMPEG(i)}$ is daily bias corrected MPEG, $P_{MPEG(i)}$ daily original MPEG rainfall estimate, $\overline{P_{obs_{mi}}}$ monthly observed average rainfall and $\overline{P_{MPEG_{mi}}}$ is monthly average original MPEG rainfall estimate.

4.2.4.2 HBV-IHMS model:

The HBV hydrologic model (Lindström et al., 1997) is a conceptual semi-distributed rainfall-runoff model for stream flow simulation. In HBV, the watershed is subdivided in to sub-basins and further into different elevation and land use zones. The hydrological and climate input data for flow simulation includes; daily data of rainfall, temperature, observed flow and long-term

average monthly potential evapotranspiration. Long-term potential evaporation is estimated by using the Penman-combination equation using Dangila station data. Digital Elevation Model (DEM) from Shuttle Radar Topography Mission (SRTM) (Jarvis et al., 2008) is used to extract drainage area of Gilgel Abay watershed for the outlet location and to divide the watershed into sub-basins and elevations zones. Land use data is collected from the Ethiopia Ministry of Water, Irrigation and Energy. Here, the HBV model will be discussed briefly, a complete description of the model can be found in Lindström et al. (1997), SMHI (2006) and Wale et al. (2009) among others. HBV model consists of subroutines for soil moisture accounting procedure, runoff generation and a simple routing procedure. The soil moisture accounting routine is based on three parameters (β), FC and LP (SMHI, 2006). Beta (β) controls the contribution to the response function from each millimeter of rainfall. FC is the maximum soil moisture storage. The limit for potential evaporation (LP) dictates a soil moisture value above which evaporation reaches its potential. The runoff generation routine transforms excess water from the soil moisture zone into runoff, this routine consists of upper non-linear and lower linear reservoir connected by percolation (Perc). Khq and K4 are recession coefficients of the upper and lower reservoir, respectively. Alfa (α) is the measure of non-linearity of the upper reservoir and it is used to fit the higher picks into the observed hydrograph.

4.2.4.3 Model calibration

The calibration is done systematically by first fitting the observed flow volume followed by calibrating the shape controlling parameters. The level of sensitivity of parameters controlling the volume and shape of the hydrograph are listed in Wale et al. (2009) and SMHI (2006). HBV has seven sensitive model parameters controlling the volume and shape of the hydrograph. The model is calibrated first for volume controlling parameters FC, LP, Beta and Khq followed by

shape controlling parameters Alfa, K4 and Perc parameters. HBV model is calibrated for both gauged rainfall, original MPEG and bias corrected MPEG from 2010 to 2013. The performance of the model is evaluated by using multiple objective functions including percent bias (PBIAS), Nash-Sutcliffe Efficiency (NSE) and Coefficient of Determination (R-Square). PBIAS calculates the relative volume difference between simulated and observed volume. A negative value indicates the over-prediction and positive value indicates under-prediction of simulation. A PBIAS value of zero might not mean a perfect simulation since the distribution through time is not considered. NSE is the normalized statistics that tells about the relative magnitude of residual variance compared to the observed flow variance. NSE indicates how well the plot between observed and simulated flow fits the 1:1 line (Moriasi et al., 2007). NSE value between 0.6 and 0.8 is considered fair to good and very good when NSE is greater than 0.8. R-Square evaluates the degree of linear association between observed and simulated flow. For a perfect fit the slope and intercept has to be checked.

$$\text{PBIAS} = \frac{\sum(Q_{Obs(i)} - Q_{MPEG(i)})}{\sum Q_{Obs(i)}} * 100 \quad (3)$$

$$\text{NSE} = 1 - \frac{\sum(Q_{Obs(i)} - Q_{MPEG(i)})^2}{\sum(Q_{Obs(i)} - \overline{Q_{Obs}})^2} \quad (4)$$

$$\text{R} - \text{square} = \left(\frac{n\sum_{i=1}^{n}(Q_{obs(i)} Q_{MPEG(i)}) - (\sum_{i=1}^{n} Q_{Obs(i)})(\sum_{i=1}^{n} Q_{MPEG(i)})}{\sqrt{\left[n(\sum Q_{Obs(i)}{}^2) - (\sum Q_{Obs(i)})^2\right]\left[n(\sum Q_{MPEG(i)}{}^2) - (\sum Q_{MPEG(i)})^2\right]}} \right)^2 \quad (5)$$

Where: BIAS: Percent bias, $Q_{MPEG(i)}$: daily flow simulated by MPEG data, $Q_{Obs(i)}$: daily observed flow, NSE: Nash-Sutcliffe Efficiency, $\overline{Q_{obs}}$: long-term average observed flow, R-square: coefficient of determination and n is number of data pairs.

4.3 Result and Discussion

4.3.1 Comparison of areal observed rainfall with MPEG rainfall estimate

The areal weights of ground rainfall stations are determined by the inverse distance interpolation method, and then the areal average rainfall of gauged rainfall of Gilgel Abay is determined. For MPEG data, the areal rainfall is determined by aggregating the 15 minutes interval rainfall data to daily. Figure 4-2 shows the long-term average annual gauged and MPEG rainfall estimate from 2010 to 2013.

The monthly areal gauged rainfall and MPEG satellite rainfall from 2010 to 2013 indicated a higher correlation coefficient of 0.81 (Figure 4-3), which indicates MPEG areal rainfall capturing 81% of the ground rainfall variation. But, despite capturing the observed rainfall pattern, MPEG rainfall estimate suffers by underestimating the gauged rainfall mount by 60% (Figure 4-3) which is consistent with Worqlul et al. (2014b) findings. Thus, the consistence bias with a higher correlation, MPEG rainfall estimate can be approximately corrected by a linear correction factor.

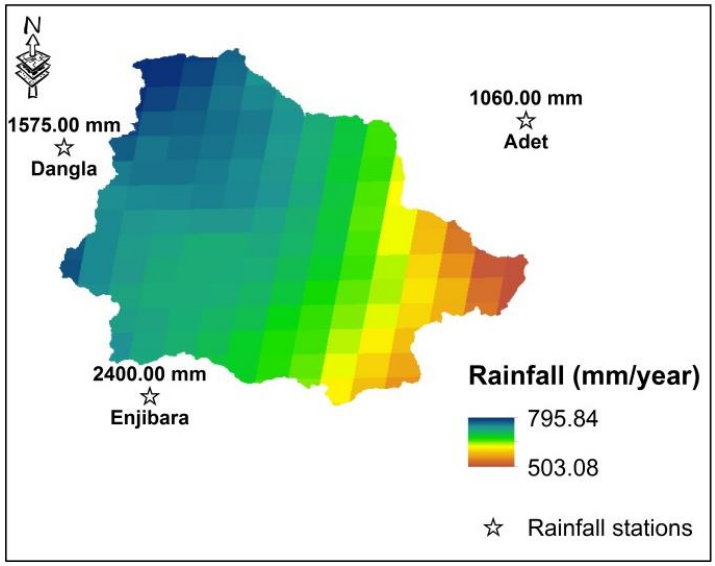

Figure 4-2: Long-term annual average observed and MPEG rainfall estimate of Gilgel Abay basin (2010 to 2013).

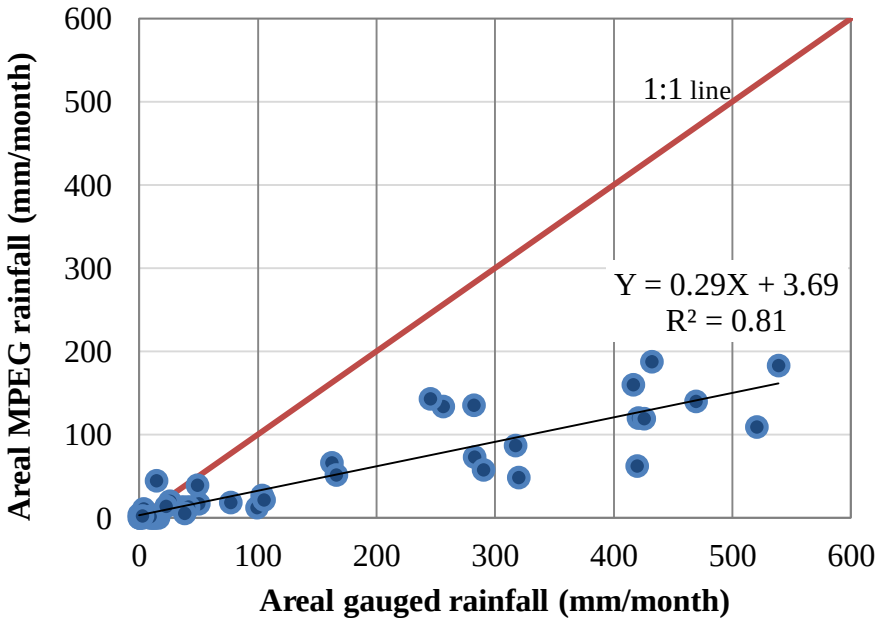

Figure 4-3: Comparison of long-term monthly areal rainfall from gauge and MPEG estimate Gilgel Abay basin 2010 – 2013.

4.3.2 Performance of Bias corrected MPEG data

The bias associated with MPEG data is corrected to match with monthly average gauged rainfall data. This is done by multiplying the daily MPEG rainfall estimate by the ratio of monthly average gauged rainfall and original MPEG rainfall estimates (Eq. 1). Figure 4-4 presents the daily rainfall difference between original and corrected MPEG from the gauged areal rainfall (2010 to 2013).

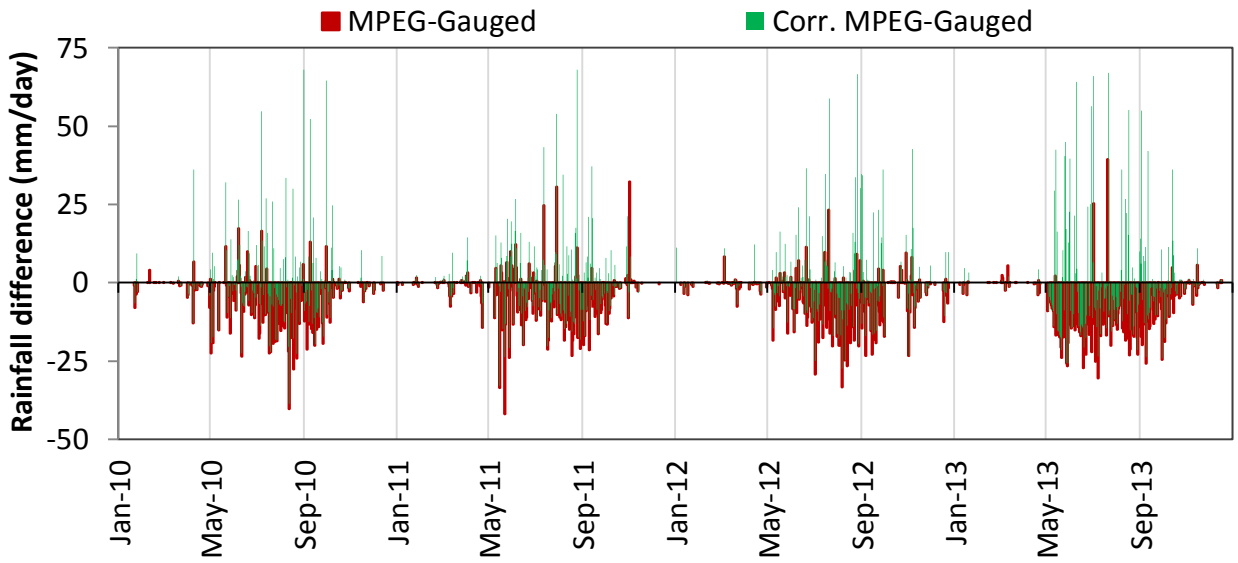

Figure 4-4: Comparison of daily rainfall difference between original MPEG and corrected MPEG form observed gauged rainfall from (2010 to 2013).

Throughout the study period more than 87% of the time original MPEG areal rainfall estimates are less than the gauged areal rainfall on daily basis (Figure 4-4). After bias correction, approximately 63% of the events have a rainfall record less than the gauge record (Figure 4-4).

The annual cumulative rainfall in Figure 4-5 indicated that original MPEG data has captured the rainfall duration but it indicated a distinct lower slope compared to gauged rainfall indicating

underprediction. The bias corrected MPEG rainfall estimate has captured the total annual volume of the gauged rainfall for the study period.

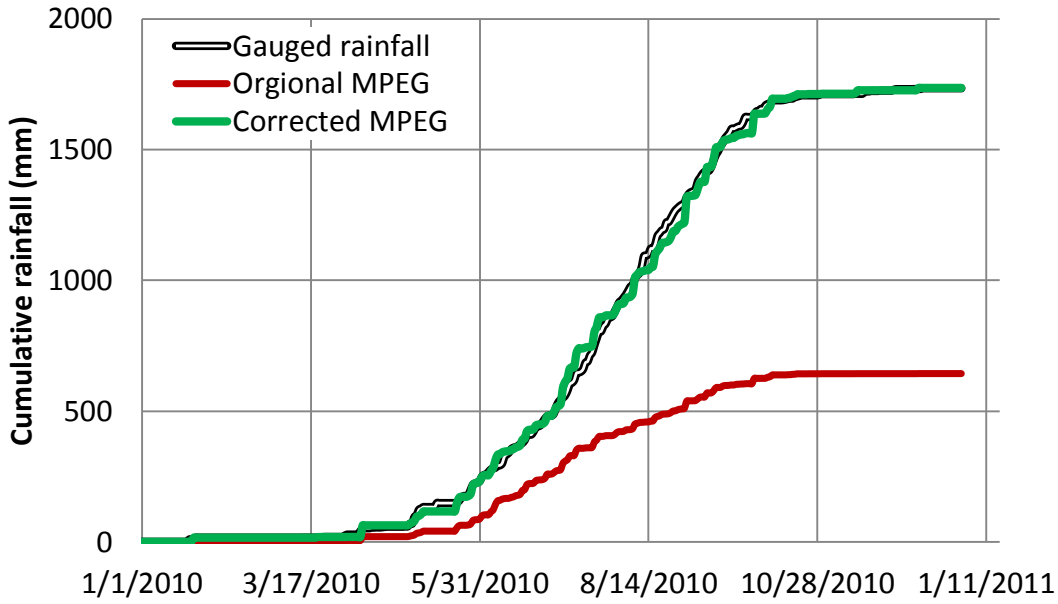

Figure 4-5: Cumulative rainfall of gauged, original and bias corrected MPEG for year 2010.

The monthly mean bias correction factors of MPEG data compared for the study period indicated a similar value for the main rainy season from May to September which accounts 90% of the annual rainfall. The monthly correction factors for dry season have a significant variation as both satellite and gauged rainfall estimates have poor performance on capturing lower rainfall amounts (Berg et al., 2012; Toté et al., 2015). Figure 4-6 shows the correction factors of the MPEG data on monthly basis for the main rainfall season. The line in Figure 4-6 indicates the average values of the monthly average correction coefficients for the main rainfall season. Generally, in Ethiopia, it will take approximately a year or more for the meteorological and hydrological data to be recorded manually, decoded to electronic format and transferred to the head office to be available for research use. So, the average values indicated in Figure 4-6 can be used to correct the MPEG data to make use of the data available at near-real time.

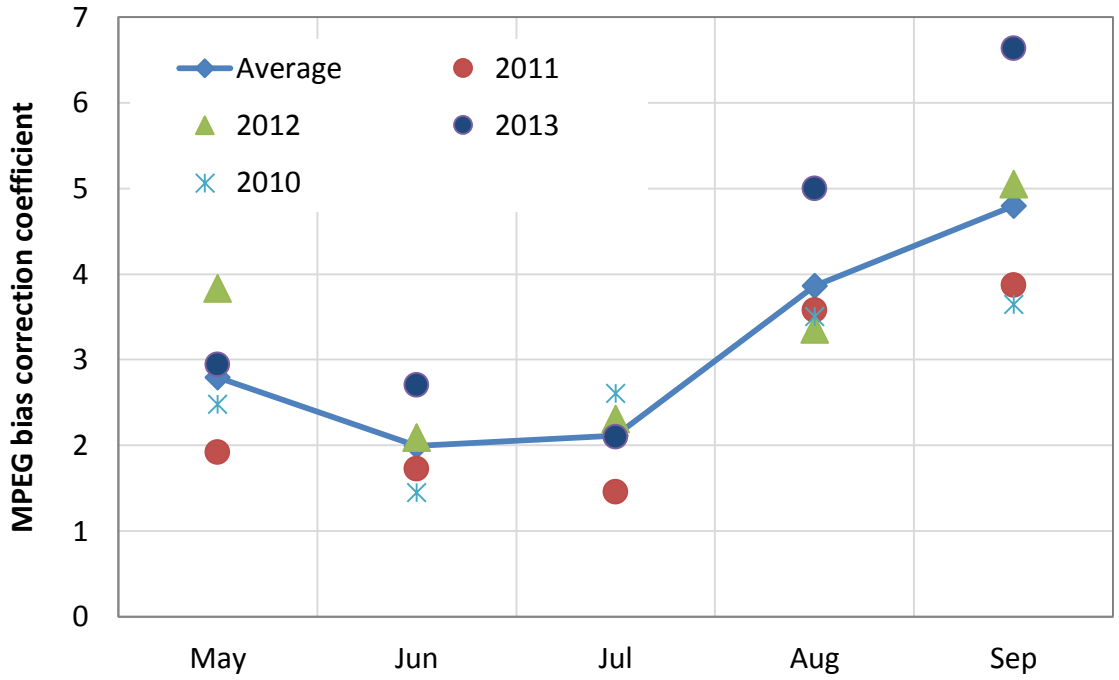

Figure 4-6: Monthly MPEG bias correction factors and long-term bias correction factor for the study period.

4.3.3 Discharge simulation with gauged rainfall, original MPEG and bias corrected MPEG data

The hydrologic model HBV is calibrated for the observed rainfall, original and bias-corrected MPEG data. The calibration was approached systematically by calibrating the volume controlling parameters first flowed by fine twining shape controlling parameters which influence the shape of the hydrograph by distributing the calculated discharge in time. List of volume and shape contriving parameters of HBV are tabulated in SMHI (2006) and Wale et al. (2009). Table 4-1 shows the optimized model parameter sets and model performance of gauged rainfall, original and bias corrected MPEG rainfall estimates.

Table 4-1: Optimized model parameter sets of HBV model and its performance for gauged rainfall, original and bias corrected MPEG data.

HBV model parameters	Gauged rainfall	Original MPEG	Corrected MPEG
Alfa	0.5	0.5	0.5
Beta	1.0	1.0	1.0
Fc	340	100	460
K4	0.08	0.07	0.10
Khq	0.18	0.01	0.08
Lp	0.70	0.90	0.80
Perc	6.0	6.0	6.0
PBIAS (%)	8.5	70.0	5.9
NSE	0.78	0.16	0.80
R-square	0.84	0.60	0.82

The performance of the simulated flow using gauged and bias corrected MPEG indicated a very good performance with a NSH of 0.78 and 0.80, respectively and with a PBIAS of less than 10% (Table 4-1, Figure 4-7 and Figure 4-8). The performance of original MPEG data was poor in capturing the observed flow through model calibration with a NSH value of 0.28 and a very high PBIAS value of 70% indicating under-prediction.

Even though percolation parameter (Perc) which links the upper and lower reservoir was kept the maximum value, the model did not capture the dry season flow very well. Otherwise, the model has captured the rising and recession limb of the hydrograph for the gauged rainfall and for the bias corrected MPEG data. The effort made to get the rating curve data at the EMWIE was not successful, we recommend a further examination of the dry season flow (January to May) after 2006 as it has increased significantly by 200% compared to the long-term average from 1980 to 2005.

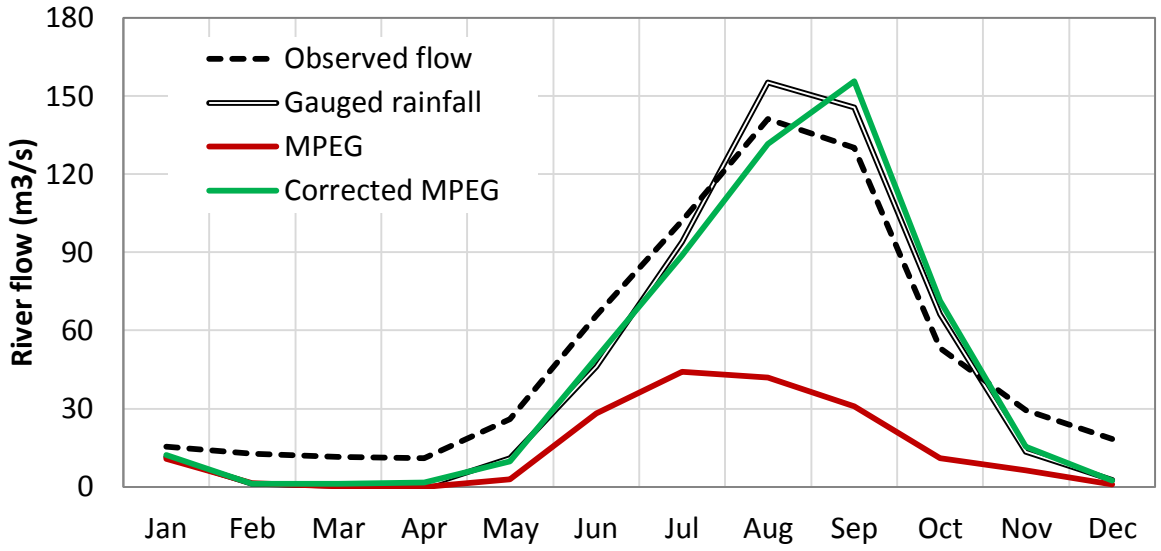

Figure 4-7: Long-term monthly average flow of observed flow and HBV simulation by gauged rainfall, MPEG and bias corrected MPEG data (2010 to 2013)

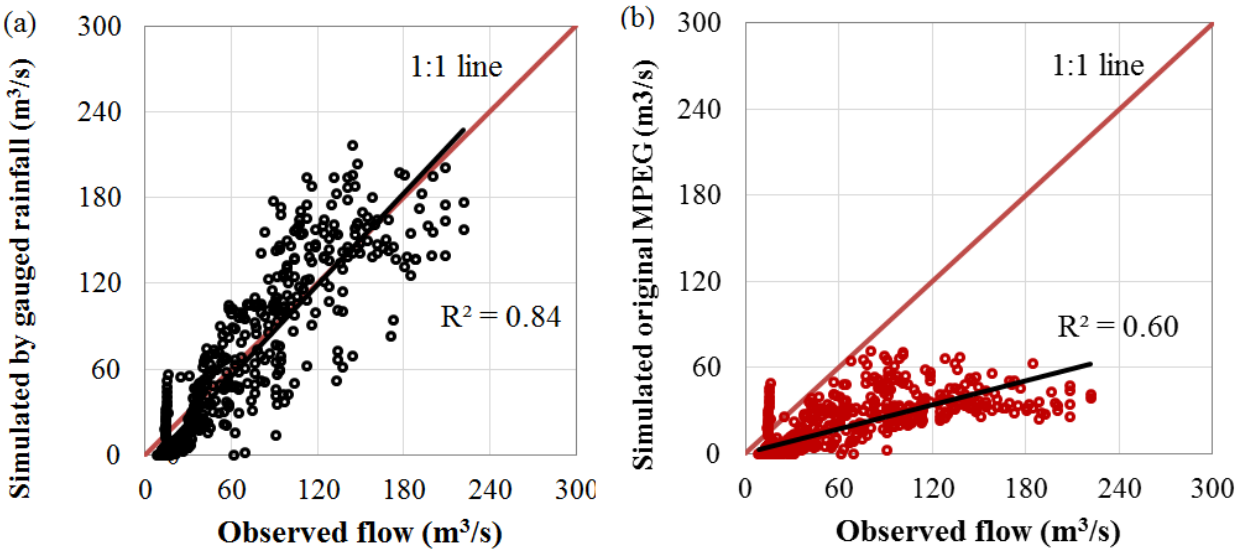

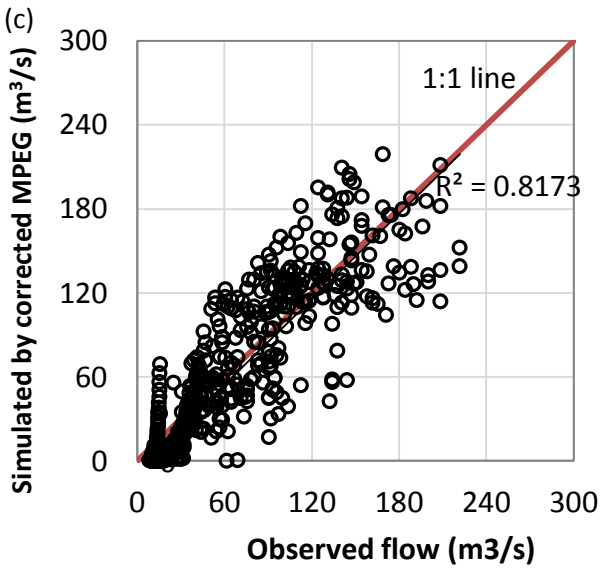

Figure 4-8: Correlation between observed and simulated flow for the calibration period using (a) gauged rainfall, (b) original MPEG, (c) bias corrected MPEG.

4.3.4 Cross validation of bias corrected MPEG data

The calibrated model parameter sets of the gauged rainfall data are used to validate the performance of bias corrected MPEG by predicting the observed flow. The calibration model parameters of the gauged rainfall and bias corrected MPEG in Table 4-1 have a similar value except for the FC, Khq and Lp. The bias corrected MPEG has a higher FC and Lp which indicates a larger active soil layer to store water and to emptied it by evaporation. This is caused by the stronger effect of the multiplication correction coefficient on higher values. Simulation of bias corrected MPEG rainfall estimate by gauged rainfall parameters captured the observed flow well with a NSE value of 0.74 and with fair PBIAS value of 8% (2010 to 2013). The long-term monthly bias correction factors under Figure 4-6 are also used to correct MPEG rainfall data to up-to-date from 2010 to May 10-2015 and runoff is simulated where the observed flow is available. The gauged rainfall calibration parameters are used to simulate the bias corrected

MPEG. Figure 4-9 indicates the monthly gauged and simulated flow of bias corrected MPEG data using long-term average bias correction factors. Due to the absence of temperature and observed flow data after 2013 the performance of bias corrected MPEG data is not evaluated.

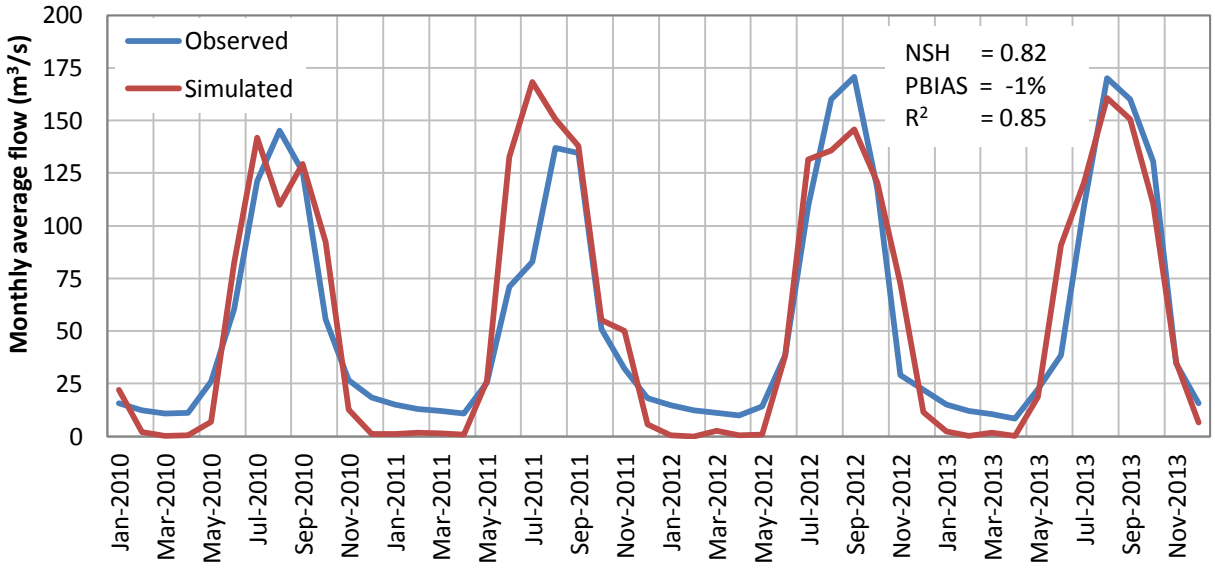

Figure 4-9: Flow simulated by bias corrected MPEG using long-term correction coefficients vs. gauged flow 2010 to 2013.

4.4 Conclusion

Rainfall is one of the dominant water balance component and it is highly variable in both space and time. Ground rainfall measurements can capture the temporal variation, but in developing countries the rain gauge networks is scarce and it is declining rapidly (Overeem et al., 2013). Satellite rainfall estimates can capture the spatial and temporal variation of rainfall using passive microwave and/or thermal infrared part of the electromagnetic spectrum. But, satellite rainfall estimate is prone to systematic error; understanding and correcting the bias associated within should be a mandatory procedure before enforcing a hydrological model. In this study, we have validated the performance of MPEG rainfall estimate by in situ rainfall measurements from the

Ethiopian Meteorological Agency and associated bias is adjusted with the gauged rainfall data. Finally the performance of bias corrected MPEG data is validated by its prediction capacity of observed flow of Gilgel Abay watershed in the Ethiopian highland.

The MPEG rainfall estimate compared with the gauged rainfall data indicated a higher correlation coefficient, capturing 81% of the gauged rainfall variation. But, despite capturing the spatial variation, the MPEG rainfall underestimated the gauged rainfall by 60%. The associated bias of MPEG rainfall estimate was consistent for the study period and it is in agreement with the previous study by Worqlul et al. (2014a). The consistent bias of MPEG data is adjusted with gauged rainfall to match with the mean of gauged rainfall data. The performance of bias corrected MPEG data is validated by its prediction capacity of the observed flow though model calibration. The result indicated that, the bias corrected MPEG data with the multiplication correction factor to match with mean of gauged rainfall data has performed as good as or better than gauged rainfall data. The long-term mean MPEG rainfall correction coefficients estimated from 2010 to 2013 has also performed well in capturing the observed flow of Gilgel Abay watershed using gauged rainfall parameters. This will allow as to use the near-real-time rainfall data from MPEG to study flood in the Lake Tana area.

References

Abdo, K., Fiseha, B., Rientjes, T., Gieske, A., and Haile, A.: Assessment of climate change impacts on the hydrology of Gilgel Abay catchment in Lake Tana basin, Ethiopia, Hydrological Processes, 23, 3661-3669, 2009.

Ali, A., Amani, A., Diedhiou, A., and Lebel, T.: Rainfall estimation in the Sahel. Part II: Evaluation of rain gauge networks in the CILSS countries and objective intercomparison of rainfall products, Journal of Applied Meteorology, 44, 1707-1722, 2005.

Aonashi, K., Awaka, J., Hirose, M., Kozu, T., Kubota, T., Liu, G., Shige, S., Kida, S., Seto, S., and Takahashi, N.: GSMaP passive microwave precipitation retrieval algorithm: Algorithm description and validation, 気象集誌. 第 2 輯, 87, 119-136, 2009.

Barrett, E. C.: Satellite remote sensing of rainfall. In: Applications of remote sensing to agrometeorology, Springer, 1989.

Behrangi, A., Khakbaz, B., Jaw, T. C., AghaKouchak, A., Hsu, K., and Sorooshian, S.: Hydrologic evaluation of satellite precipitation products over a mid-size basin, Journal of Hydrology, 397, 225-237, 2011.

Berg, P., Feldmann, H., and Panitz, H.-J.: Bias correction of high resolution regional climate model data, Journal of Hydrology, 448, 80-92, 2012.

Bitew, M. and Gebremichael, M.: Assessment of satellite rainfall products for streamflow simulation in medium watersheds of the Ethiopian highlands, Hydrology and Earth System Sciences, 15, 1147-1155, 2011.

Bitew, M. M., Gebremichael, M., Ghebremichael, L. T., and Bayissa, Y. A.: Evaluation of high-resolution satellite rainfall products through streamflow simulation in a hydrological modeling of a small mountainous watershed in Ethiopia, Journal of Hydrometeorology, 13, 338-350, 2012.

Cohen Liechti, T., Matos, J., Boillat, J.-L., and Schleiss, A.: Comparison and evaluation of satellite derived precipitation products for hydrological modeling of the Zambezi River Basin, Hydrology and Earth System Sciences, 16, 489-500, 2012.

Dinku, T., Ceccato, P., Grover-Kopec, E., Lemma, M., Connor, S., and Ropelewski, C.: Validation of satellite rainfall products over East Africa's complex topography, International Journal of Remote Sensing, 28, 1503-1526, 2007.

Dinku, T., Chidzambwa, S., Ceccato, P., Connor, S., and Ropelewski, C.: Validation of high-resolution satellite rainfall products over complex terrain, International Journal of Remote Sensing, 29, 4097-4110, 2008.

Dozier, J.: Opportunities to improve hydrologic data, Reviews of Geophysics, 30, 315-331, 1992.

Ebert, E. and McBride, J.: Verification of precipitation in weather systems: Determination of systematic errors, Journal of Hydrology, 239, 179-202, 2000.

Enku, T., Tadesse, A., Yilak, D. L., Gessesse, A. A., Addisie, M. B., Abate, M., Zimale, F. A., Moges, M. A., Tilahun, S. A., and Steenhuis, T. S.: Biohydrology of low flows in the humid Ethiopian highlands: The Gilgel Abay catchment, Biologia, 69, 1502-1509, 2014.

Ferriday, J. G.: Satellite remote sensing of global rainfall using passive microwave radiometry, Univ. of Colorado, Colorado Center For Astrodynamics Research, Boulder, CO (United States), 1994.

Fuka, D. R., Walter, M. T., MacAlister, C., Degaetano, A. T., Steenhuis, T. S., and Easton, Z. M.: Using the Climate Forecast System Reanalysis as weather input data for watershed models, Hydrological Processes, 2013. 2013.

Haerter, J., Hagemann, S., Moseley, C., and Piani, C.: Climate model bias correction and the role of timescales, Hydrology and Earth System Sciences, 15, 1065-1079, 2011.

Heinemann, T. and Kerényi, J.: The EUMETSAT multi sensor precipitation estimate (MPE): Concept and validation, 2003.

Hong, Y.: Precipitation Estimation from Remotely Sensed Information using Artificial Neural Network-Cloud Classification System, 2003. 2003.

Huffman, G. J., Bolvin, D. T., Nelkin, E. J., Wolff, D. B., Adler, R. F., Gu, G., Hong, Y., Bowman, K. P., and Stocker, E. F.: The TRMM multisatellite precipitation analysis (TMPA): Quasi-global, multiyear, combined-sensor precipitation estimates at fine scales, Journal of Hydrometeorology, 8, 38-55, 2007.

Jarvis, A., Reuter, H. I., Nelson, A., and Guevara, E.: Hole-filled seamless SRTM data V4, International Centre for Tropical Agriculture (CIAT), 2008. 2008.

Jobard, I., Chopin, F., Bergés, J., Ali, A., Lebel, T., and Desbois, M.: Presentation of the EPSAT-SG method and comparison with other satellite precipitation estimations in the frame of Precip-AMMA, 2007, 10062.

Joyce, R. J., Janowiak, J. E., Arkin, P. A., and Xie, P.: CMORPH: A method that produces global precipitation estimates from passive microwave and infrared data at high spatial and temporal resolution, Journal of Hydrometeorology, 5, 487-503, 2004.

Kidd, C.: Satellite rainfall climatology: A review, International Journal of Climatology, 21, 1041-1066, 2001.

Kidd, C., Kniveton, D. R., Todd, M. C., and Bellerby, T. J.: Satellite rainfall estimation using combined passive microwave and infrared algorithms, Journal of Hydrometeorology, 4, 1088-1104, 2003.

Kirchner, J. W.: Getting the right answers for the right reasons: Linking measurements, analyses, and models to advance the science of hydrology, Water Resources Research, 42, 2006.

Kokkonen, T. S., Jakeman, A. J., Young, P. C., and Koivusalo, H. J.: Predicting daily flows in ungauged catchments: model regionalization from catchment descriptors at the Coweeta Hydrologic Laboratory, North Carolina, Hydrological Processes, 17, 2219-2238, 2003.

Lindström, G., Johansson, B., Persson, M., Gardelin, M., and Bergström, S.: Development and test of the distributed HBV-96 hydrological model, Journal of hydrology, 201, 272-288, 1997.

Michéli, E., Schad, P., Spaargaren, O., Dent, D., and Nachtergaele, F.: World reference base for soil resources 2006. World Soil Resources ISBN 92-5-105511-4, Rome, (161 pp.) pp., 2006.

Moriasi, D., Arnold, J., Van Liew, M., Bingner, R., Harmel, R., and Veith, T.: Model evaluation guidelines for systematic quantification of accuracy in watershed simulations, Trans. Asabe, 50, 885-900, 2007.

Ochoa, A., Pineda, L., Crespo, P., and Willems, P.: Evaluation of TRMM 3B42 precipitation estimates and WRF retrospective precipitation simulation over the Pacific–Andean region of Ecuador and Peru, Hydrology and Earth System Sciences, 18, 3179-3193, 2014.

Overeem, A., Leijnse, H., and Uijlenhoet, R.: Country-wide rainfall maps from cellular communication networks, Proceedings of the National Academy of Sciences, 110, 2741-2745, 2013.

Piani, C., Haerter, J., and Coppola, E.: Statistical bias correction for daily precipitation in regional climate models over Europe, Theoretical and Applied Climatology, 99, 187-192, 2010a.

Piani, C., Weedon, G., Best, M., Gomes, S., Viterbo, P., Hagemann, S., and Haerter, J.: Statistical bias correction of global simulated daily precipitation and temperature for the application of hydrological models, Journal of Hydrology, 395, 199-215, 2010b.

Romilly, T. and Gebremichael, M.: Evaluation of satellite rainfall estimates over Ethiopian river basins, Hydrology and Earth System Sciences, 15, 1505-1514, 2011.

Scofield, R. A. and Kuligowski, R. J.: Status and outlook of operational satellite precipitation algorithms for extreme-precipitation events, Weather and Forecasting, 18, 1037-1051, 2003.

Seibert, J.: Regionalisation of parameters for a conceptual rainfall-runoff model, Agricultural and forest meteorology, 98, 279-293, 1999.

Silberstein, R.: Hydrological models are so good, do we still need data?, Environmental Modelling & Software, 21, 1340-1352, 2006.

SMHI: Integrated Hydrological Modelling System (IHMS). Manual Version 5.10. Swedish Meteorological and Hydrological Institute., 2006.

Sorooshian, S., Hsu, K.-L., Gao, X., Gupta, H. V., Imam, B., and Braithwaite, D.: Evaluation of PERSIANN system satellite-based estimates of tropical rainfall, Bulletin of the American Meteorological Society, 81, 2035-2046, 2000.

Teutschbein, C. and Seibert, J.: Bias correction of regional climate model simulations for hydrological climate-change impact studies: Review and evaluation of different methods, Journal of Hydrology, 456, 12-29, 2012a.

Teutschbein, C. and Seibert, J.: Is bias correction of Regional Climate Model (RCM) simulations possible for non-stationary conditions?, Hydrology and Earth System Sciences Discussions, 9, 12765-12795, 2012b.

Thorne, V., Coakeley, P., Grimes, D., and Dugdale, G.: Comparison of TAMSAT and CPC rainfall estimates with raingauges, for southern Africa, International Journal of Remote Sensing, 22, 1951-1974, 2001.

Tian, Y., Peters-Lidard, C. D., Choudhury, B. J., and Garcia, M.: Multitemporal analysis of TRMM-based satellite precipitation products for land data assimilation applications, Journal of Hydrometeorology, 8, 1165-1183, 2007.

Toté, C., Patricio, D., Boogaard, H., van der Wijngaart, R., Tarnavsky, E., and Funk, C.: Evaluation of Satellite Rainfall Estimates for Drought and Flood Monitoring in Mozambique, Remote Sensing, 7, 1758-1776, 2015.

Uhlenbrook, S., Mohamed, Y., and Gragne, A.: Analyzing catchment behavior through catchment modeling in the Gilgel Abay, Upper Blue Nile River Basin, Ethiopia, Hydrology and Earth System Sciences, 14, 2153-2165, 2010.

Wale, A., Kaba, E., Mengeste, A., Workaferahu, A., Mulken, M., and Aemro, B.: Opportunities of the Low-Cost Satellite Image Reception Station Established at GIS & RS Center of Bahir Dar University, Institute of Technology, 2nd Symposium on biodiversity and Natural Conservation at Arba Minch University, Ethiopia (June 03-05, 2010), 2011.

Wale, A., Rientjes, T., Gieske, A., and Getachew, H.: Ungauged catchment contributions to Lake Tana's water balance, Hydrological processes, 23, 3682-3693, 2009.

Worqlul, A., Collick, A., Tilahun, S., Langan, S., Rientjes, T., and Steenhuis, T.: Comparing TRMM 3B42, CFSR and ground-based rainfall estimates as input for hydrological models, in data scarce regions: the Upper Blue Nile Basin, Ethiopia, Hydrology and Earth System Sciences Discussions, 12, 2081-2112, 2015a.

Worqlul, A., Maathuis, B., Adem, A., Demissie, S., Langan, S., and Steenhuis, T.: Comparison of TRMM, MPEG and CFSR rainfall estimation with the ground observed data for the Lake Tana Basin, Ethiopia, Hydrology and Earth System Sciences Discussions, 11, 8013-8038, 2014a.

Worqlul, A. W., Collick, A. S., Rossiter, D. G., Langan, S., and Steenhuis, T. S.: Assessment of surface water irrigation potential in the Ethiopian highlands: The Lake Tana Basin, Catena, 129, 76-85, 2015b.

Worqlul, A. W., Maathuis, B., Adem, A. A., Demissie, S. S., Langan, S., and Steenhuis, T. S.: Comparison of rainfall estimations by TRMM 3B42, MPEG and CFSR with ground-observed data for the Lake Tana basin in Ethiopia, Hydrology and Earth System Sciences, 18, 4871-4881, 2014b.

CHAPTER 5: PREDICTING DISCHARGE DISPARITIES OF NEARBY WATERSHEDS USING PHYSICAL CATCHMENT CHARACTERISTICS IN THE LAKE TANA BASIN ETHIOPIA

Abstract

Stream water quantity and quality are dependent on the physical characteristics of a catchment. The effect of physical catchment characteristics (PCCs) on river flow is not adequately investigated in the upper Blue Nile River Basin. We selected two adjacent watersheds, Ribb and Gumara, of comparable area but significantly different long-term mean annual yield to investigate the effects of PCCs. To understand the characteristics which possibly affect the flow, more than twenty physical catchment characteristics were extracted for both rivers from climate data, physiographical characteristics, geological characteristics, land use, and soil, and a relative percentage difference was calculated. Subsequently the Soil and Water Assessment Tool (SWAT) was used to relate mathematically the watershed characteristic and climate with the discharge for both watersheds by calibrating against the discharge from 1995 to 2004. Finally, the areal average model parameters established in SWAT for Gumara at the hydrologic response unit (HRU) and sub-basin-levels were used to rerun the Ribb model. The percentage difference in physical catchment characteristics indicated no appreciable difference in climate and physiographic characteristics, a moderate difference was observed in land cover/land use type; and a major variation was observed in the soil types. SWAT model fitted the daily discharge well with a Nash-Sutcliffe Efficiency (NSE) of 0.68 and 0.71 for Ribb and Gumara, respectively and with a PBIAS of less than 10%. The percent difference of fitted model parameters captured the major variation of soil characteristics with significant differences in ground water, saturated

hydraulic conductivity, and soil depth parameters. The result of rerunning Ribb with Gumara areal parameters indicated a minor increase of flow in the Ribb River after Ribb calibrated parameters were rerun in combination with Gumara areal slope, soil and channel parameters. Ribb river flow significantly increased while simulated with Gumara areal runoff, evaporation and groundwater parameters. Furthermore, the Ribb model reran with Gumara rainfall, assuming Ribb watershed receives the same amount of Gumara areal rainfall, indicated annual average river flow of Ribb would increase by 4.3 %.

5.1 Introduction

The observations made on the large variation in the annual yield of two adjacent watersheds in the Lake Tana sub-basin of the upper Blue Nile Basin is a major motivation for this research. The two adjacent watersheds, Ribb and Gumara are major tributaries of Lake Tana sub-basin covering 25% of the watershed. The gauged parts of those two watersheds share a 45 km long boundary and have comparable area. However the long-term mean annual yield (1994 – 2008) of Gumera watershed at 9580 m3/ha/year is over 2 times that of Ribb which yields 3920 m3/ha/year (Wale et al., 2009). Despite an extensive existing knowledge base with respect to the stream discharge modeling for the two watersheds (Kebede et al., 2006; Rientjes et al., 2011; Setegn et al., 2008; Wale et al., 2009) this disparity in the long-term mean annual yield has not been explained. We hypothesize that given the prevailing comparable climatic conditions physical catchment characteristics (PCCs) are major drivers for the large disparity in the long-term annual yield of these watersheds.

Stream flow is governed by watershed characteristics, vis-à-vis physiographic elements, geology, land-use, soil and climate characteristics. Physiographic characteristics include size and shape as

well as elevation and its derivatives. The size of a watershed determines the yield in a given watershed. A previous report in the Lake Tana Basin by SMEC (2007) suggested that area is a dominant factor in estimating runoff, and used the area ratio method to estimate runoff from the ungauged part of the watershed. The shape of a watershed determines the way that runoff will bunch-up at the outlet and hence dictates the shape of the stream hydrograph while slope controls runoff response to a rainfall event in a given watershed. Slope also affects the time of concentration thereby contributing to the shape of the hydrograph (Singh, 1992). The geological characteristics; drainage pattern and density reflect the ease with which flow will accumulate to generate surface runoff. The higher the drainage density the more quickly water drains to a river with limited infiltration (Post and Jakeman, 1999). Land-use change affects the surface roughness, infiltration characteristics and the amount of water evaporated in to the air (Fohrer et al., 2001). Various researchers have simulated the impact of land-use change on the river flow (Bronstert et al., 2002; Hundecha and Bárdossy, 2004; Lørup et al., 1998). Some of such land-use changes include urbanization and conversion of dominantly cultivated land to woodland or vice versa. The runoff process is also dictated by the soil characteristics, with soil governing the infiltration and subsurface storage processes. Climate characteristics which include precipitation, temperature, wind speed, relative humidity can also affect the hydrological balance by affecting the proportion of evaporation and rainfall and consequently affecting the runoff volume. Climatic characteristics are of less significance for relatively small watersheds located adjacent to one another. The extraction of these watershed characteristics will be a first step to explain if yield disparities are due to these characteristics. Such characteristics of a given watershed can be used as pseudo characteristics in setting up a hydrologic model for an adjacent watershed under comparison.

In this paper we used models in the strictest sense as a mathematical construct that relates watershed characteristics, climate (including rainfall) and watershed discharge. Several models have been used in Ethiopia highlands including Parameter Efficient Distributed (PED) (Steenhuis et al., 2009; Tilahun et al., 2013) and Hydrologiska Byråns Vattenbalansavdelning (HBV) (Abdo et al., 2009; Wale et al., 2009) among others to capture the observed flow. Although they have performed well, we have chosen a physically based distributed hydrological model Soil and Water Assessment Tool (SWAT) (Arnold et al., 1998), since it is employs directly the landscape parameters measured to simulate daily observed discharges while others such as HBV and PED are lumped distributed models and do not include specific watershed characteristics. (Neitsch et al., 2005) SWAT uses topographic information, climatic data, land-use and soil data as an input for runoff simulation and can be used to examine the effect of these characteristics. The calibrated SWAT model is expected to represent the effect of those watershed characteristics. It is assumed that model parameters are closely related to physical catchment characteristics, as the parameters are calibrated to represent the functional behavior of the catchment response (Merz and Blöschl, 2004). Multiple studies of regionalization (Kokkonen et al., 2003; Seibert, 1999; Wale et al., 2009) indicated that physical catchment characteristics have a strong relation with the model parameters. To capture the effects of watershed characteristics on discharge the areal average values of Gumara model parameters will be used to rerun Ribb model.

The main objective of this research is to examine the influence of physical catchment characteristics such as climate, geography and physiographic, geology, soil, land-use and land cover conditions on the dissimilar stream flow of two neighboring watersheds. And finally to

understand the effect of watershed characteristics on Ribb River runoff yield compared to the nearby Gumara River using SWAT hydrological model.

5.2 Martials and Methods

5.2.1 Study Area

The Ribb and Gumara watersheds are located in the Lake Tana sub-basin of upper Blue Nile basin and lies between 11^{o} 30'N, 37^{o} 30'E and 12^{o} 13'N, 38^{o} 25'E. The sub-basin is labeled as a growth corridor due to its considerable water and land resource which if developed properly will have a major contribution in increased agricultural productivity and consequently reduce poverty. Selected watersheds are of considerable importance due to the extensive water resource development investment being undertaken by the government of Ethiopia. With outlets located 19 km apart (Figure 5-1) Ribb and Gumara Rivers drain a watershed area of approximately 1300 and 1285 km^2 respectively extracted from a 90 m resolution Shuttle Radar Tomographic Mission (SRTM) Digital Elevation Model (DEM) (Jarvis et al., 2008).

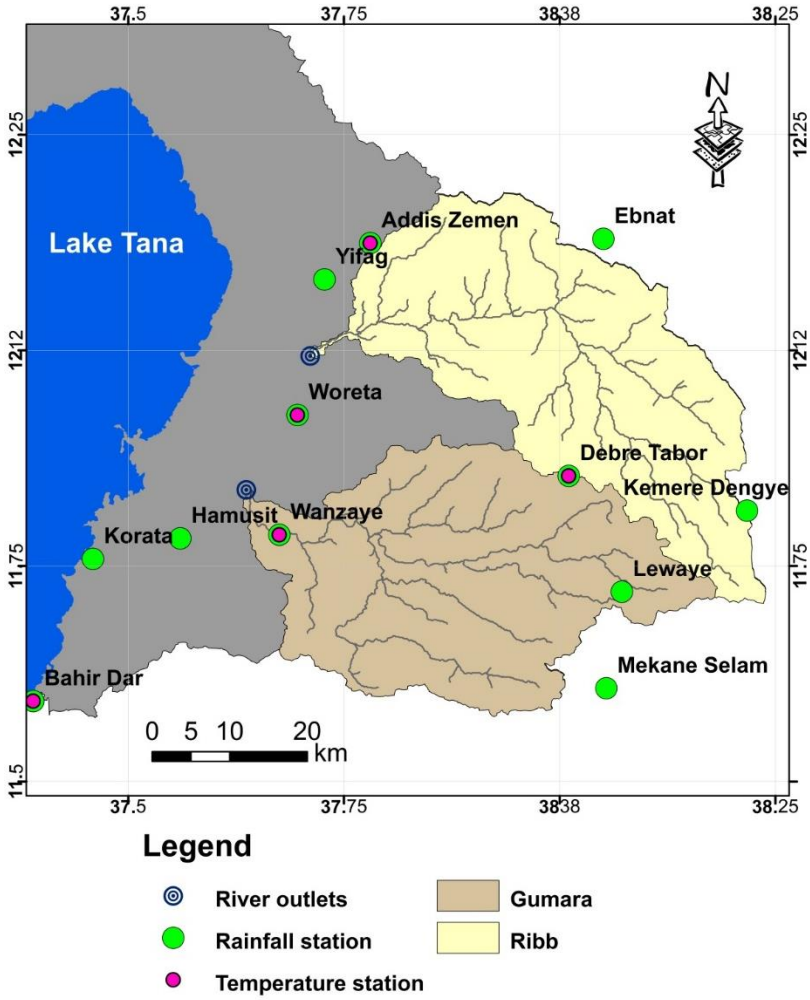

Figure 5-1: Spatial distribution of meteorological stations and river network in the Ribb and Gumara watersheds.

5.2.2 Data

Daily rainfall data of twelve nearby meteorological stations is obtained from the Metrological Agency of Ethiopia (MAE). Figure 5-1 shows the spatial distribution of rainfall and temperature measuring stations. Average annual rainfall (1994 – 2008) varies from 1000 to 1600 mm. Only five of these stations record minimum and maximum temperature. Stream flow data of the corresponding year is collected from Ministry of Water, Irrigation & Energy of Ethiopia (MWIEE) and checked for gross errors and missing data are filled using regression and spatial

interpolation methods. Ribb and Gumara rivers exhibit similar runoff pattern with a very high coefficient of determination (0.98) on a monthly basis for the study period see Figure 5-2. For both rivers the long-term average monthly discharge is maximum in August and minimum around March and April. The long-term average annual runoff (1994 – 2008) shows 480 MCm for Ribb and 1130 MCm for Gumara.

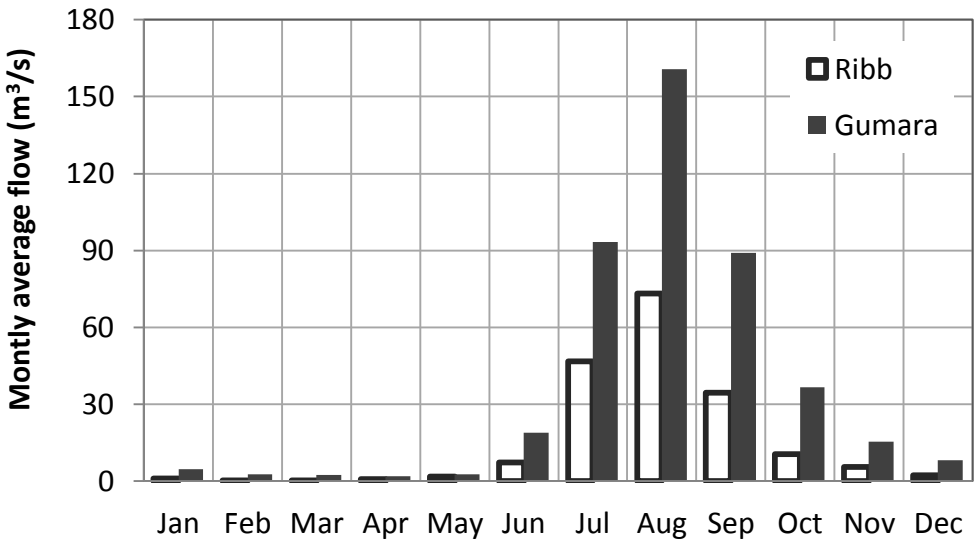

Figure 5-2: Long-term monthly average runoff of Gumara and Ribb watersheds (1994 to 2008).

The spatial data required for the SWAT model are DEM, soil, and land-use data. A 90 m resolution DEM was used to delineate the watershed, analyze the drainage patterns, characterize the terrain and analyze shape parameters. Sub-basin parameters such as slope gradient, slope length of the terrain, and the stream network characteristics such as channel slope, length, and width were derived from the DEM. The soil and land-use data were obtained from MWIEE (BCEOM, 1999). Important soil properties are derived using pedotransfer functions and a soil database were built for use in SWAT. Relative humidity and wind speed is simulated using

weather generator developed for Bahir Dar and Debre Tabor stations using a 20 years of daily data.

5.2.3 Methods

Ribb and Gumara watersheds are located in a close proximity in the Lake Tana basin and they have a comparable catchment area but, the long-term average runoff of Gumara river is approximately twice that of Ribb river flow (from 1994 to 2008). So, to understand the effect of PCCs on the river flow, the following procedures are done: (1.) A total of twenty PCCs from observed metrological data, land-use, soil and a topographic data are extracted for both watersheds, and the characteristics are compared to each other to identify the difference in characteristics which possibly affect Ribb river flow. (2.) The Soil and Water Assessment Tool (SWAT) is used to relate mathematically the watershed characteristics, rainfall and discharge through model calibration (3.) To interchange the model parameters of Ribb and Gumara watersheds, the model parameters are compared to each other to see whether the parameters have captured the effect of the PCCs or not. Then, the areal average model parameters of Gumara extracted from the hydrologic response units and sub-watersheds are used to simulate the Ribb River flow. The procedure of transferring the model parameters of Gumara to Ribb will answer the question: what if the Ribb behaves like Gumara watershed. The average values of Gumara model parameters are used to rerun Ribb model with seven scenarios listed below:

Scenario one: rerunning calibrated and validated Ribb model parameters with areal average values of Gumara evaporation and runoff controlling parameters CN2, CANMX, ESCO and EPCO.

Scenario two: rerunning calibrated and validated Ribb model parameters with areal average values of Gumara slope parameters SLSUBBSN and HRU_SLP.

Scenario three: rerunning calibrated and validated Ribb model parameters with areal average values of Gumara soil parameters SOL_AWC(1), SOL_Z(1), SOL_ALB(1) and SOL_K (1).

Scenario four and five: rerunning calibrate and validate Ribb watershed model with the areal groundwater and channel parameters of Gumara, respectively.

Scenario six: simulating Ribb model using areal average model parameters of Gumara to see the integrated effect of the model parameters on Ribb river flow.

Scenario seven: calibrated and validated Ribb watershed model is simulated using Gumara areal rainfall (1994 - 2008).

5.2.3.1 Physical Catchment Characteristics

From the perspective of a modeler, a watershed is a hydrologic unit that translates rainfall and evaporation into surface runoff, interflow and deep percolation based on physical catchment characteristics that can be grouped into five major classes, those are: climate characteristic, geography and physiography, geology, land-use and cover and soil condition.

Climate characteristics: include precipitation, temperature, wind, relative humidity and other metrological elements for a given region over a long period. Potential evaporation is estimated by Penman-Monteith approach. Using the nearby meteorological stations data from 1994 to 2008 areal rainfall and evaporation is estimated by inverse distance interpolation technique. Climate index is also computed which is the ratio of long-term annual rainfall and evapotranspiration.

Physiographical characteristics: includes size and shape of the watershed, average elevation, and slope characteristics, which are extracted using the 90 meter resolution DEM. ***Geological characteristics***: includes drainage features (pattern, drainage density, etc.). Drainage density of the watersheds is extracted from the SRTM DEM using the ArcGIS SWAT interface. ***Land-use and cover characteristics***: can affect the hydrological balance of the watershed by changing magnitude and pattern of runoff, peak flow and groundwater levels. The land-use and cover condition collected from MWIEE GIS department accomplished in 1998 as part of the Abay master plan consists of bare land, cropland, forest, grassland, woody savannah and urban. ***Soil characteristics***: runoff generally occurs when the rainfall intensity exceeds the infiltration capacity of the soil or after the soil is fully saturated. The soil map of the study area is also collected from the MWIEE. The soil map is classified into six groups consisting of: Eutric Fluvisols, Eutric Leptosols, Haplic Luvisols, Chromic Luvisols, Haplic Nitisols and Eutric Vertisols for both watersheds.

5.2.3.2 River Discharge Characteristics

Ribb and Gumara rivers exhibit similar runoff pattern with a very high coefficient of determination (0.98) on a monthly basis for the study period. Base flow of both rivers which maintains the stream flow during dry period (Hall, 1968) was separated using daily time-series flow data. Separation is performed to determine the proportion of the base flow and quick flow of the hydrograph using filter based technique.

Base Flow Index (BFI) (Lacey and Grayson, 1998) which is a measure of base flow characteristics of a catchment, defined as total volume of mean annual base flow divided by the total volume of mean annual flow is used to compare both watersheds. A digital filter by Lyne

and Hollick (1979) is used to characterize the BFI. The Lyne and Hollick (1979) method separates high frequency and low frequency signals. High frequency waves are associated with direct runoff, and low frequency waves are associated with the base flow component. Eq. (1) shows the Lyne and Hollick (1979) digital filter used for base flow separation. Base flow is separation is done by fine tuning the parameter Alpha to match with the observed flow in the recession part of the hydrograph, which has a value ranging from 0.95 to 0.99

$$q_t = \alpha * q_{t-1} + \frac{(1+\alpha)}{2} * (Q_t - Q_{t-1}) \qquad \text{Eq. (1)}$$

Where Qt is stream flow at time t and qt is the corresponding quick response component, Qt-1 is stream flow at time t-1 and qt-1 is the corresponding quick response component, Alpha (α) is the filter parameter associated with the catchments and base flow is the difference between the total discharge and the quick response component.

5.2.3.3 SWAT Description

In the Soil and Water Assessment Tool (SWAT) (Arnold et al., 1998) the watershed is first subdivide into sub-basins based on the topography, and then each sub-basin is further subdivided into a series of Hydrologic Response Units (HRUs), which have a unique soil, land-use and slope combinations. Soil water content, nutrient cycles, surface runoff, crop growth, sediment yield and management practices are simulated for each HRU and then aggregated for the sub-basin by a weighted average (Abbaspour et al., 2007). A complete detail of the model concept and its components is provided by Arnold et al. (2012). The general water balance equation used in the model is described under Eq. 2.

$$SW_t = SW_{t-1} + \sum_1^t \left(P_i - Q_{surf,i} - ET_i - Q_{loss,i} - Q_{gw,i}\right) \qquad \text{Eq. (2)}$$

Where: SW_t is the soil water content above the wilting point at the end of day t. P_i is the amount of precipitation on day i and $Q_{surf,i}$, ETi, $Q_{loss,i}$ and $Q_{gw,i}$ are the daily amounts of surface runoff, evapotranspiration, percolation into deep aquifer, and lateral subsurface flow, respectively. All components are estimated as mm water.

5.2.3.4 Calibration and validation of SWAT

The watersheds are delineated with a similar drainage threshold number of 8000 ha. This threshold was selected to balance between the spatial resolutions of the input data and to limit the number of sub watersheds for initialization. The result of watershed delineation indicated 9 and 11 sub-watersheds for Ribb and Gumara respectively. The sub-watersheds are further subdivided into multiple HRUs without excluding marginal land-use groups below a certain threshold percentage; the result indicates 222 and 227 HRUs for Ribb and Gumara, respectively.

There are two options available for calibration of the SWAT model: manual or auto-calibration using SWAT-CUP (Calibration and Uncertainty Programs) (Abbaspour et al., 2007). In this paper the Generalized Likelihood Uncertainty Estimation (GLUE) procedure of SWAT-CUP is used for sensitivity analysis and model calibration. GLUE algorithms account for several sources of uncertainties such as uncertainty in driving variables (e.g., rainfall), conceptual model, parameters, and measured data (Setegn et al., 2008).

SWAT model parameters selected to represent PCCs are identified based on the previous study in the Lake Tana area which affected river flow (Bitew and Gebremichael, 2011; Dile et al., 2013; Setegn et al., 2009; Setegn et al., 2010). In addition, a few additional parameters are included to represent PCCs soil, land-use/land cover and slope characteristics. Model parameters used for flow calibration are: SCS runoff curve number (CN2), soil evaporation compensation

factor (ESCO), Manning's "n" value for the main channel (CH_N2), available water capacity of the soil layer (SOL_AWC), depth from soil surface to bottom of layer (SOL_Z), Groundwater "revap" coefficient (GW_REVAP), groundwater delay (days) (GW_DELAY), base flow alpha factor (days) (ALPHA_BF), threshold depth of water in the shallow aquifer required for return flow to occur (mm) (GWQMN), threshold depth of water in the shallow aquifer for "revap" to occur (mm) (REVAPMN), maximum canopy storage (CANMX), plant uptake compensation factor (EPCO), average slope length (SLSUBBSN), moist soil albedo (SOL_ALB), saturated hydraulic conductivity (SOL_K), average slope steepness (HRU_SLP), average slope of main channel (CH_S2) and average slope of tributary channels (CH_S1). The types of change applied to calibrate the parameters are 'v_' meaning the existing parameter value will be replaced by a given value, 'a_' meaning a given quantity should be added to the existing parameter and 'r_' meaning the existing parameter should be multiplied by (1 + a given value) (Abbaspour et al., 2007). The soil parameters (including SOL_AWC, SOL_K, SOL_ALB) are optimized with a percentage correction of the values derived from the pedotransfer functions.

5.2.3.5 Multiple objective functions

The simulation period is split in to a warm-up (1994), calibration (1995 to 2004) and validation (2005 to 2008) periods. How well the watersheds characteristics could represent the river outflow is evaluated using multiple objective functions Percentage Bias (PBIAS), Coefficient of Determination (R-Squared) and Nash Sutcliff Efficiency (NSE). These objective functions should not be used alone. PBIAS Eq. (3): would not tell us the distribution of observed and simulated flow through time but it will tell only the cumulative volume difference between simulated and observed flow for the study period. R-Square Eq. (4): addresses the degree of linear association between the observed and simulated flow. For a perfect fit regression, slope

and intercept has to be one and zero, respectively. NSE Eq. (5): tells as the relative magnitude of the simulated residual variance compared to the observed data variance. NSE also must be used in combination with some other volumetric objective functions otherwise, it will lead as to a wrong conclusion if the standard deviation of the observed variable is too large compared to the simulated variance.

$$\mathrm{RVE} = \left(\frac{\sum_{i=1}^{n} Q_{sim(i)} - \sum_{i=1}^{n} Q_{Obs(i)}}{\sum_{i=1}^{n} Q_{Obs(i)}}\right) * 100 \qquad \text{Eq. (3)}$$

RVE: varies between negative infinity and positive infinity, but performs best when a value of zero is generated.

$$\mathrm{R-Squared} = \left(\frac{n\sum Q_{Obs(i)}Q_{sim(i)} - (\sum Q_{Obs(i)})(\sum Q_{sim(i)})}{\sqrt{\left[n(\sum Q_{Obs(i)}{}^2) - (\sum Q_{Obs(i)})^2\right]\left[n(\sum Q_{sim(i)}{}^2) - (\sum Q_{sim(i)})^2\right]}}\right)^2 \qquad \text{Eq. (4)}$$

R-squared value can range from zero to one, where zero indicates no correlation and one represents perfect correlation.

$$\mathrm{NSE} = 1 - \frac{\sum_{i=1}^{n}(Q_{sim(i)} - Q_{Obs(i)})}{\sum_{i=1}^{n}(Q_{Obs(i)} - \bar{Q}_{obs(i)})} \qquad \text{Eq. (5)}$$

NSE value can ranges between negative infinite and one, but a perfect fit between the simulated and observed data indicates a NSE value of one. NSE values less than zero indicates that, the mean of observed flow is better than the model predictions.

Where: RVE: Relative Volume Error, R-Squared: Coefficient of Determination, NSH: Nash-Sutcliff Efficiency, $Q_{sim(i)}$: simulated flow, $Q_{obs(i)}$: observed flow and n: number of simulated and observed data pairs and $\bar{Q}_{obs(i)}$: average of observed flow.

5.3 Results and Discussion

5.3.1 Physical catchment characteristics

The percentage difference in **Error! Not a valid bookmark self-reference.** indicated no appreciable difference in climate characteristic and physiographic characteristics between Ribb and Gumara watersheds. The annual average areal rainfall computed from 1994 to 2008 indicated that, on average the Gumara areal rainfall is more than Ribb areal rainfall by 170 mm/year, which accounts 13.5% of Ribb annual rainfall. Physiographic characteristics longest flow path length and circularity ratio are known to have no effect on annual river flow volume rather determine the shape of the flow hydrograph.

The moderate difference in land cover/land-use type is observed for bare land, grass land and woody savannah which represent a smaller proportion of the watershed area. Crop land constitutes a major proportion of land cover/land-use in both watersheds. With no vegetation at the onset of the rainy season the crop land generated a major proportion of the runoff. Nevertheless given the lower difference of crop land proportion and similar agricultural practices applied in the two catchments this land cover/land-use could not be a plausible explanation to the variation in the annual yield difference.

Table 5-1 below summarizes the PCCs extracted for Ribb and Gumara watersheds. The percentage difference of characteristics is computed as the difference in characteristics between Gumara and Ribb divided by the average.

The percentage difference in **Error! Not a valid bookmark self-reference.** indicated no appreciable difference in climate characteristic and physiographic characteristics between Ribb and Gumara watersheds. The annual average areal rainfall computed from 1994 to 2008 indicated that, on average the Gumara areal rainfall is more than Ribb areal rainfall by 170 mm/year, which accounts 13.5% of Ribb annual rainfall. Physiographic characteristics longest flow path length and circularity ratio are known to have no effect on annual river flow volume rather determine the shape of the flow hydrograph.

The moderate difference in land cover/land-use type is observed for bare land, grass land and woody savannah which represent a smaller proportion of the watershed area. Crop land constitutes a major proportion of land cover/land-use in both watersheds. With no vegetation at the onset of the rainy season the crop land generated a major proportion of the runoff. Nevertheless given the lower difference of crop land proportion and similar agricultural practices applied in the two catchments this land cover/land-use could not be a plausible explanation to the variation in the annual yield difference.

Table 5-1: Physical catchment characteristics of Ribb and Gumara Watersheds

Major PCCs group	**PCCs**	**Ribb**	**Gumara**	**Difference**	**Percentage difference**
Climate characteristic(from 1994 to 2008)	Areal rainfall (mm/year)	1265	1435	Moderate	6.30
	Areal Evaporation (mm/year)	1225	1234	Low	0.37
	Climate index	1.09	1.2	Low	4.80
Physiographic attributes	Catchment area (km^2)	1302	1284	Moderate	0.70
	Longest flow path length (km)	84.00	99.60	Low	8.50
	Circularity ratio	0.26	0.35	Low	14.75
	Average slope (degree)	21.55	17.88	Moderate	9.31
Geology and Soil	Drainage density (m/km^2)	301	284	Moderate	2.91
	% of Chromic Luvisols	39.70	24.40	Moderate	23.87
	% of Eutric Fluvisols	23.90	0.50	High	95.90
	% of Eutric Leptosols	36.20	8.20	High	63.06
	% of Eutric Vertisols	0.00	3.50	Low	100.0
	% of Haplic Luvisols	0.00	63.40	High	100.0
	% of Haplic Nitisols	0.20	0.00	Low	100.0
Land use/land cover	% of Bare Land	1.79	0.53	Moderate	54.31
	% of Crop Land	70.48	71.12	Low	0.45
	% of Forest	1.06	0.81	Low	13.37
	% of Grass Land	15.28	10.17	Moderate	20.08
	% of Urban and Build up	0.07	0.07	Low	0.00
	% of Woody savannah	11.31	17.29	Moderate	20.91
Base flow	Base flow index (BFI)	0.45	0.51	Moderate	6.25

A major variation in the two catchments is observed on their soil types. The difference in Eutric Fluvisiols, Eutric Leptosols and Haplic Luvisols are the major lead to explain the annual yield variation in the two watersheds. Ribb watershed is dominated with significant proportion of

Eutric Leptosols (36%) characterizes as shallow soil and extremely gravelly (Michéli et al., 2006). With Eutric Leptosols almost a quarter of the watershed area of Ribb watershed it possesses a higher ground water recharge potential. Haplic Luvisols and Chromic Luvisols covering 87% of the watershed area in Gumara watershed are characterized as having higher clay content (60%). The average slope of Ribb and Gumara is similar with a minor difference. The percentage slope distribution computed every five-degree interval from zero to 60 degree indicated a minor difference (Figure 5-3).

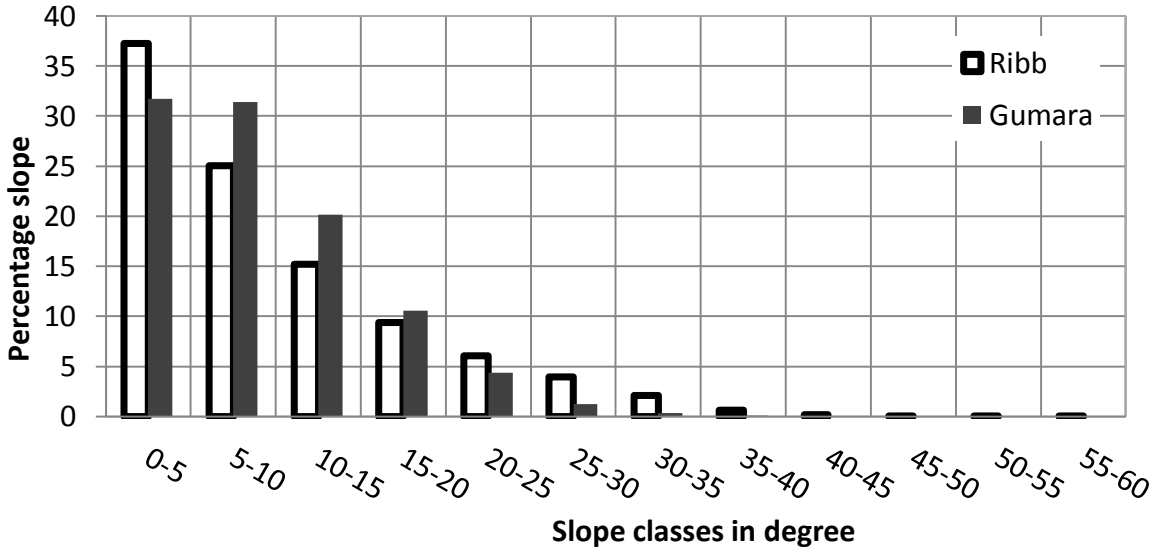

Figure 5-3: Slope distribution of Ribb and Gumara watersheds

The Baseflow separated by Lyne and Hollick (1979) approach is shown in

Table 5-2. The result indicated an average daily baseflow of 18.7m3/s and 7.0m3/s from 1994 to 2008 for Gumara and Ribb watersheds, respectively. For the study period the majority of flows in the Ribb is composed of quick flow which accounts 55% of the annual flow. Generally BFI for Gumara watershed is slightly larger than Ribb watershed; this indicates the groundwater contribution to Gumara watershed is slightly larger than Ribb watershed.

Table 5-2: Average baseflow index of Gumara and Ribb watersheds (1994-2008)

Watershed	Average stream flow m3/s	Average base flow m3/s	Base flow index (BFI)
Gumara	36.6	18.7	0.51
Ribb	15.5	7.0	0.45

5.3.2 Model sensitivity calibration and validation

Model parameters optimization and uncertainty analysis is done using GLUE algorithm incorporated within SWAT-CUP. The program allows parameter aggregation based on hydrologic group, soil, land-use and sub-basin (Abbaspour et al., 2007). Ribb and Gumara model parameter sets are iterated 14,000 times to converge to a maximum NSE for the calibration period (1995 to 2004).

The fitted model parameter sets and their relative sensitivities are tabulated in Table 5-3. The t-stat and p-value which are a measure of the significance of the sensitivity are also included. The t-stat provides a measure of sensitivity (a larger absolute values is more sensitive) and p-value determines the significance of the sensitivity (a value close to zero has more significance) Abbaspour et al. (2007). The result of relative sensitivity analysis indicated a value ranging from 92 to -34 and from 49 to -125 for Ribb and Gumara respectively. Among which, the most sensitive parameters in their relative order of sensitivity are CN2, ALPHA_BF, GWQMN and GW_REVAP for Gumara and CN2, ALPHA_BF and GWQMN for Ribb watershed.

The result of daily river flow simulation for the calibration period (1995 to 2004) indicated a reasonable performance with a NSE of 0.71 and 0.68 and RVE of 4% and 7% for Ribb and Gumara watersheds, respectively. Figure 5-4 and Figure 5-5 indicated daily calibrated vs.

observed flow of Ribb and Gumara watersheds respectively. The calibrated model validated from 2005 to 2008 has also indicated a reasonable performance with a NSE of 0.77 and 0.72 and RVE of 8% and 9% for Ribb and Gumara watersheds, respectively. See Table 5-3 the best fitted model parameter sets, there relative sensitivity and the performance of the model for calibration and validation period. Figure 5-6 indicates the spatial distribution of the long-term annual average runoff of Gumara and Ribb watersheds extracted from HRUs. Figure 5-6 indicated that most of the runoff is generated at the bottom of the hill at the flood plan area of both watersheds.

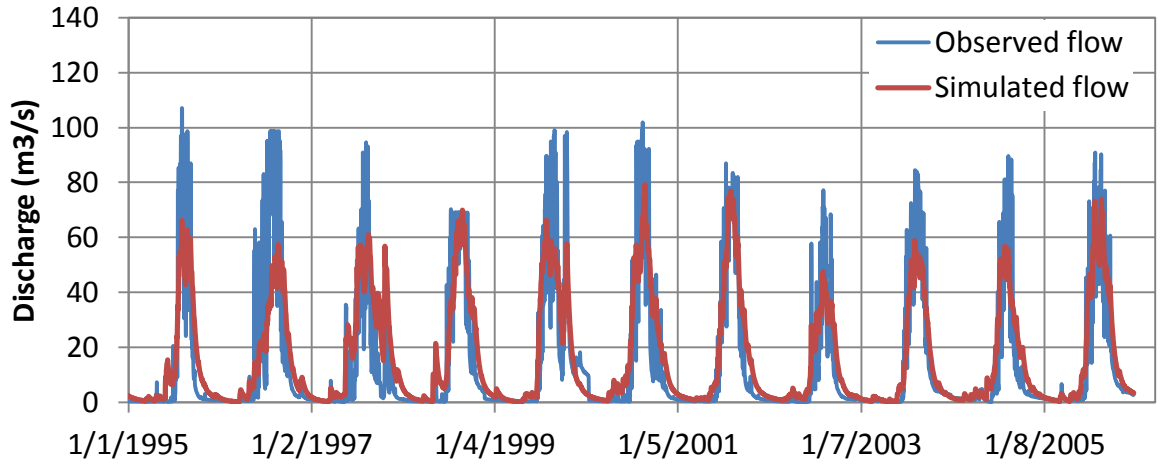

Figure 5-4: Daily simulated and observed flow of Ribb Watershed (1995 – 2005)

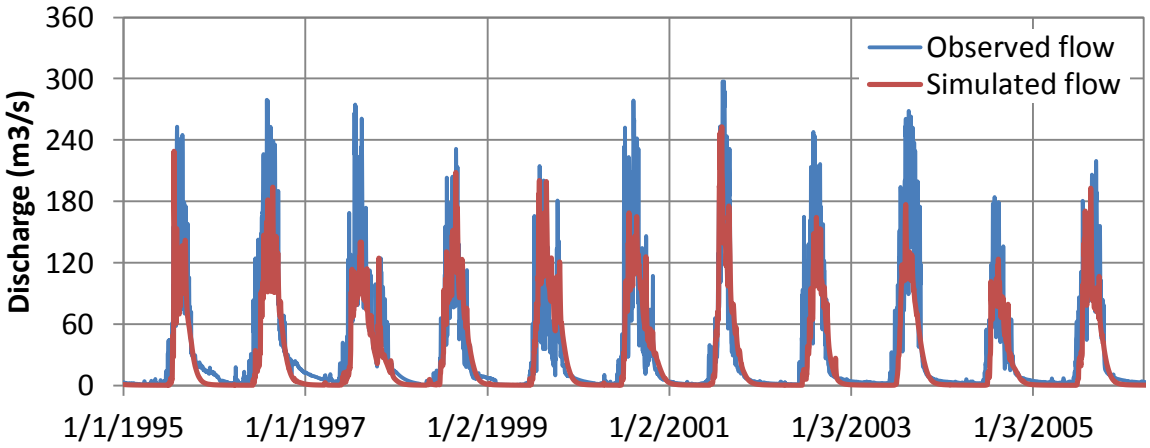

Figure 5-5: Daily simulated and observed flow of Gumara Watershed (1995 – 2005)

Table 5-3: Fitted model parameter sets with their respective relative sensitivity value for Ribb and Gumara watersheds

Model parameters	**Lower and upper bound**	**Gumara**			**Ribb**		
		Fitted value	t-stat	p-value	Fitted value	t-stat	p-value
r__CN2.mgt	±25%	4.7	41.93	0.00	-4.4	-125.86	0.00
v__CANMX.hru	±25%	4.09	-0.60	0.55	5.45	2.22	0.00
v__ESCO.hru	0 1.0	0.296	5.72	0.00	0.373	-5.13	0.00
v__EPCO.hru	0 1.0	0.399	-1.16	0.25	0.948	6.42	0.02
r__SLSUBBSN.hru	±25%	-13.0	0.67	0.50	9.3	1.45	0.15
r__HRU_SLP.hru	±25%	18.3	0.13	0.90	6.2	-0.56	0.57
r__SOL_AWC().sol	±25%	5	-8.76	0.00	-11.1	2.48	0.01
r__SOL_Z().sol	±25%	11.3	0.06	0.95	-25.6	1.74	0.08
r__SOL_ALB().sol	±25%	4.5	-0.80	0.42	-25.0	-1.13	0.26
r__SOL_K().sol	±25%	-2.8	-7.11	0.00	25.0	1.29	0.20
v__GW_REVAP.gw	0.02 0.2	0.096	-21.35	0.00	0.061	4.36	0.00
v__GW_DELAY.gw	0.0 500	19.63	-8.73	0.00	343.85	3.57	0.00
v__ALPHA_BF.gw	0.0 1.0	0.091	-34.29	0.00	0.172	-26.59	0.00
v__GWQMN.gw	0.0 5000	1969	-32.40	0.00	3570	8.11	0.00
v__REVAPMN.gw	0.0 500	67.7	4.34	0.00	416.4	1.28	0.20
r__CH_N2.rte	±30%	18.7	11.26	0.00	-20.9	-0.78	0.43
r__CH_S2.rte	±30%	-10.4	-8.33	0.00	24.6	-1.88	0.06
r__CH_S1.sub	±30%	24.8	-0.40	0.00	-24.4	0.85	0.39
Calibration period (1995-2004)	NSE		0.71			0.68	
	R-squared		0.70			0.68	
	RVE (%)		4.0			7.0	
Validation period (2005-2008)	NSE		0.77			0.72	
	R-squared						
	RVE (%)						

Note: Parameters are constructed based on 'a_', 'v_' and 'r_' meaning an absolute increase, a replacement and a relative change to the initial parameter value respectively. t-value is a measure of sensitivity(larger t-value means more sensitive). p-value indicates the significance of the sensitivity (the smaller the p-value, the less chance of a parameter being by chance assigned as sensitive).

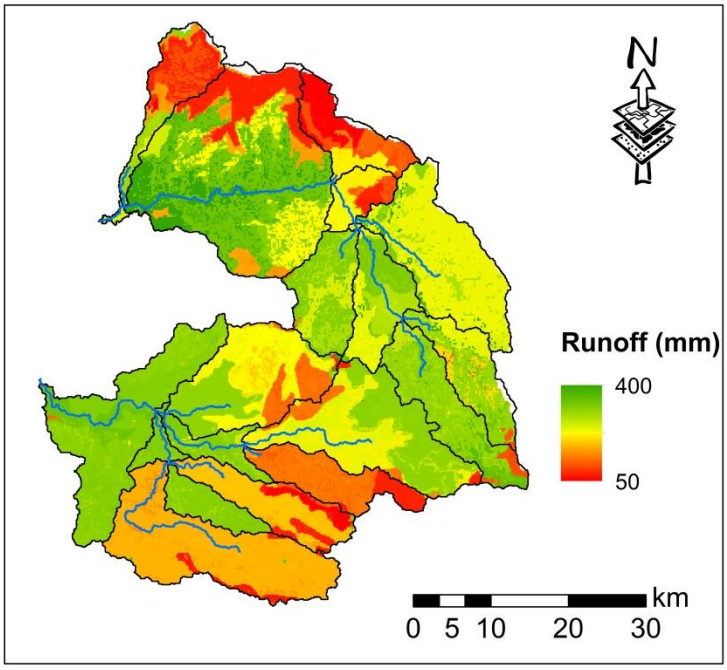

Figure 5-6: Long-term annual average surface runoff of Ribb and Gumara watersheds at HRU level

5.3.3 Effect of PCCs on the river flow

The best fitted model parameter sets of Gumara and Ribb extracted from each HRU's and sub-watersheds are used to estimate the areal average values (

Table 5-4). These areal average model parameters are categorized into six groups as runoff, evaporation, slope, soil, groundwater and channel parameters. A percentage difference of areal model parameters is computed as the difference in characteristics between Gumara and Ribb divided by the sum.

Table 5-4: Areal average model parameter value for Ribb and Gumara watersheds

Model parameters	Category	Ribb parameters	Gumara parameters	Relative percentage difference
r__CN2.mgt	Runoff	79.58	88.00	5.02
v__CANMX.hru	Runoff	5.45	4.09	14.26
v__ESCO.hru	Evaporation	0.37	0.30	10.45
v__EPCO.hru	Evaporation	0.95	0.40	40.74
r__SLSUBBSN.hru	Slope	40.61	36.09	5.89
r__HRU_SLP.hru	Slope	0.19	0.17	5.56
r__SOL_AWC(1).sol	Soil	0.13	0.10	13.04
r__SOL_Z(1).sol	Soil	156.38	237.13	20.52
r__SOL_ALB(1).sol	Soil	0.10	0.09	5.26
r__SOL_K(1).sol	Soil	4.40	2.99	19.08
v__GW_REVAP.gw	Groundwater	0.06	0.10	25.00
v__GW_DELAY.gw	Groundwater	343.85	19.63	89.20
v__ALPHA_BF.gw	Groundwater	0.17	0.09	30.77
v__GWQMN.gw	Groundwater	3570.89	1969.08	28.91
v__REVAPMN.gw	Groundwater	416.42	67.69	72.04
r__CH_N2.rte	Channel	0.01	0.02	33.33
r__CH_S2.rte	Channel	0.02	0.01	33.33
r__CH_S1.sub	Channel	0.05	0.03	25.00

The areal average values of fitted model parameters indicated a significant difference in groundwater and soil parameters which is consistent with the watershed characteristics where those two watersheds are dominated by different soil groups.

The possible effect of PCCs on annual yield of Ribb River is quantified by rerunning the calibrated and validated Ribb model with the areal average model parameters and areal rainfall of Gumara watershed. Before rerunning Ribb with Gumara average model parameters, Gumara model was simulated with areal average model parameters. The result indicated acceptable performance with a NSE of 0.62, indicating those average values are representative of Gumara characteristics.

The result of Ribb model simulated for seven scenarios as indicated in section 2.3 is shown under Table 5-5 and Figure 5-7. The result indicated a significant flow increase of Ribb when simulated in combination with Gumara areal runoff and evaporation parameters (Scenario one). Out of the runoff and evaporation parameters (Scenario one) the most sensitive parameter is CN2, which is a function of land use, soil and slope characteristics. The percentage difference of the plant uptake compensation factor (EPCO) and soil evaporation compensation factor (ESCO) is large approximately 40.7 and 10.5%, respectively and they are significantly sensitive model parameter as t-stat and p-value indicated in Table 5-3. Ribb calibrated and validated model parameters simulated with Gumara slope parameters which are less sensitive (Table 5-3) indicated insignificant effect on Ribb flow. Even though there is a significant difference between the fitted soil depth (SOL_Z), available water capacity (SOL_AWC) and saturated hydraulic conductivity (SOL_K) parameters, the result of Ribb flow simulation with Gumara soil parameters indicated insignificant difference. The relative difference between the fitted groundwater parameters was significant, and the annual flow volume increased by 13.3%. The ground water parameters have significantly affected the time to peak by one month approximately (Figure 5-7). The channel parameters which have a significant fitted value difference have a minor effect on Ribb River flow. Ribb model rerun by Gumara rainfall

assuming Ribb watershed receives the same amount of Gumara areal rainfall indicated an annual average river flow by 4.3%.

Table 5-5: Ribb model rerun with Gumara areal model parameters and areal rainfall (1995 to 2004)

Ribb rerun for different scenarios	**Average flow (m^3/s)**	**Percentage increased flow (%)**	**Annual runoff yield ($m^3/ha/year$)**
Ribb simulated flow	14.22	--	3444.9
Ribb calibrated parameters plus scenario 1	33.90	138.4	8211.0
Ribb calibrated parameters plus scenario 2	14.02	-1.5	3395.1
Ribb calibrated parameters plus scenario 3	14.36	1.0	3477.9
Ribb calibrated parameters plus scenario 4	16.12	13.3	3904.6
Ribb calibrated parameters plus scenario 5	14.22	0.01	3445.3
Ribb rerun using Gumara areal parameters	34.27	140.9	8299.5
Ribb calibrated parameters plus Gumara areal rainfall	14.82	4.3	3590.8

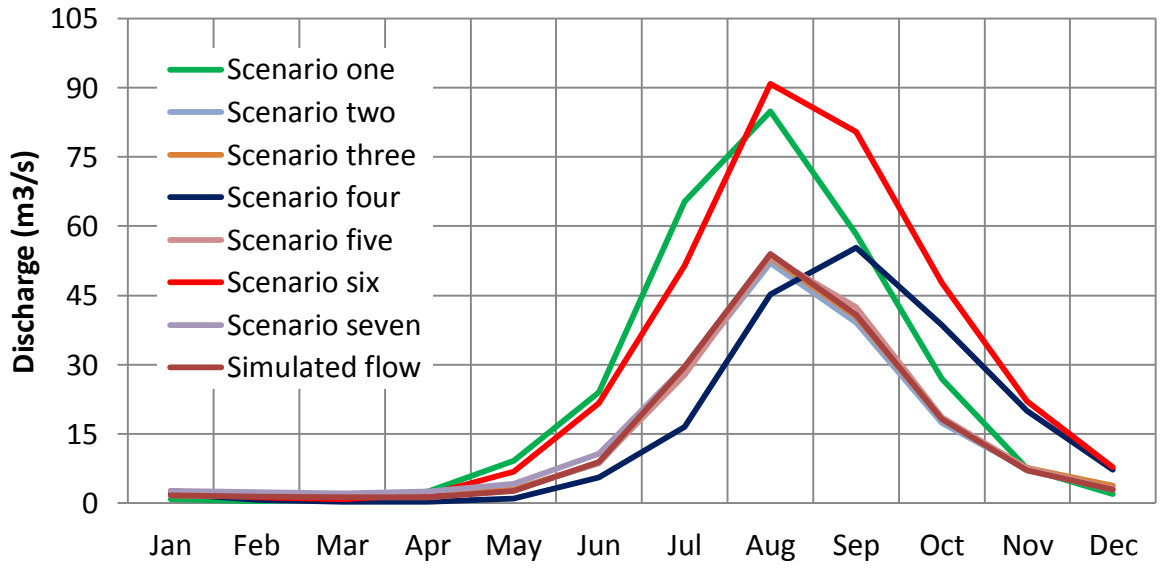

Figure 5-7: Monthly average Ribb model rerun with Gumara areal model parameters and areal rainfall (1995 to 2004)

The observed average annual runoff yield from 1994 to 2008 was 3920 and 9580 m3/ha/year for Ribb and Gumara, respectively. Ribb flow simulated by groundwater, areal rainfall and runoff parameters close the runoff difference significantly. Figure 5-7 and Table 5-5 shows the annual average long-term average flow and the percentage annual river flow increase for different scenarios.

5.4 Conclusions

This study evaluates the effect of watershed characteristics on the river flow by considering two nearby watersheds with comparable areas but with very high discharge disparities in the Upper Blue Nile Basin. To understand the effect of PCCs, the study has extracted multitude catchment characteristics from climate data, land-use, soil and topographic data. Then the percentage difference in physical catchment characteristics was identified. The spatially distributed hydrological model SWAT was used to represent the catchment characteristics through hydrological modeling with assumption that model parameters are closely related to physical catchment characteristics. Finally, the areal average model parameters values of Gumara are used to simulate Ribb river model to answer the effects of watershed characteristics on Ribb river flow. The PCCs result indicated that climate and physiographic attributes has no appreciable difference between the two watersheds. The average slope of Ribb and Gumara is similar with a minor difference in slope distribution. There is a moderate difference in land cover/land-use type. The moderate difference in land cover/land-use type is observed for bare land, grass land and woody savannah which represent a smaller proportion of the watershed area. A major variation in the two catchments is observed on their soil types. The difference in Eutric

Fluvisiols, Eutric Leptosols and Haplic Luvisols are the major lead to explain the annual yield variation in the two watersheds.

The hydrologic model SWAT has reasonably captured the observed flow through model calibration with a NSE of 0.71 and 0.68 for Gumara and Ribb watersheds, respectively from 1995 to 2004. The model was validated for a different period (2005-2008) and performed well with a NSE of 0.77 and 0.72 for Ribb and Gumara, respectively. The areal average values of fitted model parameters sets estimated averaged over the sub-watersheds and HRUs level indicated that, Ribb and Gumara have a significant difference on groundwater, channel, soil and evaporation controlling parameters. In this case we can say that SWAT has captured the major watershed characteristics difference. But the Ribb rerun with Gumara parameters indicated soil and channel parameters have insignificant effect. The ground water parameters can increase Ribb river flow by approximately 13%. The discharge disparities is mainly captured by the runoff and evaporation parameters where Ribb flow is increase by approximately 138% when simulated Gumara parameters. The discharge disparity is captured by increasing the water available for transpiration (EPCO), soil evaporation compensation factor (ESCO) and SCS curve number (CN2). The annual areal rainfall difference 170 mm/year through modelling indicated that it accounts 4.3% of Ribb River flow. After rerunning Ribb model for areal average values of Gumara watershed, it is indicated that Ribb flow will increase by 13.3%.

References

Abbaspour, K., Vejdani, M., and Haghighat, S.: SWAT-CUP calibration and uncertainty programs for SWAT, 2007.

Abdo, K., Fiseha, B., Rientjes, T., Gieske, A., and Haile, A.: Assessment of climate change impacts on the hydrology of Gilgel Abay catchment in Lake Tana basin, Ethiopia, Hydrological Processes, 23, 3661-3669, 2009.

Arnold, J., Moriasi, D., Gassman, P., Abbaspour, K., White, M., Srinivasan, R., Santhi, C., Harmel, R., Van Griensven, A., and Van Liew, M.: SWAT: Model use, calibration, and validation, Transactions of the ASABE, 55, 1491-1508, 2012.

Arnold, J. G., Srinivasan, R., Muttiah, R. S., and Williams, J. R.: Large area hydrologic modeling and assessment part I: Model development1. Wiley Online Library, 1998.

BCEOM: Abay River Basin integrated master plan, main report, Ministry of Water Resources, Addis Ababa, 1999.

Bitew, M. and Gebremichael, M.: Assessment of satellite rainfall products for streamflow simulation in medium watersheds of the Ethiopian highlands, Hydrology and Earth System Sciences, 15, 1147-1155, 2011.

Bronstert, A., Niehoff, D., and Bürger, G.: Effects of climate and land-use change on storm runoff generation: present knowledge and modelling capabilities, Hydrological Processes, 16, 509-529, 2002.

Dile, Y. T., Berndtsson, R., and Setegn, S. G.: Hydrological Response to Climate Change for Gilgel Abay River, in the Lake Tana Basin-Upper Blue Nile Basin of Ethiopia, PloS one, 8, e79296, 2013.

Fohrer, N., Haverkamp, S., Eckhardt, K., and Frede, H.-G.: Hydrologic response to land use changes on the catchment scale, Physics and Chemistry of the Earth, Part B: Hydrology, Oceans and Atmosphere, 26, 577-582, 2001.

Hall, F. R.: Base-Flow Recessions—A Review, Water Resources Research, 4, 973-983, 1968.

Hundecha, Y. and Bárdossy, A.: Modeling of the effect of land use changes on the runoff generation of a river basin through parameter regionalization of a watershed model, Journal of Hydrology, 292, 281-295, 2004.

Jarvis, A., Reuter, H. I., Nelson, A., and Guevara, E.: Hole-filled SRTM for the globe Version 4, available from the CGIAR-CSI SRTM 90m Database (http://srtm. csi. cgiar. org), 2008. 2008.

Kebede, S., Travi, Y., Alemayehu, T., and Marc, V.: Water balance of Lake Tana and its sensitivity to fluctuations in rainfall, Blue Nile basin, Ethiopia, Journal of hydrology, 316, 233-247, 2006.

Kokkonen, T. S., Jakeman, A. J., Young, P. C., and Koivusalo, H. J.: Predicting daily flows in ungauged catchments: model regionalization from catchment descriptors at the Coweeta Hydrologic Laboratory, North Carolina, Hydrological Processes, 17, 2219-2238, 2003.

Lacey, G. and Grayson, R.: Relating baseflow to catchment properties in south-eastern Australia, Journal of Hydrology, 204, 231-250, 1998.

Lørup, J. K., Refsgaard, J. C., and Mazvimavi, D.: Assessing the effect of land use change on catchment runoff by combined use of statistical tests and hydrological modelling: case studies from Zimbabwe, Journal of Hydrology, 205, 147-163, 1998.

Lyne, V. and Hollick, M.: Stochastic time-variable rainfall-runoff modelling, 1979, 89-93.

Merz, R. and Blöschl, G.: Regionalisation of catchment model parameters, Journal of Hydrology, 287, 95-123, 2004.

Michéli, E., Schad, P., Spaargaren, O., Dent, D., and Nachtergaele, F.: World reference base for soil resources: 2006: a framework for international classification, correlation and communication, FAO, 2006.

Neitsch, S. L., Arnold, J. G., Kiniry, J. R., King, K. W., and Williams, J. R.: Soil and Water Assessment Tool (SWAT) Theoretical Documentation., Blackland Research Center, 2005.

Post, D. A. and Jakeman, A. J.: Predicting the daily streamflow of ungauged catchments in SE Australia by regionalising the parameters of a lumped conceptual rainfall-runoff model, Ecological Modelling, 123, 91-104, 1999.

Rientjes, T. H., Perera, J. B., Haile, A. T., Gieske, A. S., Booij, M. J., and Reggiani, P.: Hydrological Balance of Lake Tana, Upper Blue Nile Basin, Ethiopia. In: Nile River Basin, Springer, 2011.

Seibert, J.: Regionalisation of parameters for a conceptual rainfall-runoff model, Agricultural and forest meteorology, 98, 279-293, 1999.

Setegn, S. G., Srinivasan, R., and Dargahi, B.: Hydrological modelling in the Lake Tana Basin, Ethiopia using SWAT model, The Open Hydrology Journal, 2, 49-62, 2008.

Setegn, S. G., Srinivasan, R., Dargahi, B., and Melesse, A. M.: Spatial delineation of soil erosion vulnerability in the Lake Tana Basin, Ethiopia, Hydrological Processes, 23, 3738-3750, 2009.

Setegn, S. G., Srinivasan, R., Melesse, A. M., and Dargahi, B.: SWAT model application and prediction uncertainty analysis in the Lake Tana Basin, Ethiopia, Hydrological Processes, 24, 357-367, 2010.

Singh, V. P.: Elementary hydrology, Chapter 16, Pearson College Division, Englewood Cliffs, New Jersey, 1992.

SMEC, I.: Hydrological Study of The Tana-Beles Sub-Basins." part 1, Sub-basins Groundwater Investigation Report, 2007. 2007.

Steenhuis, T. S., Collick, A. S., Easton, Z. M., Leggesse, E. S., Bayabil, H. K., White, E. D., Awulachew, S. B., Adgo, E., and Ahmed, A. A.: Predicting discharge and sediment for the Abay (Blue Nile) with a simple model, Hydrological processes, 23, 3728-3737, 2009.

Tilahun, S., Mukundan, R., Demisse, B., Engda, T., Guzman, C., Tarakegn, B., Easton, Z., Collick, A., Zegeye, A., and Schneiderman, E.: ASATURATION EXCESS EROSION MODEL, 2013. 2013.

Wale, A., Rientjes, T., Gieske, A., and Getachew, H.: Ungauged catchment contributions to Lake Tana's water balance, Hydrological processes, 23, 3682-3693, 2009.

CHAPTER 6: REALISTIC ASSESSMENT OF SURFACE WATER IRRIGATION POTENTIAL IN THE ETHIOPIAN HIGHLANDS: THE LAKE TANA BASIN[4]

Abstract

Although Ethiopia has a large potential to develop surface irrigation, only 5% of the 30 to 70 million hectares (ha) potentially available has been developed. To examine the underlying causes of this lack of irrigation development, this study evaluates the suitability of surface water irrigation for the Lake Tana Basin development corridor. Surface water availability and land potentially suitable for irrigation development were considered. Surface water potential was examined by analyzing long-term daily historical river discharges. Land suitable for irrigation was determined with a GIS-based multi-criteria evaluation, which considers the interaction of various factors such as climate, river proximity, soil type, land cover, topography/slope, and market outlets. The results indicate that nearly 20% of the Lake Tana Basin is suitable for surface irrigation. However, after analyzing 27 years of river discharge, less than 3% of the potential irrigable area (or less than 0.25% of the basin area) could be irrigated consistently with runoff from the river systems. Thus, the irrigation potential in the Lake Tana Basin can be met by increasing dry season flows, by improving upland infiltration, by supplying water from reservoirs, or by pumping water directly from Lake Tana.

[4] Worqlul, A. W., Collick, A. S., Rossiter, D. G., Langan, S., and Steenhuis, T. S.: Assessment of surface water irrigation potential in the Ethiopian highlands: The Lake Tana Basin, Catena, 129, 76-85, 2015.

6.1 Introduction

The Ethiopian highlands are comprised of land resources, which are potentially suitable for irrigation. Irrigation would provide farmers with sustained livelihoods and improve their general well-being (Belay and Bewket, 2013; Hussain and Hanjra, 2004). However, the country's irrigable land has been underutilized, and only 4 to 5% of the potential area has been developed for irrigation (Awulachew et al., 2007). Consequently, the agricultural economy of the country is largely based on rainfed cultivation, but while employing 85 percent of the population, it only contributes 50 percent to the gross domestic product (Berry, 2003). Ultimately, increasing agricultural production using irrigation is one of the main drivers to end poverty caused by insufficient output from these rainfed systems. Therefore, the study investigates the causes of the underutilization of the land resources for irrigation.

According to the Ministry of Water, Irrigation & Energy of Ethiopia irrigation command areas can be classified into three groups (Awulachew et al., 2005). The first group is small-scale irrigation area of less than 200 ha, medium scale between 200 and 3000 ha and large scale above 3000 ha. Consequently, we quantified both the potential land areas suitable for small, medium and large-scale surface irrigation; in addition, the available surface water potential for surface irrigation was identified by analyzing historical river flow data. This investigation focused on the Lake Tana basin situated in the Upper Blue Nile basin, which has been designated as one of the growth development corridors for economic development by the government of Ethiopia to end poverty.

6.2 Materials and Methods

6.2.1 Description of Study Area

The study was carried out in the 15,000 km^2 Lake Tana Basin, of which the lake covers around 3,000 km^2. The lake is located at 12º00'N, 37º15'E in the North-West highlands of Ethiopia (Wale et al., 2009). The elevation of the watershed ranges from 1,786 to 4,107 m and the slope ranges from 0 to 167% with an average slope of 47%. The study area has a minor rainy season in April and May and a major rainy phase from June to September during which approximately 75 percent of the annual rainfall occurs. The mean annual rainfall is 1,430 mm at Bahir Dar Station south of Lake Tana, and 1,090 mm at Gondar Station north of the lake (Figure 6-1). The average minimum and maximum temperatures are 20ºC and 7ºC at Debre Tabor station. The mean annual relative humidity from 1992−2006 at Bahir Dar is 58 percent and at Gondar 53 percent. It is expected that future irrigation water availability due to climate change will increase (Dile et al., 2013).

Most farmers in the Lake Tana basin grow one crop per year during the rainy phase of the monsoon from June to September when 85 % of the annual rainfall falls (Awulachew et al., 2010; Awulachew et al., 2007; Belay and Bewket, 2013). The major rainfed crops are teff, corn, sorghum, millet, barley, wheat, beans and rice. In addition Eucalyptus plantations are expanding rapidly (Chanie et al., 2013). Irrigated crops are usually of high value and include Khat, a mild narcotic leaf, onions, potatoes and vegetable crops. The acreage of irrigated crops in the Gilgil Abay basin one of the major sub-basins of Lake Tana is in the order of 1% (Enku et al., 2014) and it is in the same order as in the other basins in the Lake Tana. Both surface and ground water

are used for irrigation, with surface water irrigation dominant in the uplands and ground water use in the plains around Lake Tana.

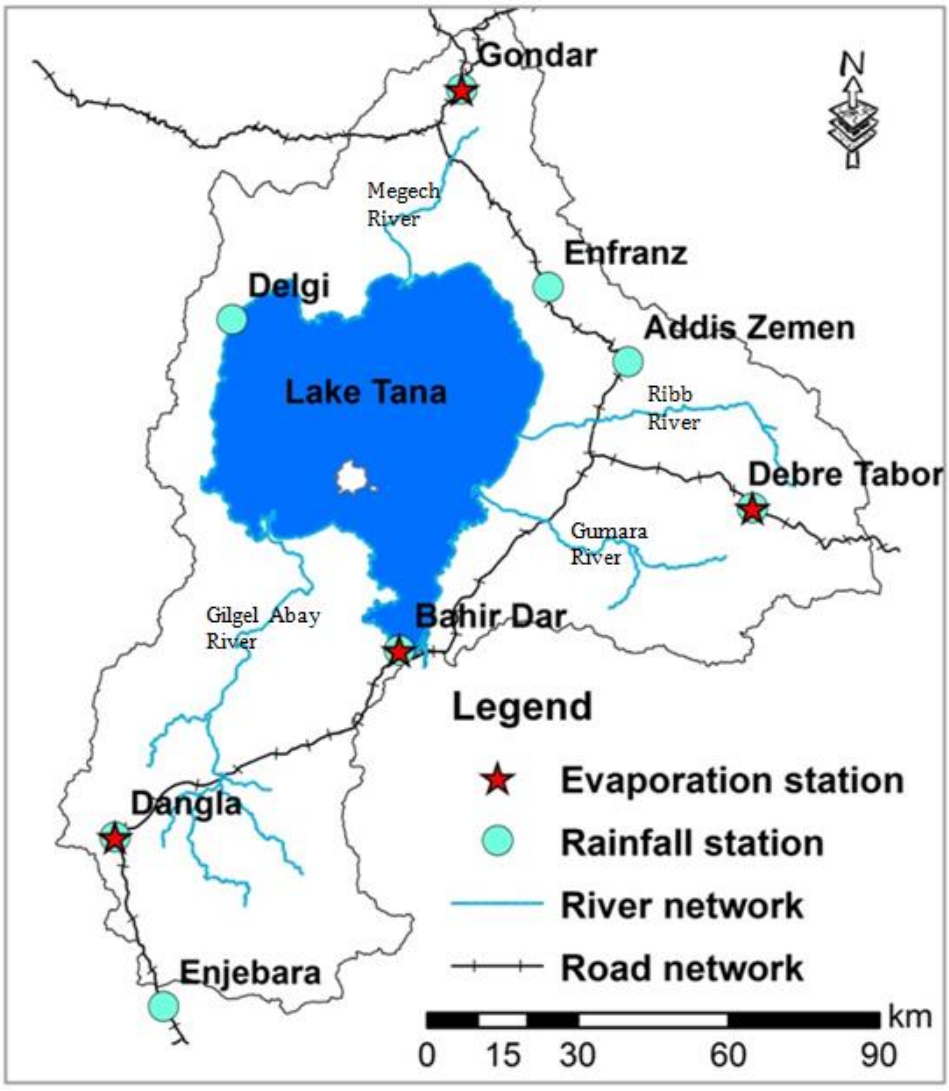

Figure 6-1: Study area with paved road network, major towns and rivers

6.2.2 Source of Data Used

In this study we have first identified potential land areas suitable for surface irrigation using a GIS based Multi-Criteria Evaluation (MCE) technique and then second quantified the available surface water potential for surface irrigation by analyzing historical river flow data of the major rivers in the Lake Tana Basin. To achieve this, the following datasets for the Lake Tana watershed were collected.

6.2.2.1 Climate

Precipitation, temperature, wind speed, and relative humidity were collected from the Ethiopian Metrological Agency (EMA). Monthly long-term rainfall was available from 1992 to 2006 for eight stations (Figure 6-1). For calculating evaporation with the Penman-Monteith equation (Monteith, 1965) the daily measurements of temperature, humidity, wind speed and sunshine hours were collected from four of the synoptic stations at Bahir Dar, Gondar, Dangla and Debre Tabor (Figure 6-1).

6.2.2.2 Land features:

Soil and land use data were obtained from the Ethiopian Ministry of Water and Energy (EMWE). The dominant soil groups according to FAO soil classification (GroupWRB, 2006) in the Lake Tana area are Haplic Luvisols (26%), Chromic Luvisols (20%), Eutric Leptosols (16%), Eutric Vertisols (15%) and Eutric Fluvisols (14%) (Figure 6-2 a). The land use map indicated that the study area was dominated by agricultural land covering approximately 74 percent followed by the lake itself accounting for approximately 22 percent, and bush land and grassland at 6 percent (Figure 6-2b). A 90 m resolution Shuttle Radar Topography Mission (SRTM) Digital Elevation

Model (DEM) was used to determine the percentage slope of the watershed on a pixel-by-pixel basis (Figure 6-2g).

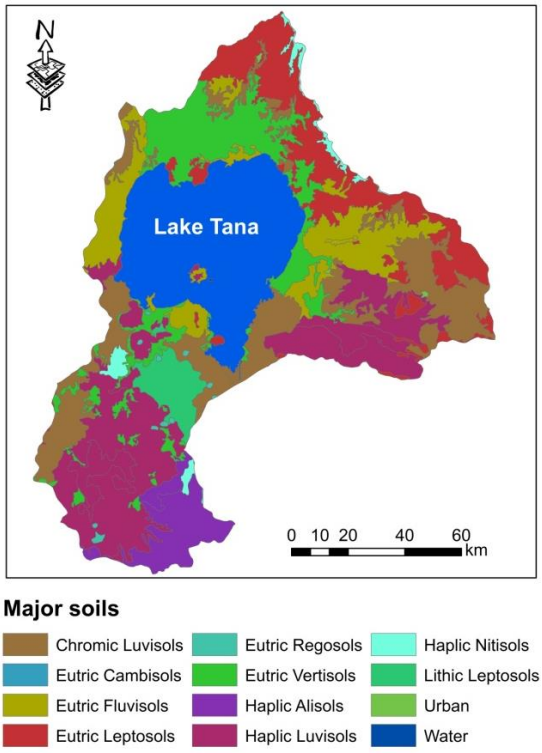

(a) Lake Tana soil

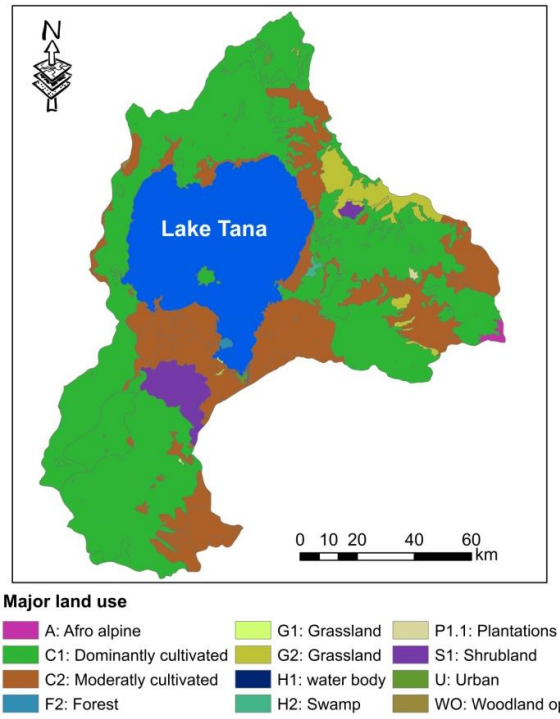

(b) Lake Tana land use

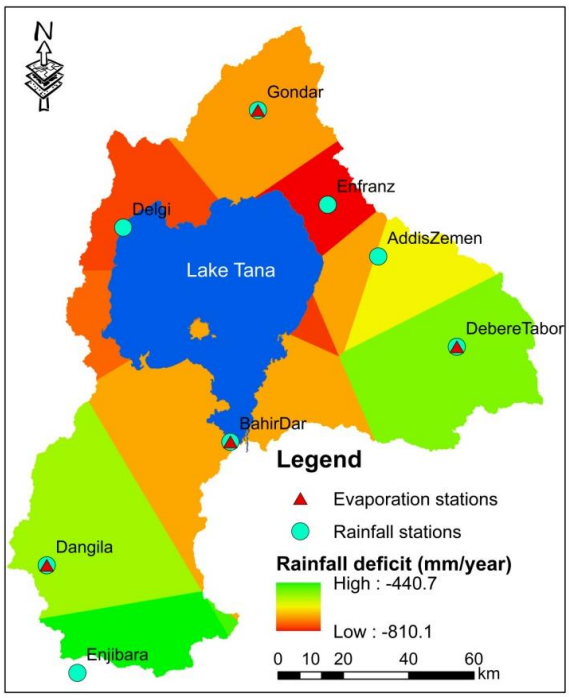

(c) Rainfall deficit

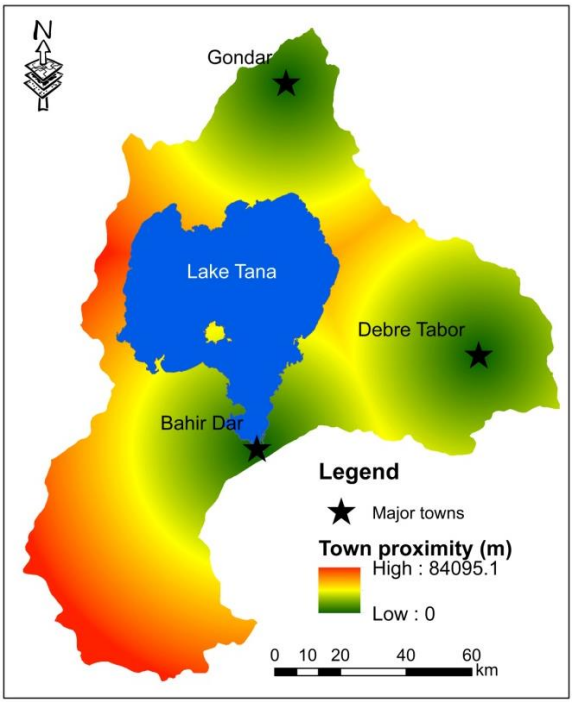

(d) Distance from town

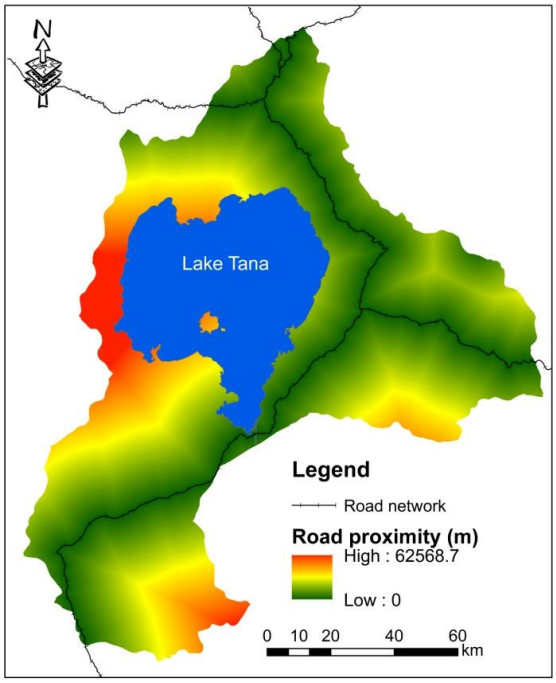

(e) Distance to road

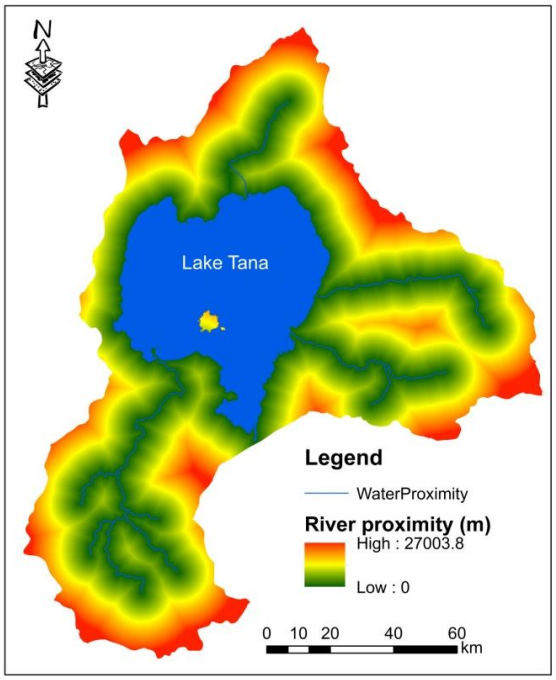

(f) Distance to river

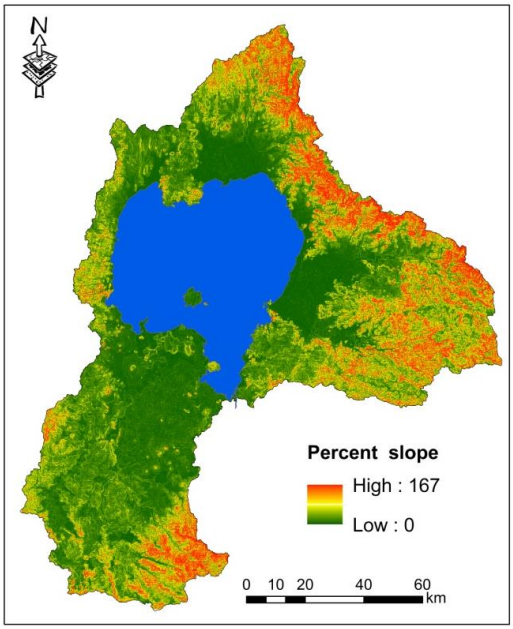

(g) Percent slope of Lake Tana

Figure 6-2: Major features affecting land suitability for surface water irrigation [soil (a), land use (b), rainfall deficit (c), distance to town (d), distance to road (e), distance to river (f) and percentage slope (g)].

6.2.2.3 Market outlets

Market access was determined by using the GPS location of the three major towns with a population of more than 50,000 identified using 2007 Population and Housing Census of Ethiopia and by the network of paved roads. The major paved road networks in the watershed were digitized manually from geo-referenced Google™ Earth images in ArcMAP 10.2 (Figure 6-2d and 2e).

6.2.2.4 Rivers proximity

The four main perennial tributary river networks contribute 93% of the total inflow of the lake (Kebede et al., 2006) and were extracted digitally from the 90m SRTM DEM using the DEM hydro-processing operations of ILWIS (Land and Water Information System, Figure 6-2f).

6.2.2.5 Historical river flow data

Daily river flow data from 1980 to 2007 of the four major rivers (Gilgel Abay, Gumara, Ribb and Megech) were obtained from EMWE. The data was checked for gross errors, and missed recordings were filled using regression and spatial interpolation methods.

6.2.3 Methodology

This study consists of two parts. First, we determined the land most suitable for surface irrigation then we quantified the river water available during the dry season. Land suitability was determined by assigning weights (or ranks) to the factors that likely affect the irrigation potential of a certain land area. Factors considered are climate characteristics (rainfall and evaporation), land features (soil type, land use and slope), market access and proximity to a perennial river. Second, the amount of water available during the dry season (October to May) was determined by analyzing long-term discharge records for the four main rivers in the Lake Tana basin.

6.2.3.1 Land Suitability Factors

Each factor determining the suitability of the land (parcel) for irrigation is classified into four classes according to (FAO, 1976; FAO, 1981) framework ranging from highly suitable (class S1) to not suitable (Class S4, Table 6-1).

Table 6-1: Framework of land suitability classification of FAO (1976 and 1981)

Class S1 Highly Suitable:	Land without significant limitations. This land is the best possible and does not reduce productivity or require increased inputs.
Class S2 Moderately Suitable:	Land that is clearly suitable but has limitations that either reduce productivity or require an increase of inputs to sustain productivity compared with those needed on S1 land.
Class S3 Marginally Suitable:	Land with limitations so severe that benefits are reduced and/or the inputs required to sustain production need to be increased so that this cost is only marginally justified.
Class S4 (N1) Currently Not Suitable:	Land that cannot support the particular land use on a sustained basis, or land on which benefits do not justify inputs

The suitability class of a land parcel with respect to market access and river proximity is determined by its distance in relation to the road network, a large town and perennial rivers. The distances were calculated by projecting the locations to a Mercator (UTM) Zone 37N. After categorizing the distance map in to four classes of equal ranges, the farthest distances are in class S4 and closer distances were classified as S1.

The climate suitability classes for the land parcels were found by calculating the annual irrigation water requirement by aggregating monthly deficits, or the difference of the average monthly rainfall and potential evaporation. The areal long-term averaged monthly rainfall and potential evapotranspiration (from 1992 to 2006) were determined by Thiessen Polygon method. The long-term average monthly deficit in rainfall is computed as rainfall minus evapotranspiration. Monthly deficits were accumulated to yearly on pixel basis (Figure 6-2c). For the overlay analysis, the average rainfall deficit values were divided into four classes by equal interval ranging technique. Pixels with small deficits were classified in the S1 group meaning land

without significant limitations for surface irrigation and pixels with the largest deficits were classified in the S4 class. Note that the deficits are theoretically equal to the irrigation water requirements at the site.

The land-characteristic suitability is based on slope soil type and land use. The slope map computed from a 90m resolution DEM has four suitability classes for surface irrigation suitability (FAO, 1999). Slope from 0 to 2 percent is classified as S1, from 2 to 4 percent as S2, from 4 to 8 percent as S3 and slope above 8 percent is classified as S4. Finally, land use and soil maps of the study area are reclassified to four different ranges of suitability groups based on their suitability and FAO soil definition (GroupWRB, 2006). Agricultural land use is considered as S1, grass land as S2, shrub land as S3 and forest area as S4. Soils with natural fertility and the suitability for a wide range of agricultural uses (Luvisols) and very productive soils (Nitisols) were classified as S1; Vertisols, Fluvisols and Cambisols with good natural fertility and considerable agricultural potential were classified as S2; Regosols and Alisols with low moisture holding capacity and poor fertility were considered to be S3; and Leptosols which are extremely gravely and stony are classified as S4.

6.2.3.2 Irrigation potential

The irrigation potential of a parcel pixel is determined by weighting the factors discussed above in Section 2.2.1. In this study, two types of weighting approaches were applied: the ranking technique and pair-wise comparison technique. The ranking technique involves ordering of decision factors (from 1 to "n") according to their importance (Rossiter et al., 1999). Rank ordering would involve assigning 1 to the most important factor, 2 to the second most important factor, and so forth until "n" is assigned to the least important factor (Rossiter et al., 1999). In

pair-wise comparison (Saaty, 1977), each factor was matched head-to-head (one-to-one) with each other, and a pair-wise or comparison matrix was prepared to express the relative importance. A scale of importance is broken down from a value of 1 to 9 (Table 6-2). The highest value 9 corresponds to absolute importance, and the reciprocal of all scaled ratios is entered in the transpose position (1/9 shows an absolute triviality).

Table 6-2: Pair wise comparison scale and definition (Saaty, 1977).

Intensity of importance	Definition	Explanation
1	Equal importance	Two factors contribute equally to the objective
3	Somewhat more important	Experience and judgment slightly favor one over the other
5	Much more important	Experience and judgment strongly favor one over the other.
7	Very much more important	Experience and judgment very strongly favor one over the other. Its importance is demonstrated in practice.
9.	Absolutely more important	The evidence favoring one over the other is of the highest possible validity.
2,4,6,8	Intermediate values	When compromise is needed

A preliminary surface irrigation area suitability map was computed for the two different weighting scenarios using the Weighted Overlay tool of ArcGIS Spatial Analyst Toolbox. The preliminary suitable area was multiplied by a constraint map, which consists of water bodies, wetlands, urban areas, forest, and protected areas. These areas were given a value of zero indicating that they ultimately limit the surface irrigation area suitability and are defined as permanently not suitable by the FAO (1976 and 1981) framework. The final map indicating

continuous areas suitable for small, medium and large irrigation was then obtained by identifying pixels (with values greater than 85).

6.2.3.3 Surface Water Availability

Information on low flows was required to quantify the amount of water available for surface water irrigation application during the dry monsoon phase. The low flows were calculated for the major tributaries of Lake Tana (i.e., Gilgel Abay, Gumara, Ribb and Megech rivers) with daily average discharges for the years from 1980 to 2007. These four rivers contribute more than 93% of the total lake inflow (Kebede et al., 2006). The daily discharge data were obtained from the Ethiopian Ministry of Water and Energy. Low-flow characteristics were estimated using a flow duration curve and by determining the 90 percentile available flow. The 90 percentile flow is described as the flow exceeded 90% (Q90) of the time for a particular year. The 90 percentile available flows were determined by ranking all daily discharge and finding the discharge exceeded by 90 percent of all values (Eslamian et al., 2010; Reilly and Kroll, 2003).

6.2.3.4 Irrigation potential as determined by water availability

The irrigated area was estimated as the quotient of the Q90 (discharge exceeds 9 out of 10 years) and the crop water requirement (CWR) during the growing season of the crop. The crop water requirement was calculated by summing maximum crop evapotranspiration (ET) plus loses which include application losses, La, conveyance loss, Lc, and special needs, Ls.

$$\mathrm{CWR} = \mathrm{ET} + \mathrm{L_a} + \mathrm{L_c} + \mathrm{L_s} \qquad \text{Eq. (1)}$$

We note that, the dominant crops in the Lake Tana basin include barley, corn, millet, wheat, sorghum, teff, beans and rice. According to FAO “56” (Allen et al., 1998) the maximum value of

the crop coefficient, Kc, for the dominant crop is 1.15 which covers barley, wheat and rice. According to FAO 56 (Allen et al., 1998) crop evapotranspiration is the product of potential evapotranspiration, Eto and crop coefficient, hence,

$$ET = Kc * Eto = 1.15 * Eto \quad \text{Eq. (2)}$$

The potential evaporation was computed using the Penman-Monteith method.

Inefficiencies in irrigation water application and water requirements for special applications, such as land preparation and leaching, are assumed to be 60% (Yohannes and Tadesse, 1998). Consequently,

$$L_a + L_c + L_s = 0.6\ ET \quad \text{Eq. (3)}$$

Combining Eqs. 1 to 3 we find that:

$$CWR = 1.84Eto \quad \text{Eq. (4)}$$

6.3 Results and Discussion

6.3.1 Weighting of factors and suitable areas for irrigation

The pair-wise comparison matrix Table 6-3 (using Table 6-2) was constructed first. The seven factors ranging from soil to slope are listed in the first seven columns and the first seven rows in Table 6-3. The column factors were compared with the factors in the rows for their significance to surface irrigation, then using the scoring of Saaty (1977) in Table 6-2, the pair-wise matrix Table 6-3 was prepared. Thus, for example in Table 6-3, the “river proximity” (in the column) is much more important for determining the suitability of a parcel of land than the factor "land use"

(in the row). Hence, we assign the value of 7 at the intersection of “river proximity” in the column and "land use" in the row. Conversely, “land use” (in the column) of Table 6-3 is much less important than “river proximity” (in the row) and we assign the reciprocal of 7 to the intersection of these two factors. Next, after completing the pair-wise comparison matrix, the weights of the factors are computed by normalizing the respective eigenvector by the cumulative eigenvector. Eigenvalue vector is the nth root of the product of rows (Podvezko, 2009).

The results in Table 6-3 show that the factor "river proximity" is the most important factor, since all its values are greater than 1 in its row followed by "road proximity" that only has one value less than 1. The least important factor in considering surface water irrigation suitability is "land use" with all its row values less than 1. In the ranking technique, factors were ordered according to their priority. The judgment is subjective, weighting of decision factors is determined based on the importance of each factors and involves knowledge of those familiar with irrigation in the area. The factors road proximity, river proximity and slope were judged as very important because they are associated with a large initial investment. Rainfall deficit and soil were considered as important, but the remaining factors of land use and urban proximity were ranked as least important.

These calculated weights of pair-wise and the weights assigned by ranking technique are listed in the last two columns of Table 6-3 where the greater the value, the more important the factor. The sum of each of the last two columns is 100. Both weighting approaches ranked the factors in the same order: river proximity was the most important factor followed by the proximity of the road and slope of the land. The factors weights in pair-wise comparison have a higher standard deviation than ranking technique (11 and 5 respectively).

Table 6-3: Pair-wise comparison matrix and weighting by ranking technique.

Factors	Soil	Land use	River proximity	Urban proximity	Road proximity	Rain deficit	Slope	Pair-wise weighting	Ranking weighting
Soil	1	4	1/3	4	1/2	2	1/3	12	15
Land use	1/4	1	1/7	1/2	1/6	1/3	1/5	3	7
River Proximity	3	7	1	6	2	4	2	32	20
Urban Proximity	1/4	2	1/6	1	1/5	1/2	1/4	4	9
Road Proximity	2	6	1/2	5	1	2	2	22	18
Rainfall deficit	1/2	3	1/4	2	1/2	1	1/3	8	14
Slope	3	5	1/2	4	1/2	3	1	19	17

6.3.2 Surface area suitability

The weights of each factor in last two columns of Table 6-3 were further subdivided into four intervals of equal ranges for each suitability group: highly suitable, moderately suitable, marginally suitable and currently not suitable. For example, the “river proximity” factor in the pair-wise weighting method of the pixels closest to the river is given a value of 32*4/4 (32) and is considered highly suitable. If the pixel was considered moderately suitable a value of 32*3/4 (24) was assigned and a value of 32*2/4 (16) and 32*1/4 (8) is assigned for marginally suitable and currently not suitable pixels, respectively. Each of the factors in Figure 6-2 was reclassified in to Figure 6-3. Figure 6-3 indicates the reclassified factor maps with their assigned weights by pair-wise and ranking techniques and the constraint map.

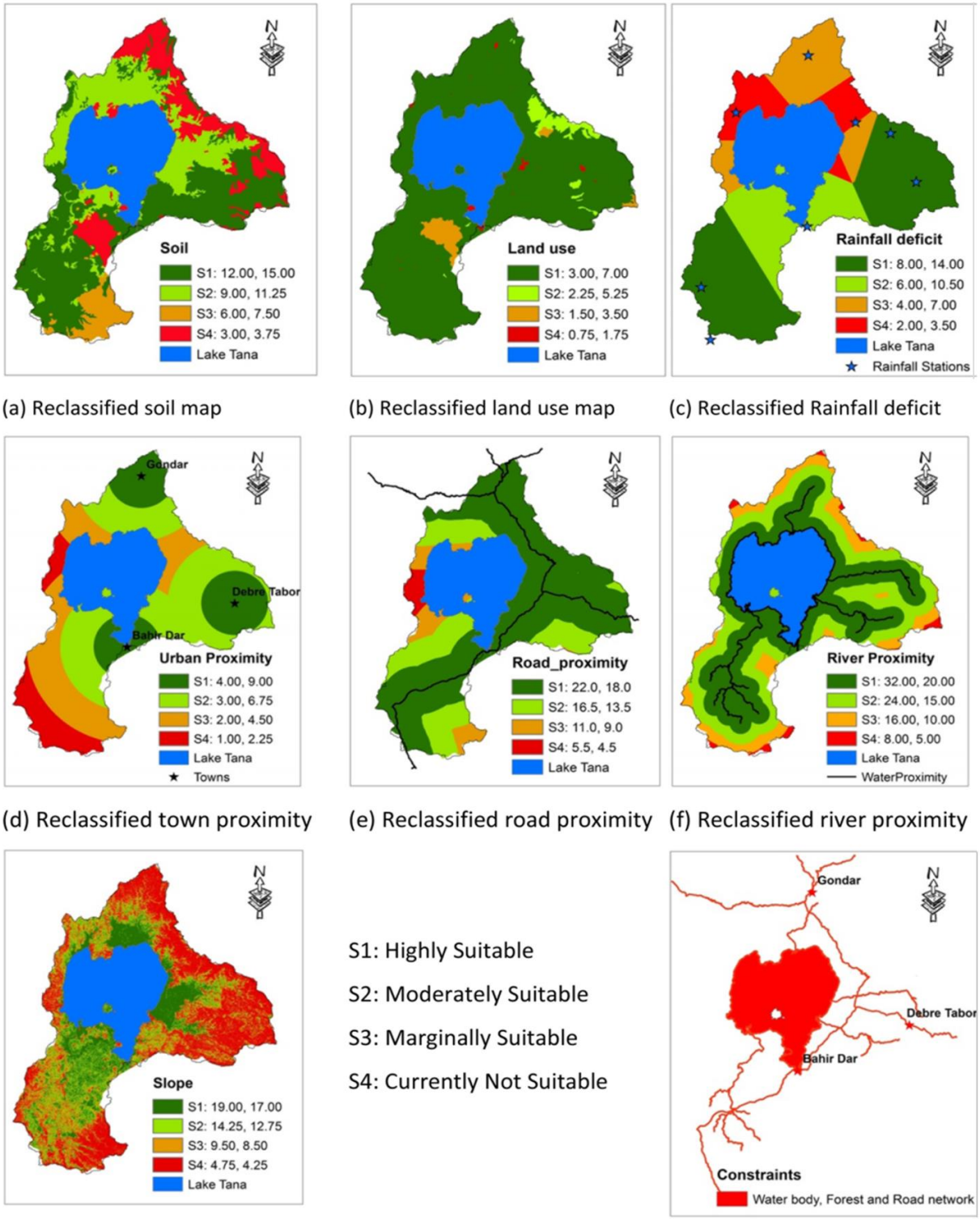

Figure 6-3: Classified factor maps of the study site [soil (a), land use (b), rainfall deficit (c), town proximity (d), road proximity (e), river proximity, (f) and slope (g)] and irrigation area constraint map (h).

A preliminary surface irrigation area suitability map was computed using the Weighted Overlay Tool available in ArcGIS Spatial Analyst Toolbox for the two weighting scenarios (Figure 6-4). Subsequently, the preliminary suitable areas are multiplied by the constraint map to exclude the permanently non-suitable areas.

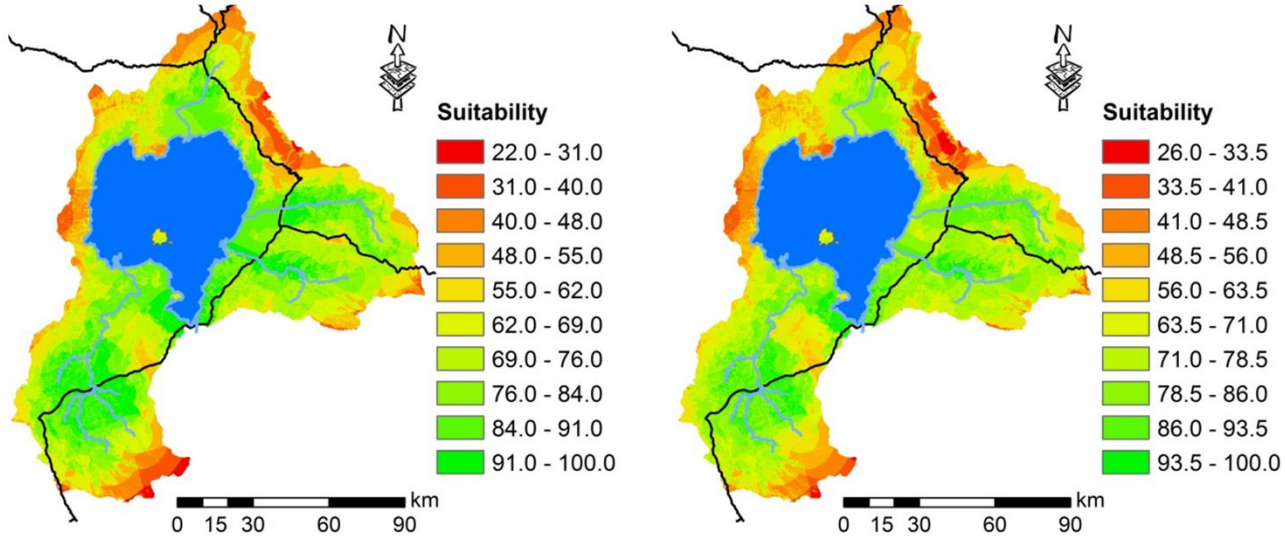

Figure 6-4: A preliminary surface irrigation area suitability map factors weighted by a. pair-wise and b. ranking. Suitability value of hundred indicates all of the factors are being classified as S1 and if one or more of the factors are classified as S2, S3 or S4 the suitability is less than hundred. The suitability value indicates the potential of the land for surface irrigation, the higher the value the higher the irrigation potential.

The preliminary suitability area map was optimized by a user defined threshold number. The threshold number used was greater than 85. Pixels with a suitability value of greater than 85 were identified as suitable areas. The optimized suitable area indicated thousands of suitable areas across the watershed. Area of suitable polygons ranges from 0.81ha (single pixel 90 by 90 meter) to 9,059 ha by ranking and from 0.81 ha (single pixel 90 by 90 meter) to 14,726 ha by

pair-wise weighting technique. The total percentage of suitable land for small scale, medium and large scale surface irrigation accounts approximately 20% and 16% of the Lake Tana Basin by pair-wise and ranking technique, respectively. There are multiple small scale suitable areas smaller than 1 ha approximately 11,500 and 10,700 ha by pair-wise and ranking technique, respectively. The optimized areas are filtered to identify medium- and large-scale suitable areas greater than 200ha. The result indicated that 11% and 5% of the land are suitable for surface irrigation by pair-wise and ranking technique, respectively. The result of the pair-wise comparison was in the same range as Awulachew et al., (2007). However, the method in this study reduced the bias associated with assigning weights to the factors and reasonably captured the existing irrigation area. For that reason, the pair-wise weighting is preferred over the result of suitability by the ranking-weighting technique. In

Table 6-4 the potential irrigable areas suitable for areas larger than 200 ha as determined by the pair-wise weighting method are shown for each of the major tributary rivers of Lake Tana Basin. The distribution of the suitable areas for each basin is shown in Figure 6-5, where the green color indicates the areas suitable for irrigation in the Gilgel Abay basin, yellow for the Ribb, cyan for the Gumara and gray for the Megech. The light blue color is Lake Tana.

Table 6-4 and Figure 6-5 show that the Gilgel Abay has the largest suitable area of approximately 54,900ha but at the same time, the smallest portion of the total basin (12%) compared to the other basins.

Table 6-4 also indicates that the highest portion of suitable area 19% is in the Megech watershed but at the same time has the lowest total area. Most of the large and medium scale suitable areas for irrigation are located in the Gilgel Abay basin (Figure 6-5 and

Table 6-4).

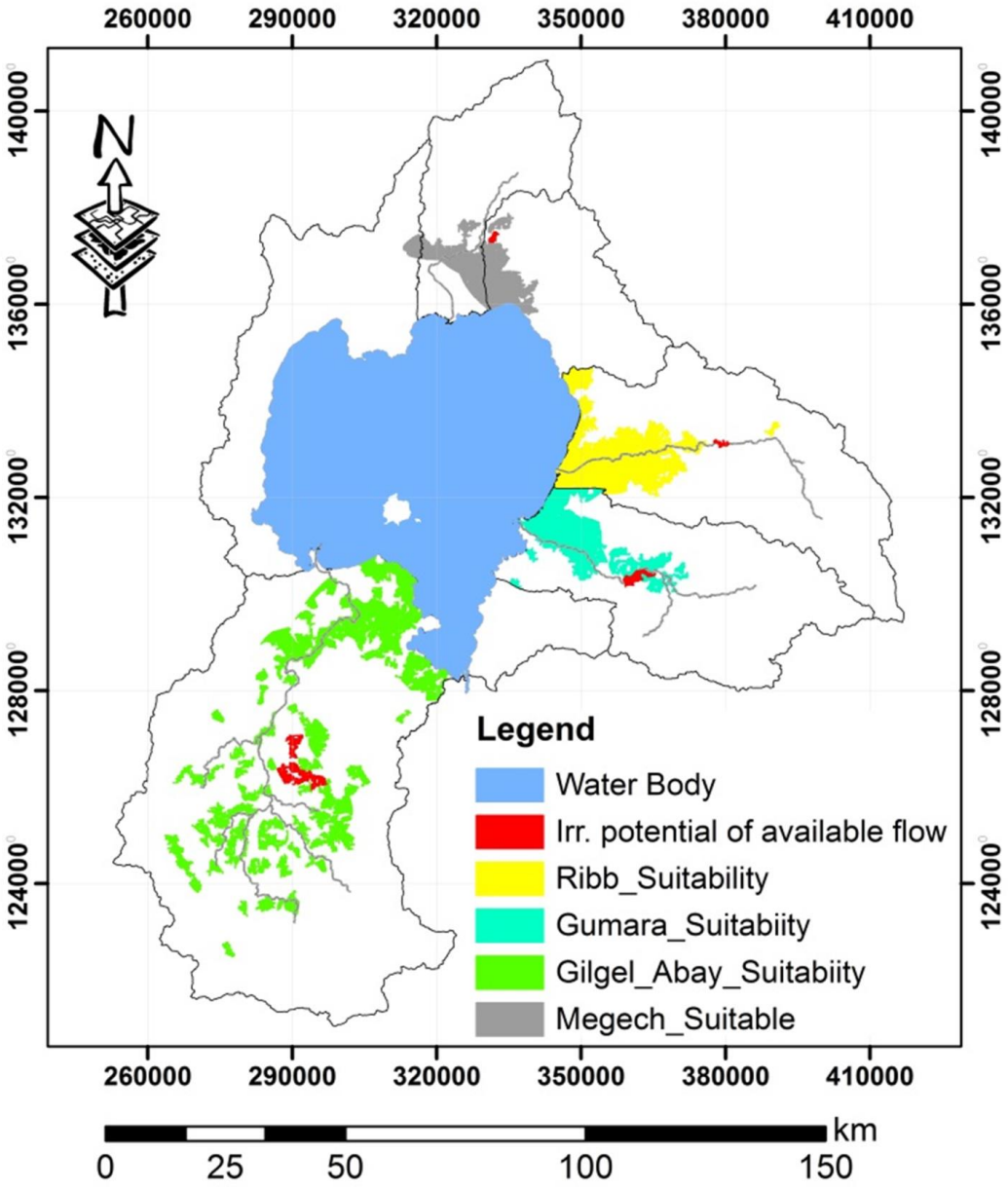

Figure 6-5: Surface irrigation potential of Lake Tana indicated by green for the Gilgil Abay, yellow for the Ribb, light blue for the Gumara and the gray for Megech. The red area is the

irrigation potential area that can be irrigated during the dry monsoon phase for 9 out of 10 years and are located in those areas that have the greatest irrigation potential.

Table 6-4: Spatial distribution of irrigation area suitable in major tributaries of Lake Tana Basin.

	Suitable Area (ha)	Number of large scale surface irrigation suitable areas (>3000 ha)	Number of medium scale surface irrigation suitable areas (>200ha and < 3000ha)	Percentage of suitable area for surface irrigation (%)
Gilgel Abay	54,894	4	78	12
Ribb	31,780	3	4	16
Gumara	24,805	2	16	14
Megech	19,029	2	8	19
Total	130,508	11	106	61

6.3.3 Surface water availability

The 90 percentile available flow is determined by generating flow-duration curves (FDC). FDC provides the percentage of time (duration) a daily or monthly stream flow was exceeded for the 27-year period from 1980 to 2007. The FDC graph of logarithmic daily river flow versus exceedance frequency is plotted for the major tributaries as shown below in Figure 6-6. The FDC of Megech has steep gradient, which indicates high variability of daily flow, with 1 per cent of all days for the study period have zero flow. The FDC of Ribb River indicates a distinct dry season with steep gradient showing about 5 per cent of all days have zero flow. FDC of Gilgel Abay indicated no distinct dry season and it has relatively little variability in stream flow. The Q90 obtained from flow duration curves in Figure 6 and that is exceeded 9 out of every 10 years

are given in Table 6-5. The Gilgel Abay has the greatest Q90 flows has also the largest suitable area. The Megech has the lowest Q90 and has the smallest suitable area.

Table 6-5: Average flow and extracted Q90 for the major tributaries of Lake Tana Basin.

	Gilgel Abay (m3/s)	Gumara (m3/s)	Ribb (m3/s)	Megech (m3/s)
90% exceedance probability	1.90	0.70	0.12	0.06
Average daily flow (1992 to 2006)	54.40	33.39	14.82	6.26

6.3.3.1 Areas suitable for irrigation versus surface water availability

The result of the rainfall deficit analysis indicated that rainfall in the wet season June through September is well above crop evapotranspiration. So, for the rainy season there is no need for irrigation. To calculate the crop water requirements in different months a potential evaporation rate was calculated using the Penman-Monteith approach, and the potential evaporation ranged from 2.8mm/day in June (cold and rainy month) to 4.4mm day-1 in April (the warmest and driest month). The total crop water requirement computed on a monthly basis using Equation 4 ranged from 5.2mm/day to 8.1mm/day. The irrigation potential of the 90 percentile available water was computed by dividing the available water in each sub-basin by the total crop water requirement. The result indicated that November and December had the maximum irrigation potential of approximately 4100ha, and April had the minimum potential of 3000ha. This area accounts less than 3% of the potential irrigable area (or less than 0.25% of the basin area). In Figure 6-5, the irrigation potential of the 90 percentile available flow in the major sub-basins of Lake Tana is

shown in red and is located in the most desirable places. Figure 6-5 also indicated that the irrigation potential of the available water was very small, and in the Ribb and Megech basin was insignificant. The irrigation potential of the 90 percentile available flow computed for another crop, such as millet, with a crop coefficient of 1.0 at the mid-season increased the irrigation potential of the 90 percentile flow by 15% in all sub-basins. Still the change is insignificant compared to the potential irrigable land.

Thus, to increase the irrigation in the potentially irrigable areas, water falling and flowing during the rainy monsoon phase needs to be stored for the dry phase. To find the irrigable area if all water was stored, we divided the average daily flow (from 1992 to 2006 in the major sub-basins of Lake Tana, Table 6-5) by the crop water requirements. The result indicated that the average flow of Gilgel Abay and Gumara Rivers is sufficient to irrigate the irrigation potential land in the dry season. However, the average flow of the Ribb and Megech is not sufficient to irrigate the potential area; they would be sufficient to irrigate only 50 and 35 percent of this area.

6.4 Conclusions

In this study, the surface water irrigation potential of the Lake Tana Basin was mapped based on factors, which affect the suitability of land for surface irrigation, such as proximity to river, slope, land use, soil, rainfall deficit and market outlets. The suitable land was filtered to identify medium (between 200 and 3000 ha) and large scale (>3000 ha) suitable areas. The result indicated that, approximately 130,000 ha (11 percent of the land) of the Lake Tana watershed is suitable for surface irrigation. Gilgel Abay sub-basin has the largest potential area for surface irrigation and Megech has the smallest potential area. However, the 90 percentile of the available daily flow from 1980 to 2007 in the major rivers of Lake Tana sub-basin can only irrigate 3

percent of the potentially irrigable land. We conclude that the main limitation for surface irrigation in the Ethiopian highlands is the available water and not land suitable for irrigation. Future estimates of irrigation potential should take into account the surface water availability, and any future expansion and planning of surface irrigation in the Lake Tana Basin may involve construction of dams across the river to store runoff during the rainy season.

Acknowledgements: This research was supported by a graduate student fellowship for the senior author by the Norman E. Borlaug Leadership Enhancement in Agriculture Program funded by the USAID and the International Water Management Institute. The National Meteorological Agency of Ethiopia and Ethiopian Ministry Water and Energy provided daily rainfall and discharge data free of charge. We would like to acknowledge IWMI's financial support for the research. The Partnership for Enhanced Engagement in Research (PEER) Science financed part of the research cost as well.

References

Allen, R.G., Pereira, L., Raes, D., Smith, M., 1998. FAO Irrigation and drainage paper No. 56. Rome: Food and Agriculture Organization of the United Nations, 26-40.

Awulachew, S., Erkossa, T., Namara, R., 2010. Irrigation potential in Ethiopia: Constraints and opportunities for enhancing the system. Unpublished Report to the Bill and Melinda Gates Foundation.

Awulachew, S.B., Loulseged, A., Loiskandl, M., Ayana, W., M Alamirew, T., 2007. Water resources and irrigation development in Ethiopia. IWMI.

Awulachew, S.B. et al., 2005. Experiences and opportunities for promoting small-scale/micro irrigation and rainwater harvesting for food security in Ethiopia, International Water Management Institute Addis Ababa.

Belay, M., Bewket, W., 2013. Traditional irrigation and water management practices in highland Ethiopia: case study in Dangila Woreda. Irrigation and Drainage, 62, 435-448.

Berry, L., 2003. Land degradation in Ethiopia: Its extent and impact. Commissioned by the GM with WB support, Global-Mechanism/World Bank. Available at http://lada.virtualcentre.org/eims/download.asp? pub_id=92120 (retrieved 1 October 2013).

Chanie, T., Collick, A.S., Adgo, E., Lehmann, C.J., Steenhuis, T.S., 2013. Eco-hydrological impacts of Eucalyptus in the semi humid Ethiopian Highlands: the Lake Tana Plain. Journal of Hydrology and Hydromechanics, 61, 21-29b.

Dile, Y.T., Berndtsson, R., Setegn, S.G., 2013. Hydrological Response to Climate Change for Gilgel Abay River, in the Lake Tana Basin-Upper Blue Nile Basin of Ethiopia. PloS one, 8, e79296.

Enku, T. et al., 2014 Biohydrology of low flows in the humid Ethiopian highlands: The Gilgel Abay catchment. Biologia 69: , 1502-1509.

Eslamian, S., Ghasemizadeh, M., Biabanaki, M., Talebizadeh, M., 2010. A principal component regression method for estimating low flow index. Water resources management, 24, 2553-2566.

FAO, 1976. A Framework for Land Evaluation, Soils Bulletin 32., FAO and Agriculture Organization of the United Nations, Rome, Rome.

FAO, 1981. Guidelines for designing and evaluating surface irrigation systems. Irrigation and Drainage Paper 45. , FAO and Agriculture Organization of the United Nations, Rome, Rome.

FAO, 1999. The future of our land Facing the challenge. Guidelines for integrated planning for sustainable management of land resources., FAO and Agriculture Organization of the United Nations, Rome, Rome.

GroupWRB, I.W., 2006. World reference base for soil resources 2006. World Soil Resources Reports No 103/FAO, Rome. 161p, ISBN 92-5-105511-4.

Hussain, I., Hanjra, M.A., 2004. Irrigation and poverty alleviation: review of the empirical evidence. Irrigation and Drainage, 53, 1-15.

Kebede, S., Travi, Y., Alemayehu, T., Marc, V., 2006. Water balance of Lake Tana and its sensitivity to fluctuations in rainfall, Blue Nile basin, Ethiopia. Journal of hydrology, 316, 233-247.

Monteith, J., 1965. Evaporation and environment, Symp. Soc. Exp. Biol, pp. 4.

Podvezko, V., 2009. Application of AHP technique. Journal of Business Economics and Management, 181-189.

Reilly, C.F., Kroll, C.N., 2003. Estimation of 7-day, 10-year low-streamflow statistics using baseflow correlation. Water Resources Research, 39(9): 1236, DOI:10.1029/2002WR001740.

Rossiter, D.H.F., and, L., Lipták, B.G., 1999. Environmental Engineers' Handbook. 2.5 Decision-Focused Checklists. CRC press LLC 1431 pages.

Saaty, T.L., 1977. A scaling method for priorities in hierarchical structures. Journal of mathematical psychology, 15, 234-281.

Wale, A., Rientjes, T., Gieske, A., Getachew, H., 2009. Ungauged catchment contributions to Lake Tana's water balance. Hydrological processes, 23, 3682-3693.

Yohannes, F., Tadesse, T., 1998. Effect of drip and furrow irrigation and plant spacing on yield of tomato at Dire Dawa, Ethiopia. Agricultural Water Management, 35, 201-207.

APPENDIX A: CHAPTER TWO

Appendix A1: Multi-Sensor Precipitation Estimate-Geostationary (MPEG)

MPEG is one of the products from MPEF as part of the Meteosat Second Generation (MSG) Ground Segment. The MPEF primary function is to generate meteorological products from the Level 1.5 image data supplied like those from the SEVIRI instrument on-board of the MSG series of geostationary satellites by the Image Processing Facility (IMPF) (EUMETSAT). Multi-sensor Precipitation Estimate (MPE) is an instantaneous rain rate product which is derived from the Infrared data (IR-data) of the geo-stationary EUMETSAT satellites by continuous re-calibration of the algorithm with rain-rate data derived from polar orbiting microwave sensors.

The algorithm is based on a combination of MSG images from the Infrared IR10.8 micro m channel and passive microwave data from the Special Sensor Microwave/Imager (SSM/I) instrument on the United States Defence Meteorological Satellite Program (DMSP) polar satellites. The role model for the MPE algorithm was the algorithm developed by (Turk et al., 1999). The product is most suitable for convective precipitation, and is intended mainly for areas with poor radar coverage (Heinemann and Kerényi, 2003). The MPEG data is available through the GEONETCast near real time, global network of satellite-based data dissemination systems designed to distribute space-based, air-borne and in-situ data. A ground GEONETCast reception station is established at the compound of Bahir Dar University, Engineering Faculty (Wale et al., 2011) in collaboration with Tana Sub-basin Organization (TaSBO) and with the University of Twente, Faculty ITC, the Netherlands. The MPEG data is available at a temporal resolution of 15 minutes with a spatial resolution of 3 km for the whole field of view of MSG. The 15 minute

MPEG data is aggregated to daily, monthly and annual rainfall for the study area for 2010, using a daily aggregation time between 00:00 and 23:45 UTC.

Appendix A2: Tropical Rainfall Measuring Mission (TRMM)

TRMM, Tropical Rainfall Measuring Mission, was launched by the H-II rocket from Tanegashima Space Centre of The National Space Development Agency of Japan (NASDA), on November 28, 1997. This satellite has been developed as a joint project between Japan and US, which is the first space mission dedicated to measure rainfall (NASDA, 2001).

TRMM works by combining both TIR and MW sensors (Dinku et al., 2011). The MW channel carefully measures the minute amounts of microwave energy emitted and scattered by the Earth and its atmospheric constituents. TRMM also operates in active radar. TRMM satellite orbits the earth at a 35o inclination angle with respect to the equator. TRMM covers an area of the earth's surface that extends well beyond the tropics, covering a swath between 38°N to 38°S. TRMM makes these data available in both near-real time and delayed research-quality formats. The TRMM rainfall product has a spatial resolution of 0.25 degree and a temporal resolution of 3 hours. For this study the TRMM product 3B42 version 7 is used. The TRMM-3B42 estimates are produced in four steps (Dinku et al., 2010): (i) the PM estimates are adjusted and combined, (ii) TIR precipitation estimates are created using the PM estimates for calibration, (iii) PM and TIR estimates are combined, and (iv) the data is rescaled to monthly totals where by gauge observations are used indirectly to adjust the satellite product. The major inputs into the 3B42 algorithm are IR data from geostationary satellites and PM data from the TRMM microwave imager (TMI), Special Sensor Microwave/Imager (SSM/I), Advanced Microwave Sounding Unit (AMSU), MHS (Microwave Humidity Sounder) and Advanced Microwave Sounding Radiometer-Earth Observing System (AMSR-E) (Ouma et al., 2012). The successor GPM is

launched in February 2014, with advanced radar and passive microwave sensors and will provide continuous precipitation estimates for the next years to come.

Appendix A3: Climate Forecast System Reanalysis (CFSR)

The CFSR was designed and executed as a global, high-resolution coupled atmosphere–ocean–land surface–sea ice system to provide the best estimate of the state of these coupled domains for the study period (Saha et al., 2014). New features in the CFSR according to (Wang et al., 2011) include: (1) it is the first reanalysis system in which the guess fields are taken as the 6-h forecast from a coupled atmosphere–ocean climate system with an interactive sea ice component; and (2) it assimilates satellite radiances rather than the retrieved temperature and humidity values. In addition, the CFSR is forced with observed estimates of evolving greenhouse gas (GHG) concentrations, aerosols, and solar variations (Wang et al., 2011). The CFSR global atmosphere data has a spatial resolution of approximately 38 km and the data is available from 1979.